Exploring controls of the early and stepped deglaciation on the western margin of the British Irish Ice Sheet.

Benetti, Sara; Chiverrell, Richard C.; Ó Cofaigh, Colm; Burke, Matthew; Medialdea, Alicia; Small, David; Ballantyne, Colin; Bateman, Mark; Callard, Sarah Louise; Wilson, Peter; Fabel, Derek; Clark, Chris; Arosio, Riccardo; Bradley, Sarah L.; Dunlop, Paul; Ely, Jeremy C.; Gales, Jenny; Livingstone, Stephen J.; Moreton, Steven; Purcell, Catriona; Saher, Margot; Schiele, Kevin; Van Landeghem, Katrien; Weilbach, Kasper

Journal of Quaternary Science

DOI:
10.1002/jqs.3315

Published: 01/07/2021

Peer reviewed version

Exploring controls of the early and stepped deglaciation on the western margin of the British Irish Ice Sheet

Sara Benetti[1#], Richard C. Chiverrell[2], Colm Ó Cofaigh[3], Matt Burke[2], Alicia Medialdea[4*], David Small[3], Colin Ballantyne[5], Mark D. Bateman[4], S. Louise Callard[6], Peter Wilson[1], Derek Fabel[7], Chris D. Clark[4], Riccardo Arosio[8**], Sarah Bradley[4], Paul Dunlop[1], Jeremy C. Ely[4], Jenny Gales[9***], Stephen J. Livingstone[4], Steven G. Moreton[10], Catriona Purcell[11], Margot Saher[11], Kevin Schiele[1], Katrien Van Landeghem[11], Kasper Weilbach[3]

[1] School of Geography and Environmental Sciences, Ulster University, Coleraine, UK

[2] School of Environmental Sciences, University of Liverpool, Liverpool, UK

[3] Department of Geography, Durham University, Durham, UK

[4] Department of Geography, University of Sheffield, Sheffield, UK

[5] School of Geography and Sustainable Development, University of St. Andrews, Scotland, UK

[6] School of Geography, Politics and Sociology, University of Newcastle, Newcastle, UK

[7] Scottish Universities Environmental Research Centre, East Kilbride, UK

[8] Scottish Association for Marine Science, Oban PA37 1QA, UK**

[9] National Oceanography Centre, Southampton, UK***

[10] NERC Radiocarbon Laboratory, East Kilbride, UK

[11] School of Ocean Sciences, Bangor University, Menai Bridge, UK

[#] *Corresponding author*

** Present address:*
National Research Centre on Human Evolution (CENIEH), Burgos, Spain

*** Present address: Centre for Environment, Fisheries and Aquaculture Science, Lowestoft NR33 0HT, UK*

**** Present address: School of Biological & Marine Sciences, Plymouth University, UK*

Running title: Deglacial rates and controls for BIIS western margin

ABSTRACT

New optically-stimulated luminescence dating and Bayesian models integrating all legacy and BRITICE-CHRONO geochronology facilitated exploration of the controls on the deglaciation of two former sectors of the British-Irish Ice Sheet, the Donegal Bay (DBIS) and Malin Sea ice-streams (MSIS). Shelf-edge glaciation occurred ~27ka, prior to the global Last Glacial Maximum, and shelf-wide retreat began 26-26.5ka at a rate of ~18.7-20.7m/a. MSIS grounding zone wedges and DBIS recessional moraines show episodic retreat punctuated by prolonged still-stands. By ~23-22ka the outer shelf (~25,000 km^2) was free of grounded ice. After this time, MSIS retreat was faster (~20m/a vs. ~2-6m/a of DBIS). Separation of Irish and Scottish ice sources occurred ~20-19.5ka, leaving an autonomous Donegal ice dome. Inner Malin shelf deglaciation followed the submarine troughs reaching the Hebridean coast ~19ka. DBIS retreat formed the extensive complex of moraines in outer Donegal Bay at 20.5-19ka. DBIS retreated on land by ~17-16ka. Isolated ice caps in Scotland and Ireland persisted until ~14.5ka. Early retreat of this marine-terminating margin margins is best explained by local ice loading increasing water depths and promoting calving ice losses rather than by changes in global temperatures. Topographical controls governed the differences between the ice-stream retreat from mid-shelf to the coast.

Keywords: Malin Sea; Donegal; ice streams; deglaciation; retreat rate

1. INTRODUCTION

The assessment of the rate and style of ice sheet retreat closely relates to many globally important scientific and socio-economic questions (Stocker, 2014). Constraining the pace of ice-sheet retreat for both past and present ice sheets can improve our understanding of how large ice masses respond to local and global, internal and external forcing, such as glaciological, climatic, and oceanographic changes. Once insights gained from such knowledge are incorporated in ice sheet models, they can improve the predictions on how modern ice sheets will evolve with the current changing climate, ocean temperature and sea-level (Joughin, et al., 2014, Rignot, et al., 2010). The behaviour of ice streams is of interest as they are a major regulator of the mass balance of ice sheets (Payne, et al., 2004, Roberts, et al., 2010, Stokes, 2018, Stokes and Clark, 1999, Stokes and Clark, 2001). At ice stream termini, the reduction or loss of buttressing ice shelves can lead to thinning of upstream based ice and the acceleration of ice flow and this behaviour has been recorded in modern ice streams in Greenland and West Antarctica (Krabill, et al., 2000, Krabill, et al., 2004, Pritchard, et al., 2009, Rignot, et al., 2004a, Sonntag, et al., 2012). Additionally, ice streams react more readily than other parts of the ice margin to any perturbation in ocean circulation, atmospheric temperature and sea-ice distribution as a consequence of both thermal (melting) and mechanical (floatation and calving) stressors that occur along the margins of marine-terminating ice sheets (e.g. Hulbe, et al., 2004, Joughin, et al., 2012, Payne, et al., 2004, Scambos, et al., 2004, Shepherd, et al., 2004).

While modern ice streams are being extensively studied, the temporal resolution of such studies is limited. Numerical-glaciological, isostatic and palaeoclimatic models all require empirical constraints on past ice-sheet extent and dynamics either to direct their formulation or for the testing of model outputs (Hughes, et al., 2016). Such information over centuries and millennia can only come from palaeo-analogues, where a complete record of deglaciation may be better visible and quantifiable (Bradwell, et al., 2008, Chiverrell, et al., 2013, Hughes, et al., 2016, Svendsen, et al., 2004). The last British Irish Ice Sheet (BIIS) has been proposed as a potential analogue for sensitive areas of modern ice sheets (Clark, et al., 2012). The BIIS, at several times in the past, had an abundance of marine-terminating ice, which would have been sensitive to both climatic and oceanic forcing, and was drained by radiating ice streams, which were likely critical to BIIS dynamics and overall mass balance during retreat (e.g. Boulton and Hagdorn, 2006, Boulton, 1990, Hubbard, et al., 2009b, Pritchard, et al., 2009, Rignot, et al., 2004b, Sole, et al., 2008).

The Malin Sea includes the continental shelf to the west of Scotland, often referred to as the Malin Shelf, and the portion of the continental shelf northwest of Ireland that includes Donegal Bay (Fig. 1). The Malin Sea received flows from two large convergent ice masses derived from the Hebridean Islands, mainland Scotland, the North Channel, and the north of Ireland. Ice radiating from the mountains of Donegal in northwest Ireland formed an independent centre of ice dispersal, that not only fed ice towards the north, but also west and southwest into Donegal Bay (Fig. 1 inset). Ice in Donegal Bay was also fed from the lowland ice domes through Counties Mayo and Sligo (Greenwood and Clark, 2009a, Greenwood and Clark, 2009b). The former ice masses occupying the Malin Shelf and

Donegal Bay meet the fundamental geomorphological criteria for ice streams (Stokes, 2018, Stokes and Clark, 1999, Stokes and Clark, 2001) in the form of convergent flows and ubiquitous elongated bedforms (Dove, et al., 2015, Dunlop, et al., 2010, Finlayson, et al., 2014). The ice on the Malin Shelf has attracted a variety of names, including Barra Fan Ice Stream (Callard, et al., 2018, Dunlop, et al., 2010, Scourse, et al., 2009), Hebrides Ice Stream (Dove, et al., 2015, Small, et al., 2017a), Malin Sea Ice Stream (Wilson, et al., 2019). In addition, sectors of the ice mass have also been referred to separately as other names including the North Channel Ice Stream (Finlayson, et al., 2014, Finlayson, et al., 2010, Hughes, et al., 2014).

Here, this marine-terminating ice stream is termed the Malin Sea Ice Stream (MSIS), it drained between 5-10% of the BIIS and fed the southernmost glaciogenic fan on the European continental margin, as well as largest sedimentary depocentre of the BIIS, the Donegal-Barra Fan (DBF - Fig. 1) (Dove, et al., 2015, Howe, et al., 2012, Knutz, et al., 2001). Deep water cores suggest that this portion of the ice sheet responded quickly to millennial scale climate oscillations suggesting a strong link between climate cycles and glaciological processes (Hibbert, et al., 2009, Knutz, et al., 2001, Scourse, et al., 2009). Its sensitivity to climatic and oceanographic changes is also captured by numerical modelling experiments (Hubbard, et al., 2009b, Patton, et al., 2017, Patton, et al., 2016, Patton, et al., 2012a, Patton, et al., 2012b). The other marine-terminating ice stream in the southern portion of the Malin Sea, was fed by ice flowing through Donegal Bay, and has surprisingly never been named and is referred to here as the Donegal Bay Ice Stream (DBIS). Less is known about the contribution of this ice stream to the evolution of the continental margin as there is no distinct glaciogenic fan on this part of the margin similar to the DBF, but there are a series of well-developed canyon systems, whose evolution was driven by meltwater and sediment delivery at the shelf edge during the stages of ice advance and retreat (Benetti et al., 2010; Sacchetti et al., 2012).

Reconstructions of the BIIS have relied heavily on onshore mapping of landforms in representations of former ice limits and ice flow directions (Ballantyne, 1989, Bennett and Boulton, 1993, Clark, et al., 2004, Sissons, 1980). More recently, advances in offshore geomorphological mapping, through the use of bathymetric and seismic data, have allowed the identification of landforms associated with ice extension and retreat on the continental shelf of the Malin Sea (Arosio, et al., 2018b, Benetti, et al., 2010, Bradwell, et al., 2008, Callard, et al., 2018, Dove, et al., 2015, Dunlop, et al., 2010, Howe, et al., 2012, Ó'Cofaigh, et al., 2012, Ó Cofaigh, et al., 2019). The marine realm has provided a better characterization of the style of retreat and of the changes in ice streaming during deglaciation. The dating of glacial and glacially-derived landforms and sediments, in both marine and terrestrial settings, carried out as part of the NERC-funded BRITICE-CHRONO project, has more recently provided key datasets, which can allow a more refined chronological reconstruction of the MSIS and DBIS behaviour during the last glaciation. Many of these results including full details of age controls and their stratigraphic and landform contexts have been reported in a series of publications (Arosio, et al., 2018a, Callard, et al., 2018, Ó Cofaigh, et al., 2019, Schiele, 2017, Small, et al., 2017a, Small, et al., 2016, Tarlati, et al., 2020, Wilson, et al., 2019). In the context of BRITICE-CHRONO, these two components of the BIIS were referred to as Transect 6 for Donegal Bay and Transect 7 for the Malin Shelf (Fig. 1 inset). Here, these geochronological reconstructions are brought together for the first time including both the offshore and onshore data by (1) presenting the Bayesian analysis of all the geochronology, including radiocarbon, optically-stimulated luminescence and cosmogenic ages, (2) using Bayesian analysis to integrate all ages produced for these former ice streams; (3) providing isochrones of ice margin retreat and allowing calculation of rates of retreat for both ice streams; (4) exploring the changing dynamics with retreat including the separation of "Scottish" and "Irish" ice masses; and (5) assessing the interplay of forcing factors in regulating the pace of ice stream retreat and ultimately deglaciation.

2. DATA & METHODS

2.1 CONTEXT AND PUBLISHED AGES

Our aim was to constrain the timing of ice margin retreat for two adjacent marine-terminating sectors of the western BIIS. This challenge was met by compiling and extending an empirical dataset of quality-controlled absolute age measurements for the DBIS and the MSIS. The BRITICE-CHRONO approach was to use sites with good stratigraphical or geomorphological integrity and incorporate the age information within Bayesian chronosequence models for the differing ice streams or glaciers (e.g. Chiverrell et al., 2013). All published and new deglaciation ages are presented here for the DBIS and MSIS, with all ages subject to a triage system assessed according to quality criteria (Small, et al., 2017b), and here only ages deemed of good quality (green and amber) are included. A few pre-LGM ages (flagged as problematic in a quality assessment of the value of legacy ages for constraining deglaciation) (Small, et al., 2017b) were nonetheless used as indicators of previous ice-free conditions (Fig. 1; Table 6) (Bos, et al., 2004, Colhoun, et al., 1972, Jardine, et al., 1988). The new deglaciation ages include offshore radiocarbon (^{14}C) ages (Table 3) (Callard, et al., 2018, Ó Cofaigh, et al., 2019) and onshore terrestrial cosmogenic nuclide (TCN) ages (Table 4) (Schiele, 2017, Small, et al., 2017a, Wilson, et al., 2019) (see Fig. 1 for all locations). In addition, fifteen new optically-stimulated luminescence (OSL) ages have been obtained and are presented here for the first time (Table 1; Fig. 1). The OSL sites were selected targeting spatial gaps in the retreat sequences and to reassess sites yielding conflicting ages in the existing deglacial chronology for the region.

Details on the methods used to process all TCN and ^{14}C samples are reported in the relevant publications (see Tables 3 and 4 for references). The original ^{14}C measurements have been calibrated using OxCal 4.2, with for marine-derived samples the Marine-13 calibration curve and applying a marine reservoir correction of 0 years (Bronk Ramsey, 2009a, Reimer, et al., 2013). They are reported to two decimal places as cal. ka BP. ^{14}C ages were calibrated afresh using consistent marine C reservoir during the Bayesian modelling. Only ^{14}C ages representing latest glacial and deglaciation ages are included in this paper (i.e. not younger ones). Cosmogenic ages include ^{10}Be and ^{36}Cl exposure ages and, in the text, all TCN ages are rounded to the nearest 0.1 ka and shown with the ±1 sigma external uncertainty, unless otherwise stated. To be consistent across all BRITICE-Chrono publications, ^{10}Be ages presented here have been calculated using the calculator formerly known as the CRONUS-Earth calculator (Developmental version; Wrapper script 2.3, Main calculator 2.1, constants 2.2.1, muons 1.1; Balco, et al., 2008). ^{10}Be ages are calibrated using the Loch Lomond local production rate (LLPR: Fabel, et al., 2012, Small and Fabel, 2015) which is linked to direct independent age control provided by limiting radiocarbon ages (MacLeod, et al., 2011). All other Scottish calibration sites rely on an assumed Younger Dryas deglaciation age (Borchers, et al., 2016, Marrero, et al., 2016), assumed tephra age within a varve chronology (Small and Fabel, 2015), and a contested radiocarbon chronology (Lowe, et al., 2019, Putnam, et al., 2019). Variation between these different production rates change calculated ^{10}Be ages from 2.5% older to 6.3% younger compared to LLPR. For comparison we also provide the TCN ages calculated with the CRONUScalc v2.0 calculator (Marrero, et al., 2016)and using the global mean ^{10}Be production rate (Borchers, et al., 2016). The resulting ages using LLPR and the global production rate are statistically the same at 1 sigma (Tables 4 and 5). All ages are calculated assuming a rock surface erosion rate of 1mm ka^{-1} and the LM scaling method (Balco, et al., 2008). All details necessary to recalculate the TCN ages in Table 4 with different calculators, reference production rates, or scaling methods can be found in the original publications. Small, et al. (2017b) conveniently provides the legacy data, except for the two legacy ^{36}Cl ages for which there was insufficient information in the original publication. For individual locations multiple samples have been analysed typically, with the site repeatability tested using the reduced Chi-squared test (see Balco, et al., 2008, Heyman, et al., 2011, Small, et al., 2017a). After excluding outliers, the uncertainty weighted mean and associated uncertainties for exposure ages were calculated at each site.

2.2 OPTICALLY-STIMULATED LUMINESCENCE (OSL) DATING

Samples for OSL dating were collected from eight sites across the two transects targeting glacifluvial and deltaic outwash sands and gravels. All sites were selected based on their ice-proximal context and the potential to constrain the timing for well-defined ice margins (Fig. 1 and Table 2). OSL dating is underpinned by the principle that exposure to sunlight zeros or bleaches an OSL signal that develops within mineral grains (typically quartz or K-feldspar). The OSL signal increases with the duration of burial in sediments as the materials are exposed to natural radiation increasing the charge stored within quartz or feldspar. Here we use small aliquots (SA; ~20 grains) of sand-sized quartz grains separated from sediments to measure the OSL signal (Duller, 2008, Murray and Wintle, 2000). For samples that have been bleached heterogeneously, the measurement of multiple replicates (typically here ~50) can identify those grains exposed to sunlight most recently, which are referred to as a well bleached population. With heterogeneous-bleaching, statistical models are required to determine an accurate age, e.g. the Minimum Age Model (MAM) (Galbraith, et al., 1999) or the internal-external uncertainty (IEU) model (Thomsen, et al., 2007).

At all sites opaque tubes were hammered into sedimentary sections to prevent exposure to sunlight during sampling. The external gamma dose rates were determined using in-situ gamma spectrometry, with external beta dose rates calculated from U, Th, K and Rb concentrations determined by inductively coupled plasma mass spectrometry (ICP-MS). The sample preparation and analysis methods used were identical to existing studies (Bateman, et al., 2018, Evans, et al., 2017). Appropriate conversion factors (Guérin, et al., 2011, Guérin, et al., 2012) were applied to calculate the final total dose rate (Table 1) including grain size. The sites sampled all have water tables that are presently artificially low, owing to either coastal erosion or aggregate extraction. Maximum pore spaces in 180 – 250 µm sand are in the range between rhombohedral (26 %) and random (40 %) packing, which for moderately sorted rounded to sub-rounded sands equates to saturated water contents of around 30 %. In terms of palaeomoisture attenuation, contents of 23±5 % were used for shallow and drier samples and 27±5 % for deeper saturated samples.

OSL analyses were performed on the 180 – 250 µm size fraction (Table 2) and using aliquots each containing ~20 grains. The low proportion of quartz grains emitting an OSL signal for these samples suggests the OSL signal was dominated by few grains as has been the case elsewhere (e.g. Evans et al. 2017). All measured De distributions were asymmetrically distributed and display a high over-dispersion (OD; Table 2) confirming heterogeneous bleaching prior to burial. The D_e values used for age calculation (Table 2) target the well bleached component of these heterogeneously bleached D_e distributions and were identified by applying age models. Final D_e values for age calculation were calculated using as appropriate either the Minimum Age Model (MAM) (Galbraith et al., 1999) or the internal-external uncertainty (IEU) model (Thomsen, et al., 2007) with the parameters a and b used in the model determined from dose recovery tests (calculating the OD of the dose distribution at multiple given doses) for each site. Such an approach has been applied successfully to glacial sediments elsewhere in the BIIS (e.g. Bateman, et al., 2018).

2.3 BAYESIAN AGE MODELLING

Bayesian age modelling (Bronk Ramsey, 2008, Buck, et al., 1996) is an approach applied routinely to integrate sets of age measurements related typically by stratigraphy, for example ages from lake sediment sequences (Bronk Ramsey, 2008). The modelling refines the probability distributions for individual ages and is underpinned by the series of ages being presented as an order of events reasoned independently of the chronology, e.g., depth order. Increasingly the approach has been applied to spatially-distributed geochronological datasets, such as the retreat of glacial margins (e.g., Bradwell, et al., 2019, Chiverrell, et al., 2018, Chiverrell, et al., 2020, Chiverrell, et al., 2013). The deglaciation sequence for both the DBIS (T6) and MSIS (T7) evidenced in the onshore and offshore geomorphology provides a hypothetical 'relative-order' of dated events, which in the terminology for the Bayesian modelling is the Prior model (Bronk Ramsey, 2008, Buck, et al., 1996). The Bayesian Prior models for both ice streams were developed independently of the age information and included all the geochronological samples in the model structures (Bronk Ramsey, 2008, Bronk Ramsey, 2009a, Bronk Ramsey, 2009b, Bronk Ramsey and Lee, 2013). These Prior models cover the ice marginal retreat from maximum limits near the continental shelf breaks fronting DBIS and MSIS through a series of well-defined ice margin configurations identified on the seafloor and stepping-back on to land in Ireland and western Scotland (Callard, et al., 2018, Ó'Cofaigh, et al., 2012, Ó Cofaigh, et al., 2019, Peters, et al., 2015, Peters, et al., 2016, Small, et al., 2017a, Wilson, et al., 2019). The Bayesian analysis of the MSIS was not straightforward because of the interaction between the MSIS draining the main ice sheet divides and more local "Irish" ice that fed laterally into the ice stream. The recently mapped features in the Malin Sea provided the framework for the context of ice movement (Callard, et al., 2018).

The Bayesian modelling was coded using OxCal 4.3 (Bronk Ramsey and Lee, 2013) and applied uniform phase sequence models that were punctuated by boundaries located at well-defined ice limits. Markov Chain Monte Carlo (MCMC) sampling was used to build distributions of possible solutions, thereby generating modelling probabilities termed posterior density estimates for all measured ages and boundary limits. The probabilities are the product of the Prior model and the likelihood or measured age probabilities measured for each sample. Each sequence was divided into retreat zones that were coded as a Phase, defined as groups containing age information for sites sharing relationships with the adjacent zones. In the Bayesian analysis though TCN ages at some locations were consistent within a site and could be averaged using a reduced Chi-square statistic (χ^2_R) (Bevington and Robinson, 2003), here the ages were included individually but grouped within a Phase in the Prior model. Phases were delimited by a series of Boundary commands that generated modelled age probability distributions for major ice limits. Both Sequence models were run to assess outliers in time using a scaling of $10^0 – 10^4$ years and Student's t-distributions to describe the outlier distribution (Bronk Ramsey, 2009b). Iterations of the modelling were undertaken gradually varying the outlier probabilities for individual age determinations to achieve overall model agreement indices exceeding the >60% threshold advocated by Bronk Ramsey (2009a). Thereby outliers were given a probability scaling of $P < 0.2$, $P < 0.5$, $P < 0.75$ and $P = 1$ (100%) on a scale of increasing outlier severity. Dating bottlenecks in the Prior models were handled by increasing iteratively the outlier probability for all ages in selected Phases until the model produced overall agreement, which then calculates model agreement indices for all individual ages. Outlier ages were identified statistically, and then scrutinised for reasons that might explain the outlier behaviour either in the Prior model (e.g., the sample context) or in the measurement data (e.g., nuclide inheritance). Ages were not excluded arbitrarily but identified statistically and then weighted $P = 1$. Cycles of the Bayesian modelling then continued decreasing and increasing other less severe outlier probabilities for subsequent iterations until the overall model agreement was > 60%. Samples handled as outliers ($P = 1$; 100%) are detailed in later sections.

3. RESULTS AND INTERPRETATIONS

This section presents the new OSL age assessments from land areas adjacent to the DBIS and MSIS (Figs. 2-11; Tables 1 and 2). In addition, we summarise 71 radiocarbon ages from offshore glacial and glaciomarine sediments previously presented in (Schiele, 2017), (Callard, et al., 2018) and (Ó Cofaigh, et al., 2019); and 41 TCN ages already included in (Schiele, 2017), (Small, et al., 2017a), and (Wilson, et al., 2019); and the legacy ages published previously (Small, et al., 2017b) that have been included in the Bayesian age modelling. The ages presented here may differ slightly to original published owing to differences in exposure-age calculations and statistical treatments (e.g. evaluation using the LLPR; (Fabel, et al., 2012, Small and Fabel, 2015).

3.1 OFFSHORE GEOMORPHOLOGY AND DATING

The geology of the Malin Shelf is characterised by series of northeast trending troughs and basins, and basement blocks. Home to the former MSIS, these over-deepened troughs and basins interlink from the Sea of Hebrides to the mid-shelf and were likely major flow paths for ice streaming across the Malin Shelf from the Scottish Highlands and Ireland during past glacial periods (Davies, et al., 1984, Dobson and Whittington, 1992). Two basins, the Malin Deep and the trough of the Sea of Hebrides are separated by the Stanton Bank, a bedrock high at the centre of the inner Malin Shelf (Dobson and Whittington, 1992). For the former DBIS, the shelf offshore NW Ireland in the southern part of the Malin Sea has a smoother profile with a gentle gradient from the mouth of Donegal Bay to the shelf edge, with Donegal Bay having the characteristics of an over-deepened basin like those further to the north (Fig. 1).

For the former MSIS, the geomorphological evidence shows the presence of a compound ridge close to the shelf edge comprising a series of moraines and grounding-zone wedges (GZWs) mapped from 55°30'N to 56°30'N (Callard, et al., 2018, Dunlop, et al., 2010). Further to the north, a series of morainal banks with a similar N-S orientation have been broadly mapped from seismic data down to 150 m water depth and are likely to be the continuation of the same ice margin and to be related to the extension of the Outer Hebrides Ice Cap on the Scottish continental shelf (Bradwell, et al., This volume). Moraines of different orientations are observed at the boundary between the DBIS (T6) and MSIS (T7) on the Malin Shelf (trending respectively NW-SE and NE-SW; Figs. 1 inset, 13, 14) and it was suggested that they mark the retreat of the two ice streams in the direction of the inner Malin Shelf to the north and northern Donegal to the south (Benetti, et al., 2010, Dunlop, et al., 2010, Ó'Cofaigh, et al., 2012). In the inner part of the Malin Shelf series of smaller recessional moraines and GZWs step back eastwards and become increasingly abundant on the inner shelf, with De Geer moraines in the shallower waters of the sea-lochs and sounds, marking the pattern and direction of retreating ice (Dove, et al., 2015, Dunlop, et al., 2010, Small, et al., 2016). It has been suggested that, because of presence of the over deepened troughs, retreat from the shelf back towards the Inner Hebrides was likely rapid (Dove, et al., 2015), although previously estimated ice sheet retreat suggests that this process was slow (Clark, et al., 2012). For the DBIS, a set of arcuate, nested moraines extend across the entire continental shelf from within Donegal Bay to the shelf edge up to distance of 90 to 120 km from the coastline (Benetti, et al., 2010, Dunlop, et al., 2010, Ó'Cofaigh, et al., 2012), and they are indicative of grounded ice and a stepped glacial retreat across the shelf.

The dating of these glacial and glacially-derived landforms and sediments provides key datasets to support a more refined chronological reconstruction of the behaviour of the two ice streams during the last glaciation (Arosio, et al., 2018a, Callard, et al., 2018, Ó Cofaigh, et al., 2019, Tarlati, et al., 2020). Constraining a maximum extent of the BIIS across the Malin Sea has not been straightforward due to the presence of intense iceberg turbation at the shelf edge in correspondence with the margin of the MSIS at the shelf edge. However, the youngest radiocarbon ages obtained from shell fragments in subglacial diamicton constrains shelf edge glaciation to after 26.3 ka BP for both the MSIS and the DBIS (JC106-125VC and JC106-112VC in Table 3) (Callard, et al., 2018, Ó Cofaigh, et al., 2019). Retreat from the shelf edge has been dated using mixed foraminifera assemblages in glaciomarine muds between 26.3 and 23-24 ka BP and extensive iceberg scouring at the shelf edge across the entire margin of the Malin Sea indicate that it happened initially through intense calving. All foraminiferal and sedimentological data suggest that glaciomarine conditions prevailed during retreat. By 21 ka BP (i.e. global LGM; Clark, et al., 2009b, Hughes and Gibbard, 2015, Hughes, et al., 2013), most of the Malin Sea was free of grounded ice with glaciomarine conditions recorded offshore Tiree (JC106-149VC; Table 3) (Callard, et al., 2018) and a morainic complex of a similar age at the mouth of Donegal Bay (JC106-92VC and JC106-97VC; Table 3) (Ó Cofaigh, et al., 2019). Sedimentological evidence from the DBF suggest some marine extension of the BIIS until ~16.5 ka BP that allowed glaciomarine sediment deposition on the fan, with discrete episodes of calving recorded as peaks in ice-rafted debris (Tarlati, et al., 2020).

3.2 OSL GEOCHRONOLOGY

On the BRITICE-CHRONO project, the timing and pace of deglaciation in other sectors of the BIIS has been in part secured by optically-stimulated luminescence (OSL) dating of proglacial and ice-marginal sediments (Bateman, et al., 2018, Chiverrell, et al., 2018, Chiverrell, et al., 2020, Evans, et al., 2017, Small, et al., 2018, Smedley, et al., 2017a, Smedley, et al., 2017b). Here, we report sixteen new OSL ages, sampled between 2014 and 2016, from glacigenic sediments at eight terrestrial sites, three associated with DBIS and five from the north of Ireland constraining the MSIS (Tables 1-2). Exposures were logged using field sketches, vertical lithofacies logs and photo-montages following standard procedures (Evans and Benn, 2004, Thomas, et al., 2004). Other characteristics recorded included textural classifications, sorting and grain size, palaeocurrents or till fabric indicators, sedimentary structures, nature of contacts and the lithofacies.

3.2.1 OSL sites from the MSIS

OSL samples were collected from natural and quarried sediment exposures extending from in the west Altwinny Bay and Fawnmore (Co. Donegal) progressing west to east to Castleroe, Glenshesk Valley and Carey Valley in Co. Antrim, Northern Ireland (Fig. 1).

3.2.1.1 Altwinny Bay (55.1432 N, 8.2929 W)

A continuous coastal section is exposed at Altwinny Bay (Cullen, 2012), which is composed of sands, gravels and diamictons (Fig. 2). The sequence, from stratigraphically oldest to youngest comprises basal laminated gravels, sands, and fines, that interdigitate with largely massive gravels which are atop a weathered and granite bedrock that has been mobilised glacially. The massive gravels are interpreted as the product of ice-marginal debris flows, with the more stratified gravel, sand, and mud interbed units suggestive of deposition into a water body. Above this, there is a massive diamict containing evidence of deformation including sandy hydro-fractures injected from above. This in turn is capped by two over-consolidated matrix-supported diamicts displaying a strong clast orientation to the south and boulder pavements that suggest a subglacial origin. In the centre of the exposures these subglacial tills are capped by planar cross-stratified sands, which have flow directions to the south, probably reflecting outwash deposition with ice margin retreat. These sands appear to have been tilted and deformed suggesting proximity to and override by ice following deposition. The exposures are capped by a further series of matrix supported diamictons and finally a clast-supported massive gravel with some stratification that is associated either with later re-advance of ice and/or deposition as flow diamicts during ice retreat.

Cullen (2012) interpreted the sequence to record ice-marginal and glaciomarine debris flows from efflux jets draining ice from inland Donegal. That interpretation conflicts with the exposures observed in 2014, which show growth of the units in a southerly direction, flow directions to the southwest in the outwash sands, and lithologies of erratic clasts in the diamicts that are all consistent with an ice mass sourced from the Malin Sea rather than inland Donegal. Two OSL samples were collected T7ALTB01 (not measured) and T7ALTB02. T7ALTB01 was taken from a unit of horizontally stratified sand that forms the oldest water-lain deposits identified stratigraphically within the section (Fig. 2B). T7ALTB02 was taken from the youngest water-lain deposit in the sequence, which was composed of deformed (tilted) planar cross-stratified sands (Fig. 2F). These two samples were the most westerly onshore materials collected for the MSIS.

The asymmetric De distribution (Fig. 3A) derived for T7ALTB02 (Shfd15166) suggests heterogeneous bleaching prior to burial, and that a small proportion of the grains characterises the minimum dose population. The OSL age determined for T7ALTB02 30.4±4.9 ka is considered slightly old relative to the dating of shelf-break glaciation at 26.3 ka BP. That said, the stratigraphical position buried by > 8 m of diamicts shows over-ride by ice and the 30.4±4.9 ka could constrain the expansion of the MSIS to the coast of NW Donegal. Alternatively, this age, slightly old in the sequence, reflects potentially poor bleaching of the OSL signal, which would not be surprising given the relatively short sediment transport distances implicit in an ice contact setting.

3.2.1.2 Fawnmore (55.1536 N, 8.0329 W)

Located ~10.5 km east of Altwinny Bay, Fawnmore is a sand and gravel pit that has excavated an ice-marginal terrace at ~ 30 m I.O.D., and has potential to record the step back of the MSIS eastward along the north coastline of Co. Donegal. Two sections were examined in 2014 (Fig. 4). Section 1, although degraded, was composed of sand, gravel, and fine-grained units dipping to the southeast that were capped by a massive diamicton. The active workings of Section 2 displayed delta fore-set sands and gravels dipping towards the southeast. Original observations at Fawnmore (McCabe, 1995) suggest ice retreat to the south, however the southward delta progradation is more consistent with an ice source to the north. A view supported further by the presence of erratic clasts (e.g., basalt) sourced up-ice within the MSIS. Consequently, this deposit is interpreted as a delta deposited within a lake dammed by the left-lateral margin of the MSIS to the north. Three OSL samples were collected: T7FAWN01 sampling rippled fine to medium sand with fine laminations from section 1, and from section 2 horizontally stratified fine-medium sands (T7FAWN02) and fining upward couplets of rippled to horizontally laminated fine to medium sand (T7FAWN03). T7FAWN02 and T7FAWN03 were priorities for OSL because these were taken from better exposed sediments that are indicative of deposition as ice proximal delta fore-sets. Both samples yielded broad De distributions (Fig. 3D) suggestive of heterogeneous bleaching prior to burial, thus a small proportion of the grains probably characterises the minimum dose population. The OSL ages determined T7FAWN02 (Shfd15015) 25.8±4.2 ka and T7FAWN03 (Shfd15168) 27.1±3.7 ka are slightly old relative to the geochronology for adjacent zones. These ages show wide distributions reflective of the poor bleaching of the OSL signal, not unexpected given the relatively short sediment transport distances associated with a small ice proximal delta topset.

3.2.1.3 The Armoy moraine

Armoy moraine is a major glacigenic landform in the north of Ireland and forms a series of interlinked ridges hummocks and kettle-holes that extend discontinuously for 50 km between Articlave and Ballycastle (Figs. 1 inset, 13) (Knight, 2004, Knight, 2008a, Knight, 2008b). It is generally agreed that the moraine, given the orientation of its arcuate morphology, marks advance of ice from southwestern Scotland into Northern Ireland, but the timing is not well constrained. The samples collected at Castleroe, Glenshesk Valley and Carey Valley are all distributed along the length of, or immediately down ice from, the moraine. The objective was to constrain the timing of this ice incursion into the north of Ireland.

<u>Castleroe (55.0987 N, 6.6363 W):</u> Within the outwash sands and gravels immediately down ice from the Armoy moraine, 4 km southeast of Coleraine and west of the River Bann, a small dormant sand and gravel pit is set within an undulating bench of glacigenic sediments (Knight, 2004). The sections, when visited in September 2014, showed a fragmentary sequence of what are probably high-energy outwash sands and gravels beneath a massive diamicton containing occasional gravel layers. The sequence is then capped by a unit of clay-silt glaciolacustrine rhythmites containing occasional drop-stones (Fig. 5). Three samples were taken from the middle to lower part of the sequence within the outwash sands and gravels, with T7CAST01 highest in the sequence sampling horizontally stratified coarse sand). Towards the base of a >10 m thick sequence samples of planar cross stratified sands with fine laminations (T7CAST02) and rippled and planar cross set fine to

coarse sands with fine laminations (T7CAST03) were taken (Fig. 5). All three samples targeted appropriate lithofacies for OSL dating within the lower and middle part of the sequence, but unfortunately sand-rich facies did not feature within the uppermost glaciolacustrine unit.

Both samples yielded broad De distributions with T7CAST02 asymmetric (Fig. 3C) suggestive of heterogeneous bleaching prior to burial, thus a small proportion of the grains characterises the minimum dose population. The OSL age determined for T7CAST01 (Shfd15015) is too old at 48.1±4.8 ka and predates a younger sample that was taken from lower in the sequence. T7CAST01 sampled a thin sand unit within high energy gravel outwash lain down potentially in deep channels of back-bar gravel fore-sets, which may have limited the potential for re-setting of the OSL signal. The De distribution for T7CAST02 is slightly better behaved with a younger population of aliquots and yielded an age of 38.3±3.8 ka. Chronologically 38.3±3.8 ka predates the MSIS advance to the shelf break (Callard, et al., 2018), but the stratigraphical location of these samples beneath 6 m thick diamicts and evidence for deformation of the outwash sediments samples is intriguing. Taken at face value the T7CAST02 (Shfd15168) age of 38.3±3.8 ka may relate to an earlier advance of the ice sheet during the build up towards the LGM. These older glaciofluvial/deltaic sediments at Castleroe were then incorporated within the Armoy Moraine, with ice advance adding the diamict and the uppermost proglacial glaciolacustrine muds as a lake formed between the MSIS and inland 'Irish' ice. The alternative hypothesis is that the Castleroe outwash units are younger and relate to the most recent deglaciation, but where the OSL signals have not been reset for these samples.

<u>Glenshesk Valley (55.1447 N, 6.2211 W):</u> East of the Armoy Moraine and 7 km south from Ballycastle, Glenshesk is one of a series of valleys where water ponded when dammed by ice to the west at Armoy and in the north towards the coast at Ballycastle. Within the Glenshesk valley a set of broad and relatively flat drift surfaces occur, which are stratigraphically above glacigenic features (drumlinized till) associated with Irish ice (Knight, 2008a). These drift surfaces are believed to be associated with water flow and damming between Irish and Scottish ice and could only be deposited when Scottish sourced ice formed margins at the Armoy moraine (Knight, 2004). A small gravel pit within one of these surfaces reveals it to be composed of distal glaciofluvial sands and gravels, with the uppermost near-surface sequence showing sands capped by planar cross-stratified gravels. Two samples (T7GLEN01 and T7GLEN02) were collected from units of rippled medium sands (Fig. 6), both yielding asymmetric De distributions (Fig. 3E) suggestive of heterogeneous bleaching and a small minimum dose population. The De distribution for T7GLEN02 (Shfd15170) is better behaved and yields a younger age of 23.6±3.4 ka, with T7GLEN01 (Shfd15017) 30.4±4.2 ka probably too old. Both samples were lain down in similar environments and so the between sample differences in signal resetting probably simply reflect the heterogeneity of bleaching in these environments.

<u>Carey Valley</u> 55.1918 N, 6.1555 W: Further east still, the Carey Valley is ~6 km east of Ballycastle and ~2 km inland of the present coastline to the north. Situated down-ice from the most eastern end of the Armoy moraine, the valley contains a set of terraced flat-topped

surfaces that form a deltaic sequence, which has been subsequently incised. This sequence, which is described by McCabe and Eyles (1988), is composed of two lower diamictons separated by gravelly debris flows. The upper sequence comprises a classic Gilbert-type delta sequence of horizontal fine-grained silty bottom-sets, gently dipping gravel and sand fore-set beds, and planar massive top-set gravels (Fig. 7). These sediments were interpreted to reflect deposition into an open marine setting to the north (McCabe and Eyles, 1988). Given the high elevation of the deposit surface at 113 m above O.D. this seems unlikely and instead we suggest it was deposited within a lake dammed by Scottish ice at the Armoy Moraine near the coast. Two OSL samples were taken from the deltaic sequence, targeting horizontally stratified fine to medium sands in the bottom-set units (T7CARV01) and an upper sample (T7CARV02) from planar cross-stratified sand in the delta fore-sets. Both samples yielded broad and slightly asymmetric De distributions (Fig. 3B) suggestive of heterogeneous bleaching, but contain small minimum dose populations producing similar ages of 22.6±2.4 ka (T7CARV01: Shfd15169) and 22.1 ±2.4 ka (T7CARV02: Shfd15018).

Taken as a group these sites constraining the Armoy Moraine highlight the challenges of dating heterogeneously bleached materials, but the cluster of three OSL ages ranging 23.6±3.4 to 22.1±2.4 ka from Glenshesk and Carey Valley are in broad agreement. The OSL ages from Castleroe are interesting, but suboptimal in terms of their stratigraphical position and the youngest of the age measurements may instead constrain the build-up of regional ice to ~ 38.3±3.8 ka. Those sediments were perhaps deposited, and then later ridden over by MSIS ice and incorporated into the Armoy Moraine. Alternatively, given ~38.3±3.8 ka predates evidence for ice free conditions in western Scotland (Jardine, et al., 1988), potentially the OSL signal were not reset completely for those samples during the last depositional cycle.

3.2.2 OSL dating sites in the Donegal Mountains and flanking the DBIS

3.2.2.1 Lough Nacung (55.0405 N, 8.2132 W)

Located in the Donegal Mountains, the Gweedore Valley contains the Clady River which drains these uplands westwards to the coast near Bunbeg (Fig. 1). Immediately downstream of Lough Nacung and south of the Clady River, a large sand and gravel pit has been excavated into dome-shaped low valley-side hillocks at elevations of 93 m (Cullen, 2012). The setting is within the mountain interior of Donegal and glacigenic landforms therein are more likely to relate to the Donegal Ice Dome, though the exit to the valley reaches the coast between the DBIS (T6) and MSIS (T7). The exposures, visited in September 2014, comprised a Gilbert-type deltaic sequence of massive basal gravels, capped by steeply dipping sand- and gravel fore-sets, and capped by planar gravel top-sets (Fig. 8). The sequence has been interpreted by Cullen (2012) as subaqueous fan sediments capped by an ice-distal deltaic sequence. The apparent dip direction of the deltaic fore-sets suggests delta progradation toward the northwest. Deltaic sedimentation was likely within a lake dammed to the north and west by coalesced MSIS and DBIS ice masses and fed by ice sourced to the east in Poisoned Glen, Donegal Mountains. Two samples were collected from units of rippled medium sands (T6LNAC01) and rippled medium to coarse sands (T6LNAC02) located toward the top of the fore-sets. These samples potentially constrain sedimentation within a lake that could only have existed whilst ice was present to the northwest. Both samples yielded broad De distributions (Fig. 9C) suggestive of heterogeneous bleaching and contain a small minimum dose population. They produced ages of 109.4±8.4 ka (T6LNAC01: Shfd15173) and 132.0±10.5 ka (T6LNAC02: Shfd15014) that though similar do not overlap within uncertainties.

The ages for the Lough Nacung delta are substantially too old relative to the LGM shelf-break maxima for the MSIS and DBIS (Callard, et al., 2018, Peters, et al., 2015, Peters, et al., 2016). The lack of evidence for overriding by ice in the sequence in the form of deformation and disruption of the Gilbert-type delta poses questions about the Donegal ice dome. It seems implausible having ice margins at the shelf break and ice-free enclaves in the Donegal Mountains, and so a more likely explanation is poor resetting of the OSL signal in these uppermost fore-set sands of this ice proximal delta. TCN ages for three glacially transported granite boulders at Poisoned Glen ~8 km up ice from the delta produced a mean age of 16.9±0.7 ka and indicate that the Derryveagh Mountains (north Donegal) were largely deglaciated by ~18–17 ka (Wilson, et al., 2019). The relatively short sediment transport distances implicit in this ice proximal delta lend further support to the poor resetting of the OSL signal.

3.2.2.2 Glenulra (54.3023 N, 9.4330 W)

Located near the coast on the southern flanks of Donegal Bay, the exposures at Glenulra are a small aggregate pit and natural river-cut exposures in part incised probably by glacial meltwater. The exposures show a sequence cut into an ice contact delta with a surface at 80 m I.O.D. (Ballantyne and Ó Cofaigh, 2017, Hallissy, 1911, Hinch, 1913, McCabe, et al., 2007a). The sediments at Glenulra Quarry and Farm are an important site for the evolution of the Irish Ice Sheet, though the glaciological interpretation of the sequence and the chronology is equivocal (Ballantyne and Ó Cofaigh, 2017, McCabe, et al., 2007a). McCabe, et al. (2007a) described a sequence of basal high density gravelly flows, ~ 16 m of bedded muddy fine-grained units and sands, overlain by 5 m of dipping gravelly delta fore-sets prograding northwards onshore to offshore and capped by planar massive gravel delta top-set (Fig. 10). Marine fauna occur throughout, and have been ^{14}C dated by analysing mixture of reworked *Arctica islandica* shells from the basal gravels and gravel delta top-set, and *in situ* monospecific *Elphidium clavatum* from muds interpreted as glaciomarine in origin (McCabe, et al., 2007a).

Reconstructions of regional ice flows affecting the Glenulra area show ice generated in the mountains in the southern part of Co. Mayo extended north to Donegal Bay (Greenwood and Clark, 2009a, Greenwood and Clark, 2009b, Synge, 1963, Synge, 1965). Offshore in Donegal Bay, mapping of submarine landforms affirm the extension of ice northwards from land offshore including a late stage set of moraines extending from Killala Bay 20 km east of Glenulra (Fig. 14) (Ó'Cofaigh, et al., 2012), but moraines with geometries reflecting ice extending westwards from the Irish Midlands to the continental shelf break dominate and suggest that the DBIS came close to or impinged on the north coast of Mayo (Ó'Cofaigh, et al., 2012). McCabe, et al. (2007a) interpreted the Glenulra ^{14}C ages as reflecting high relative sea levels from 26 to 45 ka, perhaps discontinuously, but implying substantial isostatic depression. That would require the proximity and some persistence of a thick ice sheet for a significant period before the LGM. Fifteen ^{14}C ages have been obtained for the sequence, with the ages ranging from 21.1 ± 0.2 to 39.5 ± 0.5 ^{14}C ka BP. The eleven ages for reworked *Arctica islandica* shells can only provide maximal constraint on the sequence and the ages may predate reworking by millennia. Ballantyne and Ó Cofaigh (2017) summarise an alternative view that ice cover in Ireland was limited before 32 ka supported by ^{14}C dating of organic and faunal remains from various sites. Were the *Arctica islandica* shells found at Glenulra reworked from the sea floor in Donegal Bay, those ^{14}C ages imply ice-free conditions in those waters prior to any build-up of land-based ice and advance to shelf-break glaciation 27.8–27.6 ka (Ballantyne and Ó Cofaigh, 2017). The four ^{14}C ages for monospecific *Elphidium clavatum* from Glenulra form a tighter cluster spanning 23.7 ± 0.1 to 21.1 ± 0.2 ^{14}C ka BP and include the youngest ^{14}C age in the sequence. The ages for these foraminifera, if in situ, suggest also significant isostatic depression and proximity to a thick ice sheet 27.8–25.3 cal ka BP (McCabe, et al., 2007a). Given the timing for shelf-break glaciation presented here, the Glenulra ^{14}C ages suggest either i) the site was not run over by ice during the LGM advance requiring an implausibly thin DBIS, ii) there was preservation of the Glenulra deposits under the ice sheet, and iii) that all the ^{14}C ages are from reworked marine fauna and only provide maximal ages for the deposits (Ballantyne and Ó Cofaigh, 2017). The third scenario potentially still requires high relative sea levels (80 m OD) after 25.3 cal ka BP during deglaciation assuming the deposits are glaciomarine (Ballantyne and Ó Cofaigh, 2017), although a niche glaciolacustrine setting is an alternative hypothesis forming between the DBIS and local ice thereby receiving reworked glacimarine fauna. Regional striae patterns on the north Mayo coast (Smith, et al., 2008) point to the deflection of ice feeding the DBIS via Bunatrahir and Killala Bays towards the west and northwest.

To address some of these palaeoenvironmental and geochronological uncertainties, this key site was revisited to apply OSL dating to the uppermost deltaic sediments. In November 2014, the upper Glenulra Quarry (54.3023 N, 9.4330 W) sequence displayed the uppermost 3 m comprising a thin diamicton beneath gently dipping sand and gravel fore-sets that were in turn capped by a planar geometry gravelly delta top-set (Fig. 10). The exposures were restricted with talus and the patchy nature of aggregate extraction, but the dip to the uppermost fore-sets appeared to vary from a W to SW which differs to McCabe, et al. (2007a) who recorded a northerly dip to the fore-sets. A summary conclusion might be that the sediment efflux direction was variable, which supported in Geological Survey Ireland mapping showing a north-flowing down valley meltwater input, but also coast parallel west flowing meltwater channels feeding towards the Glenulra delta (Meehan, 2013). A DBIS origin to the sediment efflux provides a mechanism for the reworking of marine fauna. Two samples (T6GULR01, T6GULR02) were collected for OSL dating from rippled medium to fine sands with fine laminations. These sampled units are located from the top of the sequence within the gravelly topsets. Both samples constrain potentially sedimentation within either a small ice marginal lake or proglacial glaciomarine delta flanking Donegal Bay, with two OSL ages that overlap within uncertainties at 25.2±1.9 ka (T6GULR01:

Shfd15172) and 24.1±1.9 ka (T6GULR02: Shfd15012). Both samples yielded asymmetric De distributions (Fig. 9B) suggestive of heterogeneous bleaching, contain a small minimum dose population and are probably maximal ages for the delta. The youngest of these, 24.1±1.9 ka, slightly post-dates though overlaps within uncertainties the youngest of the Glenulra ^{14}C ages at 25.4±0.3 cal ka BP. Regardless, all the chronology from Glenulra is old relative to the DBIS retreat sequence, and we favour an interpretation that the fauna is ostensibly reworked, and that the delta developed as a niche lake ponded between DBIS and inland Irish ice with an active delta topset ~24.1±1.9 ka (T6GULR02: Shfd15012).

3.2.2.3 Brockhill (54.2782 N, 9.3964 W)

McCabe, et al. (1986) described an extensive area of glaciofluvial outwash deposits west of the drumlins in the low ground feeding towards Bunatrahir Bay. Located ~8 km southeast from Glenulra and ~3 km inland of the present coast, the aggregate pit at Brockhill is excavated into a flat drift surface that appears to forms an ice-contact delta with an ice margin located to the south. McCabe, et al. (1986) encountered in >20 m of vertical thickness of deposit with a basal 6-7 m comprising horizontally bedded and rippled sands delta toe-sets, ~ 13 m of massive to normally-graded matrix-supported gravel giving way to planar cross-bed sands, a delta fore-set unit, dipping broadly north, and the sequence is capped by ~1-2m of planar cobble and pebbly top-set gravels. In November 2014, at the time of sampling, only the upper half of the sequence was exposed showing sandy delta fore-sets capped by gravel delta topsets. Two samples were collected from the middle (T6BROC01) and top (T6BROC02) of the sandy fore-sets (Fig. 11). Both samples were collected from units of rippled fine to medium sands, with the aim of constraining the unzipping of ice retreating inland into Co. Mayo. Both samples yielded asymmetric De distributions (Fig. 9A) suggestive of heterogeneous bleaching, contain a small minimum dose population and produced ages of 44.4±4.1 ka (T6BROC01: Shfd15171) and paired small aliquot and single grain (SG) measurements for the second sample of 39.1±3.8 ka (T6BROC02: Shfd15013) and 45.8±8.2 ka (T6BROC02: Shfd15013-SG). There is no real evidence for subsequent overriding by ice, and so the most likely explanation is poor resetting of the OSL signal given the relatively short sediment transport distances implicit in this ice proximal delta.

3.3 SYNTHESIS OF PUBLISHED ONSHORE AGES

The Bayesian age modelling uses the new geochronological data obtained during the BRITICE-CHRONO project (Table 4) and already published (Schiele, 2017, Small, et al., 2017a, Wilson, et al., 2019), alongside clusters of previously published geochronological information at several onshore locations in Scotland and Ireland (Tables 5 and 6). These are predominantly TCN ages (Table 5) but include some radiocarbon ages from various organic material recovered in mostly glaciomarine sediments in coastal proximal settings (Table 6).

Legacy TCN research from before BRITICE-CHRONO includes the Bloody Foreland moraine and other sites in the Donegal and Ox mountains (Ballantyne, et al., 2007, Ballantyne and Ó Cofaigh, 2017, Clark, et al., 2009a). In Hebridean ice feeders towards the MSIS, other ages come from Arran, South Uist (Ballantyne and Small, 2018, Finlayson, et al., 2014, Small, et al., 2016, Stone and Ballantyne, 2006). BRITICE-CHRONO conducted a program of sampling at 12 suitable locations distributed across the two transects aiming to fill in gaps in the existing datasets or resolve issues with the previous dating (Fig. 1 for locations). Small, et al. (2017a) presented 17 ^{10}Be exposure ages from glacial boulders and bedrock at sites across western Scotland within the area drained by the MSIS. These TCN ages include measurements on Tiree, Mull, Jura, Mingulay and Barra. Wilson, et al. (2019) presented 20 new ^{10}Be and ^{36}Cl surface exposure ages from six sites in Donegal, including Malin Head, Rosguill, and Poisoned Glen in northern Donegal and Glencolumnbkille, Kilcar and Blue Stacks Mountains in southern Donegal, and Schiele (2017) worked on 4 ^{10}Be samples from Ben Bulben in Co. Sligo. Some TCN samples at the boundary between the two transects have used for ensuing Bayesian modelling in both transects (Table 7).

Overall, all these ages provide evidence of the timing of the BIIS first landfall across the Malin Sea and ensuing retreat further inland ultimately towards isolated mountain glaciers. Sites around the coastline of Donegal (including Malin Head, Bloody Foreland, Aran Island, Belderg Pier and Fiddauntawnanoneen; Tables 5-6) indicate that the ice margin around 20.5 ka, was at the Donegal and north Mayo coasts. In Scotland, ice landfall occurred first at Tiree at around the same time (20.6±1.2 ka) and slightly later in Mingulay (18.9±1.0 ka) on the Outer Hebrides. The TCN age at Malin Head were used alongside ^{14}C chronology from Corvish to suggest an early separation of Scottish-sourced ice and Donegal-sourced ice by ~20.7 ka (Wilson, et al., 2019). This implied that by this time a marine embayment extended eastward along the north coast of Donegal, separating ice flowing north and northeast from the Donegal Ice Centre from the retreating MSIS. The northern mountains of Donegal (Poisoned Glen and Errigal Col) were largely deglaciated by ~18-17 ka (Wilson, et al., 2019) . By 17.5-16.5 ka the ice margin straddled the fjords, islands and peninsulas of the western seaboard of Scotland, and the Outer Hebrides Ice Cap had shrunk to expose most of the southern Outer Hebridean islands (Small, et al., 2017a). In north Co. Mayo, the five younger ^{10}Be exposure ages from glacially transported boulders within the moraine system on the northern slopes of the Ox Mountains (Table 5) indicate that ice persisted in much or all Donegal Bay and covered south-west Donegal as late as 17 ka. By ~15.0 ka the Donegal Ice Centre had shrunk to a small ice cap or ice field of very limited extent on the Blue Stack Mountains (Wilson, et al., 2019).

3.4 BAYESIAN MODELS

Bayesian age modelling of all the dating control for both transects has calculated the timing for the advance and retreat of the DBIS and the MSIS (Figs. 12-14, 16; Table 7). Additional coastal and inland sites with organic remains dated to before the LGM and after deglaciation in both Scotland and Ireland were used to identify ice free conditions before and after the last glacial advance and are discussed in the next section in the context of the Bayesian models (Table 6). Ultimately both Bayesian analyses produced conformable age models with an overall agreement indices of 188% for the DBIS and 119% for the MSIS, both exceeding the >60 % threshold advocated by Bronk Ramsey (2009a). Iterative cycles of the Bayesian modelling varying the outlier probabilities led to the identification of the outlier ages shown on Fig. 12. Italics from now on denote the posterior density estimates or modelled ages derived from the Bayesian modelling to distinguish them from the unmodelled individual ages obtained for samples directly-dated.

3.4.1 Malin Sea Ice Stream

Basal constraint on the retreat model for the MSIS is provided by radiocarbon ages obtained for faunal remains and organic deposits in western Scotland denoting ice free conditions before the advances to LGM limits (Bos, et al., 2004, Brown, et al., 2007, Jardine, et al., 1988). At Sourlie on the Ayrshire coast (Fig. 13) in the inner feeder zone of the MSIS (Finlayson, et al., 2014, Finlayson, et al., 2010), organic pockets of sediment in cold-stage fluviatile sediments between two glacial diamictons yielded antler of *Rangifer tarandus* with the collagen extract dated to 29,900 ± 420 BP (SRR-3023) and plant debris dated to 29,290 ± 350 BP (SRR-3146) (Bos, et al., 2004, Jardine, et al., 1988). Support for ice free conditions in the hinterland of the MSIS is provided further east in central Scotland by equivalent organic-rich sediments at Balglass Burn, north of Glasgow (Brown, et al., 2007) spanning 39.8 – 32.8 ka BP. The Bayesian modelling (Fig. 12A) has produced modelled age probability distributions for ice dynamics in the MSIS sector. Organic sites in western Scotland show ice free conditions around *34.4 ± 1.8 ka* and provide maximum constraint on the build-up and extension of ice into the Malin Sea. In zone 1, on the outer shelf, the youngest ^{14}C ages on shells reworked into over consolidated diamicts (Callard, et al., 2018) constrain shelf break glaciation to *27.9 ± 2.2 ka* (BL0), before marine fauna in the softer overlying glacimarine diamict indicated rapid retreat to the zone 2 moraines by *26.3 ± 0.3 ka* (BL1; Fig. 13).

Decline of ice in the more open Malin Sea proceeded with an ice margin >120 km wide retreating east reaching BL2 at *23.5 ± 0.3*, BL3 at *22 ± 0.3* and BL4 at *21.2 ± 0.5 ka* (Fig. 13). Deglaciation of zone 2 vacated the Malin Deep (> -150 m) and the outer portion of the Hebrides Trough (> -150 m) to establish a series of grounding zone wedges and the BL2 ice margin east and landward of Stanton Banks. Glacimarine sediments in front of BL2 yielded basal ^{14}C ages ranging 23.2 ± 0.3 to 22.1 ± 0.3 ka BP and denote ice-free conditions on the inner Malin shelf by *23.5 ± 0.3 ka* (BL2). The constraint on BL3 is provided by TCN and OSL ages from northwest Donegal, with boulders on the Bloody Foreland and Malin Head peninsulas forming a coherent grouping. Two of the Bloody Foreland granite boulder ages were treated as outliers leaving seven consistent TCN ages. The OSL age from Altwinny Bay, notwithstanding the substantial uncertainty, is an outlier in this grouping, and the age of 30.4±4.9 ka (T7ALTB02) is intriguing given that the sand unit sampled was beneath thick diamict units, which reflects later over-riding by ice. It is feasible that the thin outwash predates ice advance and may be better positioned in zone 1 of the Bayesian sequence model. The deltaic deposits at Fawnmore, though on the face of it a little old, are given the wide uncertainties conformable with the Bayesian model. Together, these ages constrain zone 3 ice margin retreat to BL3 by *22 ± 0.3 ka*. BL4 is constrained by TCN ages from Tiree (inner Hebrides) and OSL ages from outwash draining into lakes ponded by Scottish ice impinging on the lowlands of the north of Ireland broadly at the Armoy Moraine (Knight, 2004, Knight, 2008a). Evidence of ice-free conditions from zone 4/5 marine core (149VC) is provided by a shell fragment in a soft diamicton dated to 20.2 ± 0.2 cal. ka BP (Callard, et al., 2018). These ages constrain BL4 at *21.2 ± 0.5 ka* (Fig. 13).

BL5 at *20 ± 0.3 ka* and BL6 at *19.5 ± 0.3 ka* (Fig. 13) describe the MSIS dividing into increasingly separate lobes with the ice margin in the Sea of Hebrides entering the fjord landscape of western Scotland and further south, Scottish ice extended across the North Channel impinging on the lowlands north of Ireland. The cluster of TCN ages from Rosguill document the retreat of ice margins from the outer headlands of the north of Ireland into the mountains of Donegal (Wilson, et al., 2019), and across the Malin Sea, TCN measurements from Mingulay (southern Outer Hebrides) (Small, et al., 2017a) are very similar in age. In the Bayesian model, the Rosguill and Mingulay clusters are conformable as a single grouping, though the overall model performance is better with Rosguill before Mingulay. The pragmatic interpretation is that the BL5 to BL6 limits were established between *20 ± 0.3 ka* and BL6 at *19.5 ± 0.3 ka* (Fig. 13). Boundary limits documenting the step back of increasingly separated ice lobes into the fjords of western Scotland and into the mountains of Donegal integrates evidence distributed across the Malin Sea. BL7 at *19 ± 0.3 ka* is constrained between TCN ages in the southern Outer Hebrides (Mingulay), and ^{14}C dated evidence of ice-free conditions at Corvish (Donegal) (McCabe and Clark, 2003). There is strong geographical spread to the age constraint on BL8 at *18.1 ± 0.7 ka* and BL9 at *14.9 ± 1.5 ka* (Fig. 13), and this is supported by an array of dated TCN sites on Mull, Jura, North Barra and Arran. The three ages treated as outliers within zone 9 were two TCN ages from Jura that Ballantyne, et al. (2014) had previously interpreted as too young owing to the probable burial of the boulders under a former cover of sediment and/or peat. Three more TCN ages obtained more recently from Jura included a further slightly young age (S3-Jura) (Small, et al., 2017a) and was also handled as an outlier. Together four of Jura TCN ages form a coherent set within the Bayesian model. Ultimate deglaciation of the western Scottish Highlands occurred by *14.3 ± 1.8 ka* (BL10) (Fig. 13).

3.4.2 Donegal Bay Ice Stream

There are fewer locations in the hinterland of the DBIS that constrain ice free conditions predating MIS 2 advances, though Colhoun, et al. (1972) described organic freshwater silts and fine sands at Derryvree (Co Fermanagh; Fig. 14) that nestled between two thick diamict sheets from a road-cut exposure of a drumlin (54.3031 N, 7.4411 W). The Derryvree cold stage organic deposits yielded an age of 30.5 ± 1.1 ^{14}C ka BP (Birm-166) and indicate ice free conditions (Colhoun, et al., 1972). Bayesian modelling indicates a maximum constraint on the build-up and extension of ice into Donegal Bay at *35.1 ± 3.2 ka* (pre-LGM ice free conditions; Figs. 12B; 14), in a similar age range to the western coastline of Scotland, further to the north (Bos, et al., 2004, Jardine, et al., 1988).

In zone 1 (Fig. 14), on the outer shelf, the youngest ^{14}C ages on shells reworked into over consolidated diamicts constrain shelf break glaciation to *26.6 ± 1.3 ka* (BL0) and the establishment of the shelf break moraine (BL1) at *26.3 ± 0.1 ka* (BL1). In zone 2, moving landwards, a series of ^{14}C ages from glacimarine muds constrain ice free conditions in the outer Donegal Bay across a series of arcuate sea floor moraines. These ^{14}C ages with the more landwards zone 3 chronology constrains BL2 to *22.9 ± 0.7 ka*. Zone 3 contains a series of nine ^{10}Be ages from Bloody Foreland (Clark, et al., 2009a, Wilson, et al., 2019) and two from Aran Island (Cullen, 2012, Wilson, et al., 2019) both in northwest Donegal. The location of these sites is marginal to both the DBIS and MSIS, and probably developed a suture between the two ice-masses with ice margin retreat. Two of the Bloody Foreland ages plot too young and were handled as outliers, with all the others forming a coherent grouping. These sites constrain deglaciation of the outer headlands and islands of northwest Donegal and correlate with BL3 ice margins in Donegal Bay to *20.5 ± 0.3 ka* (Fig. 14). Zone 4 comprises dating of ice-free conditions moving further east into Donegal Bay and a series of marine fauna ^{14}C dated on the north coast of County Mayo. Our attempt to date the uppermost deltaic deposits by OSL dating logically form part of this cluster but form a clear 'too old' outlier in the Bayesian model. The zone 4 chronology and bracketing ages in zone 5, constrain the BL4 limit to *19 ± 0.4 ka*. Interestingly, the modelling combines together ^{14}C ages from the Donegal Bay moraine complex and the Killala Bay moraines, thus suggesting that they are not statistically differentiated and therefore part of a single phase of the ice margin. Within this phase, it is possible that the Killala Bay moraines represent a rapid and short-lived advance of an ice tongue from the north Mayo coast due to de-buttressing of northward-flowing ice caused by retreat of the DBIS.

Zones 5-7 record the stepping back of ice margins from Donegal Bay into the flanking mountain regions in counties Donegal, Mayo, and Sligo. Zone 5 integrates dating information from typically the coastal fringe around the mountains of Donegal and includes six locations yielding eighteen TCN ages. These form a coherent grouping in the Bayesian model, with three of four ^{36}Cl ages from Kilcar too old and probably compromised by nuclide inheritance though the fourth age is consistent within that grouping. Elsewhere, one of three ^{10}Be ages from Poisoned Glen, north Donegal, appears too young and one of five ^{10}Be ages from Glencolumbkille, southwest Donegal (MAL-05: Ballantyne, et al., 2007, Wilson, et al., 2019). Together, these thirteen ages form a conformable group and constrain retreat of ice margins on-land into the mountains of Donegal by *16.8 ± 0.5 ka* (BL5). In zone 6, eight ^{10}Be ages came from the northern Ox Mountains, south of Donegal Bay, and were published originally by Clark, et al. (2009a). Later authors have rationalised the division of the ages into two clusters regarding the five younger ages (mean 16.6±0.6 ka) as better constraint on deglaciation, with the older cluster affected by nuclide inheritance (Ballantyne and Ó Cofaigh, 2017, Wilson, et al., 2019). These five ages form a conformable grouping and constrain retreat of ice margins further inland to the Ox Mountains and BL6 by *15.3 ± 0.6 ka.* Deglaciation of zone 7 of the DBIS is constrained by TCN ages from Eglish Valley in the Blue Stack Mountains and Binn Ghulbain (Ben Bulben) in County Sligo. These TCN ages form a broadly conformable set, with two of the Eglish Valley ages and two of Binn Ghulbain ages handled as outliers. In total, four TCN from the two localities indicate that by *13.9 ± 0.4 ka* (BL7) the mountains of the inner DBIS had deglaciated (Fig. 14).

4. DISCUSSION

The seafloor geomorphology (Benetti, et al., 2010, Bradwell, et al., 2008, Callard, et al., 2018, Dove, et al., 2015, Dunlop, et al., 2010, Howe, et al., 2012, Ó'Cofaigh, et al., 2012, Ó Cofaigh, et al., 2019) and terrestrial landforms in western Scotland, the north of Ireland and around Donegal Bay suggest the presence of former ice streaming across both the Malin Shelf and Donegal Bay (Clark, et al., 2012, Finlayson, et al., 2014, Finlayson, et al., 2010, Greenwood and Clark, 2009a, Greenwood and Clark, 2009b, McCabe, 2008). However, these two adjoining sectors of the former BIIS display clearly different characteristics and rates of retreat during the last glaciation and deglacial period (Figs. 13-16).

The MSIS had a wide ice margin (120 km; Fig. 13) that remained so as the ice retreated across the shelf. The shelf topography is characterised by pronounced areas of deeper water, with normal and adverse slopes corresponding to the major seabed troughs, including the Malin Deep and extensions of the Hebrides Trough (Fig. 16), both separated by the Stanton Banks bedrock high (Lewisian Gneiss) (Dobson and Whittington, 1992). The geomorphological features associated with ice margin retreat across this outer to mid shelf topography are complex systems of GZWs, while moraines and much smaller GZWs are found mostly in the inner shelf and close to the coastline and are much smaller in size (Callard, et al., 2018, Dove, et al., 2015, Dunlop, et al., 2010, Howe, et al., 2012). Conversely, the DBIS was less wide (ca 80 km) decreasing in width as the ice margin retreated landward and had a very gently normal-sloped bed (only the innermost part of the bay displays an adverse slope) and a distinct pattern of closely-spaced recessional moraines across the shelf (Benetti, et al., 2010, Ó Cofaigh, et al., 2019). Some lateral moraines (Fig. 14) exist in a position that suggest the presence of a distinct small ice lobe extending northwards into the bay at some stage during deglaciation (Benetti, et al., 2010, Ó Cofaigh, et al., 2019).

From ice free conditions in the hinterlands of the MSIS and DBIS ~33 ka (Colhoun, et al., 1972, Jardine, et al., 1988), glacial landforms and the presence of radiocarbon dated subglacial diamicts at the shelf edge show that between 28 and 26.5 ka the BIIS had grown to its maximum extent with ice grounded to the shelf edge (Fig. 16). Evidence across the continental shelf of the western BIIS suggests that this ice margin extended also north and south of the Malin Sea, following predominantly the shelf edge at 140 to 150 m (current) water depth from Northern Scotland to northern Porcupine Bank, with coalescing ice from Scotland and Ireland (Benetti, et al., 2010, Bradwell, et al., This volume, Ó Cofaigh, et al., This volume, Schiele, 2017). This recognition that the BIIS extended to the edge of the Malin Shelf led Wilson, et al. (2019) to suggest that the Donegal ice dome was of sufficient thickness to have buried all mountain summits. This hypothesis is supported by thermo-mechanical models of ice-sheet build-up and decay driven by proxy climate data (Hubbard, et al., 2009a) which predict thick cold-based ice over many summits. There is further support for these ice thicknesses elsewhere in Ireland (Ballantyne, et al., 2011, Ballantyne and Ó Cofaigh, 2017, Ballantyne and Small, 2018, Ballantyne and Stone, 2015), and demonstrations that the last ice sheet overtopped all mountain summits in northwest Scotland (Ballantyne and Small, 2018, Fabel, et al., 2012). This build-up of ice, from

Greenland Stadial (GS) 4 into the beginning of GS-3, occurs relatively early within the context of the global LGM and predated the maximum in global ice volume (Fig. 15). Variations in SST across the North Atlantic Ocean and variations in air temperature prior to the global LGM may indicate that changes in ocean and atmospheric circulation patterns that could have resulted in an increase in atmospheric moisture transport from the Equator to the Poles that is concomitant with a cooling at the northern latitudes favouring the accumulation of snow and ice (Clark, et al., 2009b, Hughes and Gibbard, 2015, Hughes, et al., 2013, Khodri, et al., 2001, Lambeck, et al., 2014). In the Malin Sea, shelf edge glaciation appears to be relatively short-lived. By 26.5 ka the ice sheet had already started to retreat from the shelf edge and extensive iceberg scouring at the shelf edge across the entire margin of the Malin Sea indicates that it happened initially through intense calving. This is also prior to the global LGM and occurred during cold conditions of GS-3. It is possible, as suggested by Ó Cofaigh, et al. (2019) and Callard, et al. (2018), that this early retreat was related to the growth of the BIIS and driven by local ice loading increasing water depths and promoting calving ice loss rather than by any changes in oceanic and atmospheric temperatures. This early retreat coincides with the timing of Heinrich event 2 and the increased flux of BIIS sourced IRD to the Donegal-Barra Fan at both MD04-2822 (Hibbert, et al., 2009) and MD05-2006 (Knutz, et al., 2001, Knutz, et al., 2002) (Fig. 15D).

After the maximum extension in Donegal Bay ~26.6 ka, the retreat and pullback of the DBIS margins across the outer shelf was occurring at a rate of ca. 20 m a-1. Subsequently, we observe a clear pattern of episodic retreat and then stabilisations of the ice margin each marked by a morainic ridge on the shelf; more than 25 such moraines can be counted across the Donegal Bay shelf and even more are visible in sub-surface geophysical data (Benetti, et al., 2010, Ó Cofaigh, et al., 2019). For the Malin Shelf in contrast an extensive GZW complex (zone 2: Fig. 13) is observed on the outer shelf for the entire width of the ice stream margin (Callard, et al., 2018). This outer portion of the MSIS displays one of the lower rates in retreat for the MSIS (18.7 m a^{-1}; Fig. 15B), and this is smaller than the retreat rate for the corresponding zone of the DBIS (Fig. 15A). The timing of formation of the GZWs in this zone is consistent with the reconstructed 600 to 1500 years for the deposition of GZWs during ice stream retreat in Antarctica prior to the Holocene (paleo-Pine Island ice stream) (Jakobsson, et al., 2012). After the initial retreat from the shelf edge, there is a switch in the relative magnitude of retreat rates and in the MSIS they are five to ten times faster than the DBIS (Fig. 15A vs. 15B). This could be related to the shape of the underlying bed. The Malin Shelf displays a clear reverse-sloping bed into the Malin Deep and Hebridean Trough (zones 3 and 5: Fig. 13), where we observe retreat rates of ~25-29 m a^{-1}, that could have contributed to an accelerated ice loss compared to the much more gently inclined DBIS bed (Fig. 15A). When grounding lines retreat onto reverse-sloped beds theoretical and numerical models predict that instability of the ice margin can be triggered by increases in ice thickness at the grounding line, which in turns favours an increase in ice flow across it. This mechanism, termed marine ice-sheet instability (MISI), has been advocated in explanations of the dynamics of many West Antarctic outlets (DeConto and Pollard, 2016, Favier, et al., 2014, Schoof, 2007). Whether the water depths are sufficient for MISI to have occurred in the Malin Sea remains to be tested. Overall, the rates of retreat across the margin at this time appear to be between 1.5 and 10 times slower than those of other ice streams of the former BIIS, Laurentide Ice Sheet, Fennoscandian Ice Sheet, and for Greenland Ice Sheet (Hughes, et al., 2012, Scourse, et al., This volume, Stokes, et al., 2014, Winsborrow, et al., 2010).

Foraminiferal and sedimentological data developed for the sector suggest that glaciomarine conditions prevailed during ice margin retreat across the Malin Shelf (Callard, et al., 2018). Across the entire ice front there is a distinct reduction in retreat rates once the margins reached constrictions in width at the headlands and islands of Donegal and Scotland; this is particularly the case in the mid-Malin Shelf (10 m a^{-1} in zone 4; Fig. 13) and outer Donegal Bay (2-5.4 m a^{-1} in zones 3/4; Fig. 14). Within this area, the Donegal Bay Moraine (zone 4; Fig 14) represents a major stillstand at 20.5 - 19 ka. The assessment here of ages developed for the Donegal Bay and Killala Bay moraines cannot be differentiated statistically (Fig. 12B) to distinguish the Killala Bay moraines as a temporally distinct readvance as previously suggested (Ó'Cofaigh, et al., 2012, Ó Cofaigh, et al., 2019). Instead, it is likely that all the moraines mapped within zone 4 (Fig. 14) were the product of oscillating ice positions from different source areas around Donegal Bay and formed around the same time. It appears likely that the Donegal and Mayo headlands and underlying bedrock highs visible in the sub-bottom data (Benetti, et al., 2010, Schiele, 2017) acted as shallow and constricted pinning points during the retreat thus slowing ice loss (Favier, et al., 2012) and favouring the formation of this moraine complex, at this time fed by entirely Irish-based ice, now a separate Donegal Ice Dome. In attempting to resolve the temporal linkages between MSIS and DBIS we highlight a less well resolved region between Malin Beg and Bloody Foreland, which occupies both the developing suture between the two ice streams during their respective maximum and later retreat. This sector is rendered even more complex by the growing influence of the ice dome over the Donegal mountains on the geomorphology. The exact timing of the separation of Scottish and Irish Ice in the Malin Sea is resolved for the first time here by the MSIS Bayesian model, which brackets it between 20 and 19.5 ka (Figs. 13; 16). Thus, separation of Scottish and Irish Ice in the Malin Sea occurs quite early during deglaciation, a feature not present in previous reconstructions; (see DATED: Hughes, et al., 2016). This timing of 20-19.5 ka coincides with equivalent data from the north Irish Sea basin showing the pullback of ice on land in northeast Ireland (Ballantyne and Ó Cofaigh, 2017, Chiverrell, et al., 2018, McCabe, 2008, McCabe, et al., 2007b). Here we show the reduced contributions of ice from the North Channel into the Irish Sea, which accords with evidence for an ice-free western Irish Sea and the margins of the Irish Sea Ice-stream positioned to the north of the Isle of Man receiving flows solely from SW Scotland (Galloway Hills Ice Dome) and the English Lake District by 20-19 ka (Chiverrell, et al., 2018, Scourse, et al., This volume). Ice persisted longer over Donegal Bay than on the Malin Shelf. Compared to the DBIS sector, the ice margin of the MSIS was still straddling the entire width of the Malin Shelf, through a series of deep troughs and smaller headlands (Fig. 13). By 20 ka, Tiree was already seaward of the ice margin, but the remainder of the Inner and Outer Hebrides were still glaciated. Rapid retreat in the Minch Trough between 20 – 18.5 ka and the drawdown of ice lead to Hebridean ice masses becoming glaciologically independent shortly before ~18.5 ka

(Bradwell, et al., This volume) and leading to the development of a separate Outer Hebrides Ice Dome (Small, et al., 2017a). A differential pattern of retreat developed to the northeast and southeast once the separation of MSIS and DBIS initiated, and the Outer Hebrides Ice Dome became independent. Seismic and bathymetric data behind Stanton Bank show a stepped retreat to the southeast between Tiree and Mull (Callard, et al., 2018) but that is not resolved in terms of timing by the BRITICE-CHRONO sampling.

Around 20 to 18.5 ka, the retreat of the MSIS was proceeding at a slightly slower pace of ~20 m a^{-1} compared to earlier retreat, and which may reflect stabilisation of ice margins at constricted fjord mouths of western Scotland. The net MSIS retreat rates are between 10-28 m a^{-1} throughout and do not vary much at all, so the changes in net pace are subtle. That said, there is better geomorphological evidence for pinning and stabilisation points, for example the larger GZWs and moraines, so the actual pace of retreat may have included faster and slower episodes not resolved by the net axial ice margin retreat rate data that emerges from the Bayesian age modelling. This is a pattern of retreat observed commonly in marine-based paleo-ice streams (Bradwell, et al., This volume, Jakobsson, et al., 2012, Larter, et al., 2009, Newton and Huuse, 2017, Ottesen, et al., 2005, Shaw, et al., 2006, Winsborrow, et al., 2010). Between 21 and 15.4 ka, the reduction in the flux of subglacially-derived material, measured using radiogenic Pb isotope data, to the continental shelf is interpreted as the result of the break-up of the ice-stream in western Scotland (Arosio, et al., 2018a) and glaciomarine conditions are still indicated in the shelf sediments around the Scottish coastline (Callard, et al., 2018). Sedimentological evidence from the Donegal-Barra Fan suggests some marine extension of the BIIS until as late as ~16.5 ka that allowed glaciomarine sediment deposition on the fan, with discrete episodes of calving recorded as peaks in ice-rafted debris between 18 and ~16.5 ka (Tarlati, et al., 2020).

Between 19 and ~16.8 ka, an increase in retreat rate, from an average of around 3.7 to 25 m a^{-1}, is however observed in the inner part of Donegal Bay (Zone 5; Fig. 14), inshore of the extensive Donegal Bay and Killala Bay moraine complex that occupies the outer bay. At this location, the reverse sloped bed (Fig. 15B) is likely to have accelerated through MISI processes (DeConto and Pollard, 2016, Favier, et al., 2014, Schoof, 2007). The overall driver, beyond instability, of retreat at this stage is unclear as it is happening within Greenland Stadial 2 (GS-2) and therefore atmospheric warming is unlikely to be a significant control (Fig. 15). Lack of significant change in foraminifera assemblages across the Malin Sea also suggest that the final stages of deglaciation were not likely driven by changes in sea temperature but more probably by local sea level changes and / or thinning of the ice sheet. This is supported by modelled water depths for the inner and outer MSIS derived from a glacio-isostatic adjustment model (Bradley, et al., 2011) rerun to account for the ice thicknesses from the latest BRITICE-CHRONO ice sheet reconstruction and accounting for global ice sheet variations (Fig. 15A-B). This suggests maximum water depths occurred at 20-16 ka in the later part of GS-2. Retreat to a fully terrestrially-based Donegal Ice Dome occurred within 1-1.5 ka after 16.8 ka and corresponds with the timing of Heinrich event 1. Deglaciation at low ground around Donegal Bay was widespread by 15.3 ka when ice free conditions are also recorded in the Ox Mountains (zones 6 & 7, Fig. 14).

5. CONCLUSIONS

New OSL ages combined with Bayesian modelling of legacy and BRITICE-CHRONO ages along with consideration of their stratigraphic and landform contexts has allowed us to reconstruct ice advance to the continental shelf edge and withdrawal from here and back across the marine to terrestrial transition (Fig. 16). We summarise the main aspects and the coastal and inland radiocarbon ages show that Donegal and Scotland were ice free at low elevations around 34-35 ka. However, by 27.9-26.6 ka the BIIS had reached its maximum extent reaching the shelf break of the Malin Sea extending distances of ~190 km from the Donegal and ~280 km from the Scottish coastlines. Geomorphological and sedimentological evidence in the form of subglacial diamict, moraines and grounding zone wedges show a continuous ice margin developed at the shelf edge, fed by ice flow from two confluent ice streams, the Malin Sea and the Donegal Bay ice streams. Bayesian modelling of the geochronology shows that retreat from maximum started synchronously along the entire shelf edge of the Malin Sea by 26.3 ka. Compared with the onset of ice retreat globally this is surprisingly early. The Malin Sea Ice Stream retreated at a rate of ~19 m a^{-1} and the Donegal Bay Ice Stream at ~20 m a^{-1} both across the outer shelf between 26.3 and 22.5-23 ka. The outer shelf GZWs in the northern part of the Malin Sea and recessional moraines in the southern part, offshore NW Ireland, indicate that episodic retreat was separated by still-stand or oscillation of the ice margins. The Bayesian modelling struggles to resolve the duration of still-stands, but the scale of the landforms suggests some persistence of the ice margins at these locations.

By 23-22 ka the outer shelf (an area of about ~25,000 km^2) was already free of grounded ice and ice margin retreat continued at a slower net rate across mid-shelf between 23.5 and 20.5 ka, with the ice margin sitting across the central Malin Sea, near the NW Irish coastline, and across the outer part and mouth of Donegal Bay. The separation between Irish-based and Scottish-based ice seems to have occurred just after this time around 20-19.4 ka, leaving behind an autonomous ice dome over the uplands of Donegal. Thereafter, mass loss of ice on the inner Malin shelf was focussed along major submarine troughs and took place over the ensuing two thousand years at a net rate of 16-27 m a^{-1} with an ice margin positioned close to the present coastline within the Sea of Hebrides at 19ka. In Donegal Bay retreat during this time was punctuated by still-stands building moraines and retreat occurred at a much slower pace of 2 - 5.4 m a^{-1}. The Donegal Bay and Killala Bay moraines at the mouth of the bay record a major ice margin stillstand between 20.5 and 19 ka, with the moraines of different orientations suggesting oscillating ice positions driven by different source areas around Donegal Bay. Once the ice margin started retreating further from this position, the rate of retreat drastically accelerated to 25 m a^{-1}, likely due to the reverse-slope bed in the inner part of the bay. By 17 - 16 ka ice had retreated onto land and may have persisted as isolated ice caps in both Scotland and Ireland at least until ca 14.9-13.9 ka.

Our chronologically-constrained reconstruction suggests that the early retreat of the marine-terminating western margin of the BIIS was initially driven by local ice loading that increased water depths promoting ice losses by calving, rather than forcing by rises in ocean and atmospheric temperatures. Retreat from the mid-shelf to the coastline proceeded at differing paces between ice-streams and was affected by the presence of topographic controls, including pinning points at underlying bedrock outcrops and constrictions between coastal headlands of Scotland and Ireland, and by the presence of reverse-slope beds underneath portions of the ice streams. Thinning of the ice sheet could have also driven the onset of stages comprising relatively more rapid retreat close to the coastlines of Ireland and Scotland. The timing and rates of retreat for the two ice streams seem largely unrelated to global atmospheric and oceanographic changes, except for the final stage transition into ice-free conditions before 14-13 ka.

Acknowledgements

This research was funded by the UK Natural Environment Research Council consortium grant NE/J007196/1 BRITICE-CHRONO. The work was supported by the NERC Radiocarbon Facility and NERC Cosmogenic Isotope Facility Analysis. Thanks to the staff at the SUERC AMS Laboratory, East Kilbride for carbon isotope measurements. We thank the officers and crew of the RRS James Cook for their assistance with data acquisition, as well as the British Geological Survey and UK National Oceanography Centre for vibro- and piston core collection respectively, during cruise JC106. Also thanks to the entire BRITICE-CHRONO consortium for fruitful discussions over the duration of the project and the two anonymous reviewers for their constructive comments.

References

Arosio R, Crocket KC, Nowell GM, Callard SL, Howe JA, Benetti S, Fabel D, Moreton S, Clark CD. 2018a. Weathering fluxes and sediment provenance on the SW Scottish shelf during the last deglaciation. Marine Geology **402**: 81-98. DOI: 10.1016/j.margeo.2017.08.017

Arosio R, Dove D, Ó Cofaigh C, Howe JA. 2018b. Submarine deglacial sediment and geomorphological record of southwestern Scotland after the Last Glacial Maximum. Marine Geology **403**: 62-79. DOI: 10.1016/j.margeo.2018.04.012

Balco G, Stone JO, Lifton NA, Dunai TJ. 2008. A complete and easily accessible means of calculating surface exposure ages or erosion rates from 10Be and 26Al measurements. Quaternary Geochronology **3**: 174-195. DOI: 10.1016/j.quageo.2007.12.001

Ballantyne CK. 1989. The Loch Lomond Readvance on the Isle of Skye, Scotland: Glacier reconstruction and palaeoclimatic implications. Journal of Quaternary Science **4**: 95-108. DOI: 10.1002/jqs.3390040201

Ballantyne CK, McCarroll D, Stone JO. 2007. The Donegal ice dome, northwest Ireland: Dimensions and chronology. Journal of Quaternary Science **22**: 773-783

Ballantyne CK, McCarroll D, Stone JO. 2011. Periglacial trimlines and the extent of the Kerry-Cork Ice Cap, SW Ireland. Quaternary Science Reviews **30**: 3834-3845. DOI: 10.1016/j.quascirev.2011.10.006

Ballantyne CK, Ó Cofaigh C. 2017. The last Irish Ice Sheet: extent and chronology. In *Advances in Irish Quaternary Studies*. Springer; 101-149.

Ballantyne CK, Small D. 2018. The Last Scottish Ice Sheet. Earth and Environmental Science Transactions of the Royal Society of Edinburgh **110**: 93-131. DOI: 10.1017/s1755691018000038

Ballantyne CK, Stone JO. 2015. Trimlines, blockfields and the vertical extent of the last ice sheet in Southern Ireland. Boreas **44**: 277-287. DOI: 10.1111/bor.12109

Ballantyne CK, Wilson P, Gheorghiu D, Rodés À. 2014. Enhanced rock-slope failure following ice-sheet deglaciation: timing and causes. Earth Surface Processes and Landforms **39**: 900-913. DOI: 10.1002/esp.3495

Bateman MD, Evans DJA, Roberts DH, Medialdea A, Ely J, Clark CD. 2018. The timing and consequences of the blockage of the Humber Gap by the last British−Irish Ice Sheet. Boreas **47**: 41-61. DOI: 10.1111/bor.12256

Benetti S, Dunlop P, Ó'Cofaigh C. 2010. Glacial and glacially-related features on the continental margin of northwest ireland mapped from marine geophysical data. Journal of Maps **2010**: 14-29

Bennett MR, Boulton GS. 1993. Deglaciation of the younger dryas or Loch Lomond Stadial ice-field in the northern Highlands, Scotland. Journal of Quaternary Science **8**: 133-145. DOI: 10.1002/jqs.3390080206

Berger A, Loutre MF. 1991. Insolation values for the climate of the last 10 million years. Quaternary Science Reviews **10**: 297-317. DOI: 10.1016/0277-3791(91)90033-Q

Bevington PR, Robinson DK. 2003. Data reduction and error analysis for the physical sciences. McGraw-Hill: Boston, Mass. ; London

Bintanja R, van de Wal RSW, Oerlemans J. 2005. Modelled atmospheric temperatures and global sea levels over the past million years. Nature **437**: 125-128

Bond G, Heinrich H, Broecker W, Labeyrie L, McManus J, Andrews J, Huon S, Jantschik R, Clasen S, Simet C, Tedesco K, Klas M, Bonani G, Ivy S. 1992. Evidence for massive discharges of icebergs into the North Atlantic ocean during the last glacial period. Nature **360**: 245-249

Borchers B, Marrero S, Balco G, Caffee M, Goehring B, Lifton N, Nishiizumi K, Phillips F, Schaefer J, Stone J. 2016. Geological calibration of spallation production rates in the CRONUS-Earth project. Quaternary Geochronology **31**: 188-198. DOI: 10.1016/j.quageo.2015.01.009

Bos JAA, Dickson JH, Coope GR, Jardine WG. 2004. Flora, fauna and climate of Scotland during the Weichselian Middle Pleniglacial – palynological, macrofossil and coleopteran investigations. Palaeogeography, Palaeoclimatology, Palaeoecology **204**: 65-100. DOI: 10.1016/s0031-0182(03)00724-7

Boulton G, Hagdorn M. 2006. Glaciology of the British Isles Ice Sheet during the last glacial cycle: form, flow, streams and lobes. Quaternary Science Reviews **25**: 3359-3390. DOI: 10.1016/j.quascirev.2006.10.013

Boulton GS. 1990. Sedimentary and sea level changes during glacial cycles and their control on glacimarine facies architecture. Glacimarine environments: processes and sediments: 15-52

Bradley SL, Milne GA, Shennan I, Edwards R. 2011. An improved glacial isostatic adjustment model for the British Isles. Journal of Quaternary Science **26**: 541-552. DOI: 10.1002/jqs.1481

Bradwell T, Fabel D, Clark C, Chiverrell RC, Small D, Smedley RK, Saher M, Moreton S, Dove D, Callard SL, Duller GAT, Medialdea A, Bateman MB, Burke MJ, McDonald N, Gilgannon S, Morgan S, Roberts DH, Ó Cofaigh C. This volume. Pattern, style and timing of British-Irish Ice Sheet advance and retreat over the last 45,000 years: evidence from NW Scotland and the adjacent continental shelf. Journal of Quaternary Science:

Bradwell T, Small D, Fabel D, Clark CD, Chiverrell RC, Saher MH, Dove D, Callard SL, Burke MJ, Moreton SG, Medialdea A, Bateman MD, Roberts DH, Golledge NR, Finlayson A, Morgan S, Cofaigh CÓ. 2019. Pattern, style and timing of British–Irish Ice Sheet retreat: Shetland and northern North Sea sector. Journal of Quaternary Science. DOI: 10.1002/jqs.3163

Bradwell T, Stoker MS, Golledge NR, Wilson CK, Merritt JW, Long D, Everest JD, Hestvik OB, Stevenson AG, Hubbard AL, Finlayson AG, Mathers HE. 2008. The northern sector of the last British Ice Sheet: Maximum extent and demise. Earth-Science Reviews **88**: 207-226. DOI: 10.1016/j.earscirev.2008.01.008

Bronk Ramsey C. 2008. Deposition models for chronological records. Quaternary Science Reviews **27**: 42-60. DOI: 10.1016/j.quascirev.2007.01.019

Bronk Ramsey C. 2009a. Bayesian analysis of radiocarbon dates. Radiocarbon **51**: 337-360

Bronk Ramsey C. 2009b. Dealing with outliers and offsets in radiocarbon dating. Radiocarbon **51**: 1023-1045

Bronk Ramsey C, Lee S. 2013. Recent and Planned Developments of the Program Oxcal. Radiocarbon **55**: 720-730

Brown EJ, Rose J, Coope RG, Lowe JJ. 2007. An MIS 3 age organic deposit from Balglass Burn, central Scotland: palaeoenvironmental significance and implications for the timing of the onset of the LGM ice sheet in the vicinity of the British Isles. Journal of Quaternary Science **22**: 295-308. DOI: 10.1002/jqs.1028

Buck CE, Cavanagh WG, Litton CD. 1996. Bayesian Approach to Interpreting Archaeological Data:

Callard SL, Cofaigh CÓ, Benetti S, Chiverrell RC, Van Landeghem KJJ, Saher MH, Gales JA, Small D, Clark CD, Livingstone SJ, Fabel D, Moreton SG. 2018. Extent and retreat history of the Barra Fan Ice Stream offshore western Scotland and northern Ireland during the last glaciation. Quaternary Science Reviews **201**: 280-302. DOI: 10.1016/j.quascirev.2018.10.002

Chiverrell RC, Smedley RK, Small D, Ballantyne CK, Burke MJ, Callard SL, Clark CD, Duller GAT, Evans DJA, Fabel D, van Landeghem K, Livingstone S, Ó Cofaigh C, Thomas GSP, Roberts DH, Saher M, Scourse JD, Wilson P. 2018. Ice margin oscillations during deglaciation of the northern Irish Sea Basin. Journal of Quaternary Science. DOI: 10.1002/jqs.3057

Chiverrell RC, Thomas GSP, Burke M, Medialdea A, Smedley R, Bateman M, Clark C, Duller GAT, Fabel D, Jenkins G, Ou X, Roberts HM, Scourse J. 2020. The evolution of the terrestrial-terminating Irish Sea glacier during the last glaciation. Journal of Quaternary Science. DOI: 10.1002/jqs.3229

Chiverrell RC, Thrasher IM, Thomas GSP, Lang A, Scourse JD, van Landeghem KJJ, McCarroll D, Clark CD, Ó'Cofaigh C, Evans DJA, Ballantyne CK. 2013. Bayesian modelling the retreat of the Irish Sea Ice Stream. Journal of Quaternary Science **28**: 200-209. DOI: 10.1002/jqs.2616

Clark CD, Evans DJA, Khatwa A, Bradwell T, Jordan CJ, Marsh SH, Mitchell WA, Bateman MD. 2004. Map and GIS database of glacial landforms and features related to the last British Ice Sheet. Boreas **33**: 359-375. DOI: 10.1111/j.1502-3885.2004.tb01246.x

Clark CD, Hughes ALC, Greenwood SL, Jordan C, Sejrup HP. 2012. Pattern and timing of retreat of the last British-Irish Ice Sheet. Quaternary Science Reviews **44**: 112-146. DOI: 10.1016/j.quascirev.2010.07.019

Clark CD, Ely JC, Greenwood S.L, Hughes ALC, Meehan R, Barr I.D, Bateman MD, Bradwell T, Doole J, Evans DJA, Jordan CJ, Monteys X, Pellicer XM, Sheehy M. 2018. BRITICE Glacial Map, version 2: a map and GIS database of glacial landforms of the last British–Irish Ice Sheet. Boreas **47**: 11-27. DOI 10.1111/bor.12273.

Clark J, McCabe AM, Schnabel C, Clark PU, McCarron S, Freeman SPHT, Maden C, Xu S. 2009a. Cosmogenic 110Be chronology of the last deglaciation of western Ireland, and implications for sensitivity of the Irish ice sheet to climate change. Bulletin of the Geological Society of America **121**: 3-16

Clark PU, Dyke AS, Shakun JD, Carlson AE, Clark J, Wohlfarth B, Mitrovica JX, Hostetler SW, McCabe AM. 2009b. The Last Glacial Maximum. Science **325**: 710-4. DOI: 10.1126/science.1172873

Colhoun EA, Dickson JH, McCabe AM, Shotton FW. 1972. A Middle Midlandian freshwater series at Derryvree, Maguiresbridge, County Fermanagh, Northern Ireland. Proceedings of the Royal Society of London. Series B. Biological Sciences **180**: 273-292. DOI: 10.1098/rspb.1972.0018

Cullen C. 2012. Deciphering the geomorphic and sedimentary record of the last Irish Ice Sheet in NW Donegal, Ireland: implications for glacial dynamics and decay configurations. In *Geography and Archaeology*. National University of Ireland, Galway: NUI Galway; 434.

Davies HC, Dobson MR, Whittington RJ. 1984. A revised seismic stratigraphy for Quaternary deposits on the inner continental shelf west of Scotland between 55°30‘N and 57°30’N. Boreas **13**: 49-66. DOI: 10.1111/j.1502-3885.1984.tb00059.x

DeConto RM, Pollard D. 2016. Contribution of Antarctica to past and future sea-level rise. Nature **531**: 591-597. DOI: 10.1038/nature17145

Dietze M, Kreutzer S, Burow C, Fuchs MC, Fischer M, Schmidt C. 2016. The abanico plot: Visualising chronometric data with individual standard errors. Quaternary Geochronology **31**: 12-18. DOI: 10.1016/j.quageo.2015.09.003

Dobson MR, Whittington RJ. 1992. Aspects of the geology of the Malin Sea area. Basins on the Atlantic seaboard: 291-311

Dove D, Arosio R, Finlayson A, Bradwell T, Howe JA. 2015. Submarine glacial landforms record Late Pleistocene ice-sheet dynamics, Inner Hebrides, Scotland. Quaternary Science Reviews **123**: 76-90. DOI: 10.1016/j.quascirev.2015.06.012

Duller GAT. 2008. Single-grain optical dating of Quaternary sediments: why aliquot size matters in luminescence dating. Boreas **37**: 589-612

Dunlop P, Shannon R, McCabe M, Quinn R, Doyle E. 2010. Marine geophysical evidence for ice sheet extension and recession on the Malin Shelf: New evidence for the western limits of the British Irish Ice Sheet. Marine Geology **276**: 86-99. DOI: 10.1016/j.margeo.2010.07.010

Evans DJA, Bateman MD, Roberts DH, Medialdea A, Hayes L, Duller GAT, Fabel D, Clark CD. 2017. Glacial Lake Pickering: stratigraphy and chronology of a proglacial lake dammed by the North Sea Lobe of the British-Irish Ice Sheet. Journal of Quaternary Science **32**: 295-310. DOI: 10.1002/jqs.2833

Evans DJA, Benn DI. 2004. A Practical Guide to the Study of Glacial Sediments. A Practical Guide to the Study of Glacial Sediments:

Fabel D, Ballantyne CK, Xu S. 2012. Trimlines, blockfields, mountain-top erratics and the vertical dimensions of the last British-Irish Ice Sheet in NW Scotland. Quaternary Science Reviews **55**: 91-102. DOI: 10.1016/j.quascirev.2012.09.002

Favier L, Durand G, Cornford SL, Gudmundsson GH, Gagliardini O, Gillet-Chaulet F, Zwinger T, Payne AJ, Le Brocq AM. 2014. Retreat of Pine Island Glacier controlled by marine ice-sheet instability. Nature Climate Change **4**: 117-121. DOI: 10.1038/nclimate2094
Favier L, Gagliardini O, Durand G, Zwinger T. 2012. A three-dimensional full Stokes model of the grounding line dynamics: effect of a pinning point beneath the ice shelf. The Cryosphere **6**: 101-112. DOI: 10.5194/tc-6-101-2012
Finlayson A, Fabel D, Bradwell T, Sugden D. 2014. Growth and decay of a marine terminating sector of the last British–Irish Ice Sheet: a geomorphological reconstruction. Quaternary Science Reviews **83**: 28-45. DOI: 10.1016/j.quascirev.2013.10.009
Finlayson A, Merritt J, Browne M, Merritt J, McMillan A, Whitbread K. 2010. Ice sheet advance, dynamics, and decay configurations: evidence from west central Scotland. Quaternary Science Reviews **29**: 969-988. DOI: 10.1016/j.quascirev.2009.12.016
Galbraith RF, Roberts RG, Laslett GM, Yoshida H, Olley JM. 1999. Optical dating of single and multiple grains of quartz from Jinmium rock shelter, northern Australia: Part I, experimental design and statistical models. Archaeometry **41**: 339-364. DOI: 10.1111/j.1475-4754.1999.tb00987.x
Greenwood SL, Clark CD. 2009a. Reconstructing the last Irish Ice Sheet 1: changing flow geometries and ice flow dynamics deciphered from the glacial landform record. Quaternary Science Reviews **28**: 3085-3100. DOI: 10.1016/j.quascirev.2009.09.008
Greenwood SL, Clark CD. 2009b. Reconstructing the last Irish Ice Sheet 2: a geomorphologically-driven model of ice sheet growth, retreat and dynamics. Quaternary Science Reviews **28**: 3101-3123. DOI: 10.1016/j.quascirev.2009.09.014
Guérin G, Mercier N, Adamiec G. 2011. Dose-rate conversion factors: update. Ancient TL **29**: 5-8
Guérin G, Mercier N, Nathan R, Adamiec G, Lefrais Y. 2012. On the use of the infinite matrix assumption and associated concepts: A critical review. Radiation Measurements **47**: 778-785. DOI: 10.1016/j.radmeas.2012.04.004
Hallissy T. 1911. Part 7. Geology. Proceedings of the Royal Irish Academy. Section C: Archaeology, Celtic Studies, History, Linguistics, Literature **31**: 7.1-7.22
Heyman J, Stroeven AP, Harbor JM, Caffee MW. 2011. Too young or too old: Evaluating cosmogenic exposure dating based on an analysis of compiled boulder exposure ages. Earth and Planetary Science Letters **302**: 71-80. DOI: 10.1016/j.epsl.2010.11.040
Hibbert FD, Austin WEN, Leng MJ, Gatliff RW. 2009. British Ice Sheet dynamics inferred from North Atlantic ice-rafted debris records spanning the last 175 000 years. Journal of Quaternary Science **25**: 461-482. DOI: 10.1002/jqs.1331
Hinch JDW. 1913. The Shelly Drift of Glenulra and Belderrig, Co. Mayo. The Irish Naturalist. **22**: 1-6
Howe JA, Dove D, Bradwell T, Gafeira J. 2012. Submarine geomorphology and glacial history of the Sea of the Hebrides, UK. Marine Geology **315-318**: 64-76. DOI: 10.1016/j.margeo.2012.06.005
Hubbard A, Bradwell T, Golledge N, Hall A, Patton H, Sugden D, Cooper R, Stoker M. 2009a. Dynamic cycles, ice streams and their impact on the extent, chronology and deglaciation of the British-Irish ice sheet. Quaternary Science Reviews **28**: 758-776
Hubbard A, Bradwell T, Golledge N, Hall A, Patton H, Sugden D, Cooper R, Stoker M. 2009b. Dynamic cycles, ice streams and their impact on the extent, chronology and deglaciation of the British–Irish ice sheet. Quaternary Science Reviews **28**: 758-776. DOI: 10.1016/j.quascirev.2008.12.026
Hughes ALC, Clark CD, Jordan CJ. 2014. Flow-pattern evolution of the last British Ice Sheet. Quaternary Science Reviews **89**: 148-168. DOI: 10.1016/j.quascirev.2014.02.002

Hughes ALC, Gyllencreutz R, Lohne OS, Mangerud J, Svendsen JI. 2016. The last Eurasian ice sheets - a chronological database and time-slice reconstruction, DATED-1. Boreas **45**: 1-45. DOI: 10.1111/bor.12142
Hughes ALC, Rainsley E, Murray T, Fogwill CJ, Schnabel C, Xu S. 2012. Rapid response of Helheim Glacier, southeast Greenland, to early Holocene climate warming. Geology **40**: 427-430. DOI: 10.1130/G32730.1
Hughes PD, Gibbard PL. 2015. A stratigraphical basis for the Last Glacial Maximum (LGM). Quaternary International **383**: 174-185. DOI: 10.1016/j.quaint.2014.06.006
Hughes PD, Gibbard PL, Ehlers J. 2013. Timing of glaciation during the last glacial cycle: evaluating the concept of a global 'Last Glacial Maximum' (LGM). Earth-Science Reviews **125**: 171-198. DOI: 10.1016/j.earscirev.2013.07.003
Hulbe CL, MacAyeal DR, Denton GH, Kleman J, Lowell TV. 2004. Catastrophic ice shelf breakup as the source of Heinrich event icebergs. Paleoceanography **19**: PA1004 1-15. DOI: 10.1029/2003pa000890
Jakobsson M, Anderson JB, Nitsche FO, Gyllencreutz R, Kirshner AE, Kirchner N, O'Regan M, Mohammad R, Eriksson B. 2012. Ice sheet retreat dynamics inferred from glacial morphology of the central Pine Island Bay Trough, West Antarctica. Quaternary Science Reviews **38**: 1-10. DOI: 10.1016/j.quascirev.2011.12.017
Jardine WG, Dickson JH, Haughton PDW, Harkness DD, Bowen DQ, Sykes GA. 1988. A late Middle Devensian interstadial site at Sourlie, near Irvine, Strathclyde. Scottish Journal of Geology **24**: 288. DOI: 10.1144/sjg24030288
Joughin I, Alley RB, Holland DM. 2012. Ice-Sheet Response to Oceanic Forcing. Science **338**: 1172-1176. DOI: 10.1126/science.1226481
Joughin I, Smith BE, Medley B. 2014. Marine Ice Sheet Collapse Potentially Under Way for the Thwaites Glacier Basin, West Antarctica. Science **344**: 735-738. DOI: 10.1126/science.1249055
Khodri M, Leclalnche Y, Ramstein G, Braconnot P, Marti O, Cortijo E. 2001. Simulating the amplification of orbital forcing by ocean feedbacks in the last glaciation. Nature **410**: 570-574. DOI: 10.1038/35069044
Knight J. 2004. Sedimentary evidence for the formation mechanism of the Armoy moraine and late Devensian glacial events in the north of Ireland. Geological Journal **39**: 403-417. DOI: 10.1002/gj.964
Knight J. 2008a. Armoy Moraine. In *North of Ireland: Field Guide*, Whitehouse NJ, Roe HM, McCarron S, Knight J (eds). Quaternary Research Association: London; 187-193.
Knight J. 2008b. Carey and Glenshesk valleys. In *North of Ireland: Field Guide*, Whitehouse NJ, Roe HM, McCarron S, Knight J (eds). Quaternary Research Association: London; 194-203.
Knutz PC, Austin WEN, John W Jones E. 2001. Millennial-scale depositional cycles related to British ice sheet variability and North Atlantic paleocirculation since 45 kyr B.P., Barra Fan, U.K. margin. Paleoceanography **16**: 53-64. DOI: 10.1029/1999PA000483
Knutz PC, Hall IR, Zahn R, Rasmussen TL, Kuijpers A, Moros M, Shackleton NJ. 2002. Multidecadal ocean variability and NW European ice sheet surges during the last deglaciation. Geochemistry, Geophysics, Geosystems **3**: 1077
Krabill W, Abdalati W, Frederick E, Manizade S, Martin C, Sonntag J, Swift R, Thomas R, Wright W, Yungel J. 2000. Greenland Ice Sheet: High-elevation balance and peripheral thinning. Science **289**: 428-430. DOI: 10.1126/science.289.5478.428
Krabill W, Hanna E, Huybrechts P, Abdalati W, Cappelen J, Csatho B, Frederick E, Manizade S, Martin C, Sonntag J, Swift R, Thomas R, Yungel J. 2004. Greenland Ice Sheet: Increased coastal thinning. Geophysical Research Letters **31**: 1-4. DOI: 10.1029/2004GL021533

Lambeck K, Rouby H, Purcell A, Sun Y, Sambridge M. 2014. Sea level and global ice volumes from the Last Glacial Maximum to the Holocene. Proc Natl Acad Sci U S A **111**: 15296-303. DOI: 10.1073/pnas.1411762111
Larter RD, Graham AGC, Gohl K, Kuhn G, Hillenbrand C-D, Smith JA, Deen TJ, Livermore RA, Schenke H-W. 2009. Subglacial bedforms reveal complex basal regime in a zone of paleo–ice stream convergence, Amundsen Sea embayment, West Antarctica. Geology **37**: 411-414. DOI: 10.1130/G25505A.1
Lowe J, Matthews I, Mayfield R, Lincoln P, Palmer A, Staff R, Timms R. 2019. On the timing of retreat of the Loch Lomond ('Younger Dryas') Readvance icefield in the SW Scottish Highlands and its wider significance. Quaternary Science Reviews **219**: 171-186. DOI: 10.1016/j.quascirev.2019.06.034
MacLeod A, Palmer A, Lowe J, Rose J, Bryant C, Merritt J. 2011. Timing of glacier response to Younger Dryas climatic cooling in Scotland. Global and Planetary Change **79**: 264-274. DOI: 10.1016/j.gloplacha.2010.07.006
Marrero SM, Phillips FM, Borchers B, Lifton N, Aumer R, Balco G. 2016. Cosmogenic nuclide systematics and the CRONUScalc program. Quaternary Geochronology **31**: 160-187. DOI: 10.1016/j.quageo.2015.09.005
McCabe A, Haynes JR, MacMillan NF. 1986. Late Pleistocene tidewater glaciers and glaciomarine sequences from north County Mayo, Republic of Ireland. Journal of Quaternary Science **1**: 73-84
McCabe AM. 1995. Fawnmore - ice mareginal terrace. In *North West Donegal. Field Guide.*, Wilson P (ed). Irish Association for Quaternary Studies: Dublin; 67-70.
McCabe AM. 2008. Glacial geology and geomorphology: the landscapes of Ireland. Dunedin Academic Press, Edinburgh
McCabe AM, Clark PU. 2003. Deglacial chronology from county Donegal, Ireland: Implications for deglaciation of the British-Irish ice sheet. Journal of the Geological Society **160**: 847-855
McCabe AM, Clark PU, Clark J. 2007a. Radiocarbon constraints on the history of the western Irish ice sheet prior to the Last Glacial Maximum. Geology **35**: 147-150
McCabe AM, Clark PU, Clark J, Dunlop P. 2007b. Radiocarbon constraints on readvances of the British–Irish Ice Sheet in the northern Irish Sea Basin during the last deglaciation. Quaternary Science Reviews **26**: 1204-1211. DOI: 10.1016/j.quascirev.2007.01.010
McCabe AM, Eyles N. 1988. Sedimentology of an ice-contact glaciomarine delta, Carey Valley, Northern Ireland. Sedimentary Geology **59**: 1-14
Meehan R. 2013. North Mayo. In *Geological Survey Ireland Geological Mapping*. Geological Survey Ireland: Dublin.
Murray AS, Wintle AG. 2000. Luminescence dating of quartz using an improved single-aliquot regenerative-dose protocol. Radiation Measurements **32**: 57-73. DOI: 10.1016/S1350-4487(99)00253-X
Newton AMW, Huuse M. 2017. Glacial geomorphology of the central Barents Sea: Implications for the dynamic deglaciation of the Barents Sea Ice Sheet. Marine Geology **387**: 114-131. DOI: https://doi.org/10.1016/j.margeo.2017.04.001
Ó'Cofaigh C, Dunlop P, Benetti S. 2012. Marine geophysical evidence for Late Pleistocene ice sheet extent and recession off northwest Ireland. Quaternary Science Reviews **44**: 147-159. DOI: 10.1016/j.quascirev.2010.02.005
Ó Cofaigh C, Callard L, Roberts DH, Chiverrell RC, Ballantyne CK, Evans D, Saher M, Van Landeghem K, Benetti S, Burke MJ, Clark C, Duller G, Fabel D, Livingstone S, Medialdea A, Moreton S, Sacchetti F, Smedley RK. This volume. Timing and pace of ice-sheet withdrawal across the marineterrestrial transition west of Ireland during the last glaciation. Journal of Quaternary Science:

Ó Cofaigh C, Weilbach K, Lloyd JM, Benetti S, Callard SL, Purcell C, Chiverrell RC, Dunlop P, Saher M, Livingstone SJ, Van Landeghem KJJ, Moreton SG, Clark CD, Fabel D. 2019. Early deglaciation of the British-Irish Ice Sheet on the Atlantic shelf northwest of Ireland driven by glacioisostatic depression and high relative sea level. Quaternary Science Reviews **208**: 76-96. DOI: 10.1016/j.quascirev.2018.12.022
Ottesen D, Dowdeswell JA, Rise L. 2005. Submarine landforms and the reconstruction of fast-flowing ice streams within a large Quaternary ice sheet: The 2500-km-long Norwegian-Svalbard margin (57°–80°N). GSA Bulletin **117**: 1033-1050. DOI: 10.1130/B25577.1
Patton H, Hubbard A, Andreassen K, Auriac A, Whitehouse PL, Stroeven AP, Shackleton C, Winsborrow M, Heyman J, Hall AM. 2017. Deglaciation of the Eurasian ice sheet complex. Quaternary Science Reviews **169**: 148-172. DOI: 10.1016/j.quascirev.2017.05.019
Patton H, Hubbard A, Andreassen K, Winsborrow M, Stroeven AP. 2016. The build-up, configuration, and dynamical sensitivity of the Eurasian ice-sheet complex to Late Weichselian climatic and oceanic forcing. Quaternary Science Reviews **153**: 97-121. DOI: 10.1016/j.quascirev.2016.10.009
Patton H, Hubbard A, Glasser NF, Bradwell T, Golledge NR. 2012a. The last Welsh Ice Cap: Part 1 - Modelling its evolution, sensitivity and associated climate. Boreas: n/a-n/a. DOI: 10.1111/j.1502-3885.2012.00300.x
Patton H, Hubbard A, Glasser NF, Bradwell T, Golledge NR. 2012b. The last Welsh Ice Cap: Part 2 - Dynamics of a topographically controlled icecap. Boreas: n/a-n/a. DOI: 10.1111/j.1502-3885.2012.00301.x
Payne AJ, Vieli A, Shepherd AP, Wingham DJ, Rignot E. 2004. Recent dramatic thinning of largest West Antarctic ice stream triggered by oceans. Geophysical Research Letters **31**: 1-4. DOI: 10.1029/2004GL021284
Peck VL, Hall IR, Zahn R, Elderfield H, Grousset F, Hemming SR, Scourse JD. 2006. High resolution evidence for linkages between NW European ice sheet instability and Atlantic Meridional Overturning Circulation. Earth and Planetary Science Letters **243**: 476-488. DOI: 10.1016/j.epsl.2005.12.023
Peck VL, Hall IR, Zahn R, Grousset F, Hemming SR, Scourse JD. 2007. The relationship of Heinrich events and their European precursors over the past 60 ka BP: a multi-proxy ice-rafted debris provenance study in the North East Atlantic. Quaternary Science Reviews **26**: 862-875. DOI: 10.1016/j.quascirev.2006.12.002
Peters JL, Benetti S, Dunlop P, Ó Cofaigh C. 2015. Maximum extent and dynamic behaviour of the last British–Irish Ice Sheet west of Ireland. Quaternary Science Reviews **128**: 48-68. DOI: 10.1016/j.quascirev.2015.09.015
Peters JL, Benetti S, Dunlop P, Ó Cofaigh C, Moreton SG, Wheeler AJ, Clark CD. 2016. Sedimentology and chronology of the advance and retreat of the last British-Irish Ice Sheet on the continental shelf west of Ireland. Quaternary Science Reviews **140**: 101-124. DOI: 10.1016/j.quascirev.2016.03.012
Pritchard HD, Arthern RJ, Vaughan DG, Edwards LA. 2009. Extensive dynamic thinning on the margins of the Greenland and Antarctic ice sheets. Nature **461**: 971-5. DOI: 10.1038/nature08471
Putnam AE, Bromley GRM, Rademaker K, Schaefer JM. 2019. In situ 10Be production-rate calibration from a 14C-dated late-glacial moraine belt in Rannoch Moor, central Scottish Highlands. Quaternary Geochronology **50**: 109-125. DOI: 10.1016/j.quageo.2018.11.006
Rasmussen SO, Bigler M, Blockley SP, Blunier T, Buchardt SL, Clausen HB, Cvijanovic I, Dahl-Jensen D, Johnsen SJ, Fischer H, Gkinis V, Guillevic M, Hoek WZ, Lowe JJ, Pedro JB, Popp T, Seierstad IK, Steffensen JP, Svensson AM, Vallelonga P, Vinther BM, Walker MJC, Wheatley JJ, Winstrup M. 2014. A stratigraphic framework for abrupt climatic changes

during the Last Glacial period based on three synchronized Greenland ice-core records: Refining and extending the INTIMATE event stratigraphy. Quaternary Science Reviews **106**: 14-28. DOI: 10.1016/j.quascirev.2014.09.007
Rasmussen TL, Thomsen E, Moros M. 2016. North Atlantic warming during Dansgaard-Oeschger events synchronous with Antarctic warming and out-of-phase with Greenland climate. Sci Rep **6**: 20535. DOI: 10.1038/srep20535
Reimer PJ, Bard E, Bayliss A, Beck JW, Blackwell PG, Bronk Ramsey C, Buck CE, Cheng H, Edwards RL, Friedrich M, Grootes PM, Guilderson TP, Haflidason H, Hajdas I, Hatté C, Heaton TJ, Hoffmann DL, Hogg AG, Hughen KA, Kaiser KF, Kromer B, Manning SW, Niu M, Reimer RW, Richards DA, Scott EM, Southon JR, Staff RA, Turney CSM, van der Plicht J. 2013. IntCal13 and Marine13 radiocarbon age calibration curves 0-50,000 years cal BP. Radiocarbon **55**: 1869-1887. DOI: 10.2458/azu_js_rc.55.16947
Rignot E, Braaten D, Gogineni SP, Krabill WB, McConnell JR. 2004a. Rapid ice discharge from southeast Greenland glaciers. Geophysical Research Letters **31**: L10401 1-4. DOI: 10.1029/2004GL019474
Rignot E, Casassa G, Gogineni P, Krabill W, Rivera A, Thomas R. 2004b. Accelerated ice discharge from the Antarctic Peninsula following the collapse of Larsen B ice shelf. Geophysical Research Letters **31**: L18401 1-4. DOI: 10.1029/2004GL020697
Rignot E, Koppes M, Velicogna I. 2010. Rapid submarine melting of the calving faces of West Greenland glaciers. Nature Geoscience **3**: 187-191. DOI: 10.1038/ngeo765
Roberts DH, Long AJ, Davies BJ, Simpson MJR, Schnabel C. 2010. Ice stream influence on West Greenland Ice Sheet dynamics during the Last Glacial Maximum. Journal of Quaternary Science **25**: 850-864. DOI: https://doi.org/10.1002/jqs.1354
Scambos TA, Bohlander JA, Shuman CA, Skvarca P. 2004. Glacier acceleration and thinning after ice shelf collapse in the Larsen B embayment, Antarctica. Geophysical Research Letters **31**: L18402 1-4. DOI: 10.1029/2004GL020670
Schiele CK. 2017. Timing, forcing and onshore-offshore correlations on the western margin of the British-Irish Ice Sheet. In *School of Geography and Environmental Sciences*. Ulster University: Coleraine.
Schoof C. 2007. Ice sheet grounding line dynamics: Steady states, stability, and hysteresis. Journal of Geophysical Research: Earth Surface **112**. DOI: 10.1029/2006JF000664
Scourse JD, Chiverrell RC, Smedley RK, Small D, Burke MJ, Saher M, Landeghem KJJV, Duller GAT, Cofaigh CÓ, Bateman M, Benetti S, Bradley S, Callard SL, Evans DJA, Fabel D, Jenkins GTH, McCarron S, Medialdea A, Moreton S, Praeg D, Roberts DH, Clark CD. This volume. Maximum extent and readvance dynamics of the Irish Sea Ice Stream and Irish Sea Glacier since the Last Glacial Maximum. Journal of Quaternary Science:
Scourse JD, Haapaniemi AI, Colmenero-Hidalgo E, Peck VL, Hall IR, Austin WEN, Knutz PC, Zahn R. 2009. Growth, dynamics and deglaciation of the last British–Irish ice sheet: the deep-sea ice-rafted detritus record. Quaternary Science Reviews **28**: 3066-3084. DOI: 10.1016/j.quascirev.2009.08.009
Shaw J, Piper DJW, Fader GBJ, King EL, Todd BJ, Bell T, Batterson MJ, Liverman DGE. 2006. A conceptual model of the deglaciation of Atlantic Canada. Quaternary Science Reviews **25**: 2059-2081. DOI: 10.1016/j.quascirev.2006.03.002
Shepherd A, Wingham D, Rignot E. 2004. Warm ocean is eroding West Antactic ce Sheet. Geophys. Res. Lett. **31**:
Sissons JB. 1980. The Loch Lomond Advance in the Lake District, northern England. Transactions of the Royal Society of Edinburgh: Earth Sciences **71**: 13-27. DOI: 10.1017/S0263593300013468
Small D, Benetti S, Dove D, Ballantyne CK, Fabel D, Clark CD, Gheorghiu DM, Newall J, Xu S. 2017a. Cosmogenic exposure age constraints on deglaciation and flow behaviour of

a marine-based ice stream in western Scotland, 21–16 ka. Quaternary Science Reviews **167**: 30-46. DOI: 10.1016/j.quascirev.2017.04.021
Small D, Clark CD, Chiverrell RC, Smedley RK, Bateman MD, Duller GAT, Ely JC, Fabel D, Medialdea A, Moreton SG. 2017b. Devising quality assurance procedures for assessment of legacy geochronological data relating to deglaciation of the last British-Irish Ice Sheet. Earth-Science Reviews **164**: 232-250. DOI: 10.1016/j.earscirev.2016.11.007
Small D, Fabel D. 2015. A Lateglacial 10Be production rate from glacial lake shorelines in Scotland. Journal of Quaternary Science **30**: 509-513. DOI: 10.1002/jqs.2804
Small D, Rinterknecht V, Austin WEN, Bates R, Benn DI, Scourse JD, Bourlès DL, Hibbert FD. 2016. Implications of 36Cl exposure ages from Skye, northwest Scotland for the timing of ice stream deglaciation and deglacial ice dynamics. Quaternary Science Reviews **150**: 130-145. DOI: 10.1016/j.quascirev.2016.08.028
Small D, Smedley RK, Chiverrell RC, Scourse JD, Cofaigh C, Duller GAT, McCarron S, Burke MJ, Evans DJ, Fabel D, Gheorghiu DM, Thomas GSP, Xu S, Clark CD. 2018. Trough geometry was a greater influence than climate-ocean forcing in regulating retreat of the marine-based Irish-Sea Ice Stream. Bulletin of the Geological Society of America **130**: 1981-1999. DOI: 10.1130/B31852.1
Smedley RK, Chiverrell RC, Ballantyne CK, Burke MJ, Clark CD, Duller GAT, Fabel D, McCarroll D, Scourse JD, Small D, Thomas GSP. 2017a. Internal dynamics condition centennial-scale oscillations in marinebased ice-stream retreat. Geology **45**: 787-790. DOI: 10.1130/G38991.1
Smedley RK, Scourse JD, Small D, Hiemstra JF, Duller GAT, Bateman MD, Burke MJ, Chiverrell RC, Clark CD, Davies SM, Fabel D, Gheorghiu DM, McCarroll D, Medialdea A, Xu S. 2017b. New age constraints for the limit of the British–Irish Ice Sheet on the Isles of Scilly. Journal of Quaternary Science **32**: 48-62. DOI: 10.1002/jqs.2922
Smith MJ, Knight J, Field KS, Harrison S. 2008. Glacial striae observations for Ireland compiled from historic records. Journal of Maps **4**: 378-398. DOI: 10.4113/jom.2008.1035
Sole A, Payne T, Bamber J, Nienow P, Krabill W. 2008. Testing hypotheses of the cause of peripheral thinning of the Greenland Ice Sheet: Is land-terminating ice thinning at anomalously high rates? Cryosphere **2**: 205-218. DOI: 10.5194/tc-2-205-2008
Sonntag J, Manizade S, Krabill W, Linkswiler M, Yungel J. 2012. Progressive thinning of Greenland's west-central flank and northwest coastal margin from operation icebridge laser altimetry. 1553-1556. DOI: 10.1109/IGARSS.2012.6350815
Stocker T. 2014. Climate change 2013 : the physical science basis : Working Group I contribution to the Fifth assessment report of the Intergovernmental Panel on Climate Change
Stokes CR. 2018. Geomorphology under ice streams: Moving from form to process. Earth Surface Processes and Landforms **43**: 85-123. DOI: 10.1002/esp.4259
Stokes CR, Clark CD. 1999. Geomorphological criteria for identifying Pleistocene ice streams. Annals of Glaciology **28**: 67-74
Stokes CR, Clark CD. 2001. Palaeo-ice streams. Quaternary Science Reviews **20**: 1437-1457
Stokes CR, Corner GD, Winsborrow MCM, Husum K, Andreassen K. 2014. Asynchronous response of marine-terminating outlet glaciers during deglaciation of the Fennoscandian ice sheet. Geology **42**: 455-458. DOI: 10.1130/G35299.1
Stone JO, Ballantyne CK. 2006. Dimensions and deglacial chronology of the Outer Hebrides Ice Cap, northwest Scotland: implications of cosmic ray exposure dating. Journal of Quaternary Science **21**: 75-84. DOI: 10.1002/jqs.933
Svendsen JI, Alexanderson H, Astakhov VI, Demidov I, Dowdeswell JA, Funder S, Gataullin V, Henriksen M, Hjort C, Houmark-Nielsen M, Hubberten HW, Ingolfsson O,

Jakobsson M, Kjær KH, Larsen E, Lokrantz H, Lunkka JP, Lyså A, Mangerud J, Matiouchkov A, Murray A, Möller P, Niessen F, Nikolskaya O, Polyak L, Saarnisto M, Siegert C, Siegert MJ, Spielhagen RF, Stein R. 2004. Late Quaternary ice sheet history of northern Eurasia. Quaternary Science Reviews **23**: 1229-1271
Synge FM. 1963. The Glaciation of the Nephin Beg Range, County Mayo. Irish Geography **4**: 397-403. DOI: 10.1080/00750776309555569
Synge FM. 1965. The glaciation of west mayo. Irish Geography **5**: 372-386. DOI: 10.1080/00750776509555630
Tarlati S, Benetti S, Callard SL, Cofaigh CÓ, Dunlop P, Georgiopoulou A, Edwards R, Van Landeghem K, Saher M, Chiverrell R, Fabel D, Moreton S, Morgan S, Clark CD. 2020. Final deglaciation of the Malin Sea through meltwater release and calving events. Scottish Journal of Geology. DOI: 10.1144/sjg2019-010
Thomas GSP, Chiverrell R, Huddart D. 2004. Ice-marginal depositional responses to readvance episodes in the Late Devensian deglaciation of the Isle of Man. Quaternary Science Reviews **23**: 85-106. DOI: 10.1016/j.quascirev.2003.10.012
Thomsen KJ, Murray AS, Bøtter-Jensen L, Kinahan J. 2007. Determination of burial dose in incompletely bleached fluvial samples using single grains of quartz. Radiation Measurements **42**: 370-379. DOI: 10.1016/j.radmeas.2007.01.041
Van Kreveld S, Sarnthein M, Erlenkeuser H, Grootes P, Jung S, Nadeau MJ, Pflaumann U, Voelker A. 2000. Potential links between surging ice sheets, circulation changes, and the Dansgaard-Oeschger cycles in the Irmiger Sea, 60-80 kyr. Paleoceanography **15**: 425-442. DOI: 10.1029/1999PA000464
Waelbroeck C, Lougheed BC, Vazquez Riveiros N, Missiaen L, Pedro J, Dokken T, Hajdas I, Wacker L, Abbott P, Dumoulin JP, Thil F, Eynaud F, Rossignol L, Fersi W, Albuquerque AL, Arz H, Austin WEN, Came R, Carlson AE, Collins JA, Dennielou B, Desprat S, Dickson A, Elliot M, Farmer C, Giraudeau J, Gottschalk J, Henderiks J, Hughen K, Jung S, Knutz P, Lebreiro S, Lund DC, Lynch-Stieglitz J, Malaize B, Marchitto T, Martinez-Mendez G, Mollenhauer G, Naughton F, Nave S, Nurnberg D, Oppo D, Peck V, Peeters FJC, Penaud A, Portilho-Ramos RDC, Repschlager J, Roberts J, Ruhlemann C, Salgueiro E, Sanchez Goni MF, Schonfeld J, Scussolini P, Skinner LC, Skonieczny C, Thornalley D, Toucanne S, Rooij DV, Vidal L, Voelker AHL, Wary M, Weldeab S, Ziegler M. 2019. Consistently dated Atlantic sediment cores over the last 40 thousand years. Sci Data **6**: 165. DOI: 10.1038/s41597-019-0173-8
Wilson P, Ballantyne CK, Benetti S, Small D, Fabel D, Clark CD. 2019. Deglaciation chronology of the Donegal Ice Centre, north-west Ireland. Journal of Quaternary Science **34**: 16-28. DOI: 10.1002/jqs.3077
Winsborrow MCM, Andreassen K, Corner GD, Laberg JS. 2010. Deglaciation of a marine-based ice sheet: Late Weichselian palaeo-ice dynamics and retreat in the southern Barents Sea reconstructed from onshore and offshore glacial geomorphology. Quaternary Science Reviews **29**: 424-442. DOI: 10.1016/j.quascirev.2009.10.001

TABLES

Table 1 Radioactivity and dose rate data for luminescence samples.

Site	Sample	Depth (m)	Water (%)	U (ppm)*	Th (ppm)*	K (%) *	Rb (ppm)*	Beta dose-rate (Gy/ka)	Gamma dose-rate (Gy/ka)	Cosmic dose-rate (Gy/ka)	Total dose-rate (Gy/ka)
Brockhill Quarry	T6BROC01	7	27	1.22±0.12	3.0±0.3	1.5±0.08	42.9±4.29	0.782±0.060	0.452±0.030	0.088±0.004	1.339±0.074
	T6BROC02	5	27	1.03±0.10	2.4±0.24	1.3±0.07	39.4±3.94	0.902±0.078	0.477±0.032	0.111±0.006	1.507±0.084
Glenulra Quarry	T6GULR01	2.3	27	1.65±0.17	4.4±0.44	2.1±0.11	72.5±7.25	1.270±0.109	0.760±0.050	0.156±0.008	2.207±0.120
	T6GULR02	2	27	1.70±0.17	4.7±0.47	2.0±0.10	64.6±6.46	1.228±0.105	0.636±0.042	0.162±0.008	2.047±0.113
Lough Nacung	T6LNAC01	5	27	0.66±0.07	1.6±0.2	0.8±0.04	25.3±2.53	0.485±0.042	0.317±0.021	0.111±0.006	0.928±0.047
	T6LNAC02	3	27	0.82±0.08	3.0±0.3	2.0±0.10	53.1±5.31	1.120±0.101	0.563±0.038	0.143±0.007	1.841±0.108
Altwinny Bay	T7ALTB02	10	27	1.04±0.10	3.9±0.39	1.9±0.10	51.3±5.13	1.109±0.97	0.584±0.039	0.064±0.003	1.775±0.105
Carey Valley	T7CARV01	12	27	1.22±0.12	5.0±0.5	1.4±0.07	49.7±4.97	0.882±0.074	0.519±0.034	0.054±0.003	1.474±0.081
	T7CARV02	8	27	1.39±0.14	6.3±0.63	1.7±0.09	62.7±6.27	1.067±0.091	0.530±0.032	0.080±0.004	1.697±0.095
Castleroe	T7CAST01	10	23	0.37±0.04	1.3±0.13	0.60±0.03	16.8±1.68	0.375±0.033	0.211±0.014	0.064±0.003	0.663±0.036
	T7CAST02	15	23	0.37±0.04	1.2±0.12	0.60±0.03	15.9±1.59	0.373±0.033	0.207±0.014	0.041±0.002	0.635±0.036
Fawnmore	T7FAWN02	5	27	1.17±0.12	4.7±0.47	1.30±0.07	44.9±4.49	0.823±0.070	0.573±0.038	0.111±0.006	1.525±0.079
	T7FAWN03	3	27	1.27±0.13	6.6±0.66	1.60±0.08	53.8±5.38	1.010±0.084	0.625±0.042	0.142±0.007	1.798±0.094
Glenshesk Valley	T7GLEN01	2	27	1.06±0.11	4.3±0.43	0.80±0.04	28.2±2.82	0.555±0.044	0.440±0.030	0.164±0.008	1.178±0.054
	T7GLEN02	3	27	1.13±0.11	4.9±0.49	0.90±0.05	35.4±3.54	0.621±0.050	0.386±0.039	0.144±0.007	1.170±0.057

*The analytical chemistry laboratory did not provide uncertainties on individual U, Th, K or Rb concentrations. Based on replicate analyses, uncertainties of 10% were assumed for U, Th and Rb, and 5% for K, and these uncertainties were propagated through the dose rate calculations.

Table 2 Luminescence equivalent dose and age data.

Site	Sample	Labcode	Analysis	Grain size (μm)	DR OD (%)	Total analysed*	n	OD (%)	Age model†	a value or Sigma-b‡	D_e (Gy)	Age (ka)
Brockhill Quarry	T6BROC01	Shfd15171	SA	180-250	12	102	60	60	IEU	0.307	59.43±4.37	44.4±4.1
	T6BROC02	Shfd15013	SA	212-250		96	48	65	IEU	0.307	58.97±4.66	39.1±3.8
	T6BROC02	Shfd15013	SG	212-250		1600	29	36	IEU	0.307	68.96±11.8	45.8±8.2
Glenulra Quarry	T6GULR01	Shfd15172	SA	180-250		76	53	45	IEU	0.307	55.68±2.71	25.2±1.9
	T6GULR02	Shfd15012	SA	180-250	6	144	51	65	IEU	0.307	49.3±2.71	24.1±1.9
Lough Nacung	T6LNAC01	Shfd15173	SA	180-250		92	36	40	IEU	0.307	243±13	109±8.4
	T6LNAC01	Shfd15173	SG	180-250		3200	33	34	IEU	0.189	77.8±5.01	83.8±6.9
	T6LNAC02	Shfd15014	SA	180-250	6	48	25	71	IEU	0.307	63.6±6.32	132±11
Altwinny Bay	T7ALTB02	Shfd15166	SA	180-250		97	35	56	MAM	0.20	54.0±8.16	30.4±4.9
Carey Valley	T7CARV01	Shfd15169	SA	212-250		80	43	65	MAM	0.10	42.04±2.41	22.6±2.4
	T7CARV02	Shfd15018	SA	212-250	6	160	40	37	MAM	0.10	41.36±2.61	22.1±2.4
Castleroe	T7CAST01	Shfd15167	SA	212-250		72	57	42	MAM	0.10	31.91±2.67	48.1±4.8
	T7CAST02	Shfd15016	SA	212-250	6	70	45	58	MAM	0.10	24.29±2.02	38.3±3.8
Fawnmore	T7FAWN02	Shfd15015	SA	212-250		78	34	65	MAM	0.20	41.34±5.28	25.8±4.2
	T7FAWN03	Shfd15168	SA	212-250	20	103	45	70	MAM	0.20	46.43±7.08	27.1±3.7
Glenshesk Valley	T7GLEN01	Shfd15017	SA	212-250	17	120	52	70	MAM	0.20	36.66±3.32	30.4±4.2
	T7GLEN02	Shfd15170	SA	212-250		78	55	80	MAM	0.20	32.24±2.42	23.6±3.4

*Total analysed is the number of small aliquots or single grains measured for a sample, while the column headed 'n' is the number of small aliquots of single grains accepted for De modelling.

†Shows the age model used, either the Minimum Age Model (MAM) or the internal–external uncertainty (IEU) model.

‡Where the IEU model was used, the first parameter 'a' is given in this column. The second parameter 'b' is 1.5 for all samples. For samples analysed using the MAM, the value given here is that for sigma b.

Table 3 Previously published BRITICE-CHRONO ^{14}C ages included in this paper.

Transect	Cruise-Core	Code	Sample ID	Latitude	Longitude	Depth (m)	Sample type	Sample depth (cm)	Stratigraphical context	Conventional Radiocarbon Age (years BP)	+/- 1σ (radiocarbon yrs BP)	Reference
T6	CE08-018VC	UCIAMS-133552	CE_08-018_CC	54.98	-9.92	122	Mixed Forams	core catcher	Marine sands and gravels (deglacial), contained fine sands (w/forams)	20170	90	Ó Cofaigh *et al.* 2019
T6	JC106-92VC	Beta432793	T6-92VC-259cm	54.405517	-9.1768	75	Foraminifera-mixed benthic	259-260	Diamict	16250	60	Schiele, 2017
T6	JC106-97VC	Beta432794	T6-97VC-468cm	54.454783	-9.17203	75	Foraminifera-mixed benthic	468-469	Compact deformed mud	16350	60	Schiele, 2017
T6	JC106-099VC	UCIAMS-164429	T6-099VC-474	54.60363	-9.33564	99	Foraminifera	474	From laminated clay and silts. Mid unit, no diamict at base.	17180	80	Ó Cofaigh *et al.* 2019
T6	JC106-101VC	UCIAMS-164431	T6-101VC-548-551	54.61307	-9.42068	100	Foraminifera	548-551	From laminated clay and silts. Mid unit, no diamict at base.	20110	120	Ó Cofaigh *et al.* 2019
T6	JC106-102VC	UCIAMS-164437	T6-102VC-247	54.62345	-9.5189	90.5	Foraminifera	247	From laminated clay and silts. Mid unit, no diamict at base.	21000	110	Ó Cofaigh *et al.* 2019
T6	JC106-103VC	SUERC-63558	T6-103VC-145	54.64063	-9.59722	100	Foraminifera	145	From laminated clay and silts. Mid unit, no diamict at base.	22521	70	Ó Cofaigh *et al.* 2019
T6	JC106-112VC	SUERC-63584	T6-112VC-51	54.84513	-10.18137	125	Shell fragment	51	Diamict interpreted as subglacial till	22582	67	Ó Cofaigh *et al.* 2019
T6	JC106-112VC	SUERC-63585	T6-112VC-59.5	54.84513	-10.18137	125	Shell fragment	59.5	Diamict interpreted as subglacial till	22572	71	Ó Cofaigh *et al.* 2019
T7	JC106-125VC	SUERC-72873	T7JC106-125VC115	55.73367167	-9.251471389	91	Shell fragment	115	Diamict interpreted as subglacial till	22813	61	Callard et al., 2018
T7	JC106-125VC	SUERC-72874	T7JC106-125VC117	55.73367167	-9.251471389	91	Shell fragment	117	Diamict interpreted as subglacial till	22906	62	Callard et al., 2018
T7	JC106-146VC	UCIAMS-176382	T7-146VC-223	56.47296	-8.70696	150	Foraminifera, mixed assemblage	223-225	Glaciomarine/ice proximal: alternating laminated silt and clay with IRD rich mud, not overconsolidated	20200	80	Callard et al., 2018
T7	JC106-146VC	UCIAMS-176383	T7-146VC-369	56.48404	-8.44641	158	Foraminifera, mixed assemblage	369-372	Glaciomarine/ice proximal: alternating laminated silt and clay with IRD rich mud, not overconsolidated	22030	100	Callard et al., 2018
T7	JC106-146VC	UCIAMS-164440	T7-146VC-389	56.47296	-8.70696	150	Foraminifera	389-392	Glaciomarine/ice proximal: alternating laminated silt and clay with IRD rich mud, not overconsolidated	20730	100	Callard et al., 2018
T7	JC106-149VC	SUERC-59509	T7-149VC-421	56.39728	-7.44881	136	Shell fragment	421	Soft diamict, possibly glaciomarine/ice proximal - IRD	17155	47	Callard et al., 2018
T7	JC106-151VC	UCIAMS-179841	T7-151VC-389	56.14046	-7.53772	122	Foraminifera, mixed assemblage	389-394		19690	90	Callard et al., 2018
T7	JC106-153VC	UCIAMS-164432	T7-153VC-277	56.25168	-7.58738	113.5	Foraminifera	277-279	Glaciomarine/ice proximal in a stiffer mud unit with some IRD	19210	110	Callard et al., 2018
T7	JC106-154VC	UCIAMS-164433	T7-154VC-211	56.32525	-7.61805	138	Foraminifera	211-214	Glaciomarine/ice distal/proximal	18670	90	Callard et al., 2018

Table 4 All published BRITICE-CHRONO TCN ages.

Transect	Code	Location	Region	Latitude	Longitude	Elev. (m)	Sample	Lithology	^{10}Be age (ka)[1]	CRONUScalc v2.0 ^{10}Be age (ka)[2]	CRONUScalc v2.0 ^{36}Cl age (ka)[2]	Reference
T6	T6BS01	Eglish Valley	Blue Stack Mountains	54.7228	-8.1132	149	boulder	Conglomerate	13.1 ± 0.9 (0.7)	13.1 ± 1.3 (0.7)		Wilson et al. (2019)
T6	T6BS02	Eglish Valley	Blue Stack Mountains	54.7225	-8.114	148	boulder	Sandstone	15.4 ± 1.0 (0.7)	15.4 ± 1.4 (0.7)		Wilson et al. (2019)
T6	T6BS03	Eglish Valley	Blue Stack Mountains	54.7231	-8.1165	150	boulder	Conglomerate	14.9 ± 0.9 (0.7)	14.9 ± 1.4 (0.7)		Wilson et al. (2019)
T6	T6BS04	Eglish Valley	Blue Stack Mountains	54.7225	-8.115	163	boulder	Conglomerate	14.4 ± 0.8 (0.4)	14.4 ± 1.2 (0.4)		Wilson et al. (2019)
T6	T6GCS02	Glencolumkille	SW coast Donegal	54.7079	-8.761	41	boulder	Schist (Qtz vein)	16.2 ± 1.0 (0.7)	16.2 ± 1.5 (0.7)		Wilson et al. (2019)
T6	T6GCS03	Glencolumkille	SW coast Donegal	54.7076	-8.7589	36	boulder	Schist (Qtz vein)	17.3 ± 1.1 (0.7)	17.3 ± 1.6 (0.7)		Wilson et al. (2019)
T6	T6GCS04	Glencolumkille	SW coast Donegal	54.7076	-8.7589	34	boulder	Schist (Qtz vein)	16.5 ± 1.0 (0.7)	16.5 ± 1.5 (0.7)		Wilson et al. (2019)
T6	T6PG01	Poisoned Glen	Donegal	55.01505	-8.10675	73	Boulder	Granite	17.2 ± 1.1 (0.8)	17.2 ± 1.6 (0.8)		Wilson et al. (2019)
T6	T6PG04	Poisoned Glen	Donegal	55.01495	-8.10653	73	Boulder	Granite	16.2 ± 1.0 (0.8)	16.2 ± 1.5 (0.8)		Wilson et al. (2019)
T6	T6PG05	Poisoned Glen	Donegal	55.01498	-8.10572	75	Boulder	Granite	13.0 ± 0.9 (0.6)	13.0± 1.2 (0.6)		Wilson et al. (2019)
T6	T6ROS01	Rosguill	Donegal	55.2269	-7.84304	65	Boulder	Granite	18.7 ± 1.0 (0.6)	18.7 ± 1.6 (0.6)		Wilson et al. (2019)
T6	T6ROS02	Rosguill	Donegal	55.2252	-7.84062	105	Boulder	Granite	21.4 ± 1.4 (1.0)	21.0 ± 2.0 (1.0)		Wilson et al. (2019)
T6	T6ROS04	Rosguill	Donegal	55.22412	-7.84055	105	Boulder	Granite	18.9 ± 1.0 (0.6)	18.9 ± 1.6 (0.6)		Wilson et al. (2019)
T6	T6BEN01	Ben Bulben	Sligo	54.36215	-8.4939	204	Boulder	Sandstone	13.0 ± 0.7 (0.5)	13.0 ± 1.1 (0.5)		Schiele (2017)
T6	T6BEN02	Ben Bulben	Sligo	54.361967	-8.494217	198	Boulder	Sandstone	14.3 ± 0.8 (0.5)	14.3 ± 1.2 (0.5)		Schiele (2017)
T6	T6BEN03	Ben Bulben	Sligo	54.363433	-8.494533	203	Boulder	Sandstone	14.3 ± 0.8 (0.5)	14.3 ± 1.2 (0.5)		Schiele (2017)
T6	T6BEN04	Ben Bulben	Sligo	54.363617	-8.494717	200	Boulder	Sandstone	15.7 ± 0.9 (0.5)	15.7 ± 1.4 (0.5)		Schiele (2017)
T6	T6KC01	Kilcar	Donegal	54.6187	-8.6096	50	Boulder	Dolerite			18.2 ± 1.7 (0.7)	Wilson et al. (2019)
T6	T6KC02	Kilcar	Donegal	54.6187	-8.6096	50	Boulder	Dolerite			37.5 ± 6.3 (2.1)	Wilson et al. (2019)
T6	T6KC03	Kilcar	Donegal	54.6187	-8.6096	50	Boulder	Dolerite			42.8 ± 6.1 (2.0)	Wilson et al. (2019)
T6	T6KC04	Kilcar	Donegal	54.6189	-8.609	45	Boulder	Dolerite			37.4 ± 5.4 (1.7)	Wilson et al. (2019)
T6/T7	T7MH02	Malin Head	N Coast Donegal	55.38112	-7.37255	65	Bedrock	Quartzite	23.2 ± 1.4 (0.9)	23.2 ± 2.1 (0.9)		Wilson et al. (2019)
T6/T7	T7MH03	Malin Head	N Coast Donegal	55.38156	-7.37716	30	Bedrock	Quartz vein (Quartzite)	20.7 ± 1.1 (0.7)	20.7 ± 1.8 (0.7)		Wilson et al. (2019)
T6/T7	T7MH04	Malin Head	N Coast Donegal	55.38033	-7.37458	55	Bedrock	Quartzite	25.5 ± 2.1 (1.8)	25.8 ± 2.8 (1.8)		Wilson et al. (2019)
T7	T7CAR02	Carnan Mor	Tiree	56.45521	-6.92344	136	Boulder	Lewisian Gneiss	21.1 ± 1.2 (0.7)	21.1 ± 1.8 (0.7)		Small et al. (2017)
T7	T7CAR05	Carnan Mor	Tiree	56.45464	-6.92271	133	Boulder	Lewisian Gneiss	20.2 ± 1.1 (0.6)	20.2 ± 1.7 (0.6)		Small et al. (2017)
T7	T7CAR07	Carnan Mor	Tiree	56.45236	-6.91878	111	Boulder	Lewisian Gneiss	20.8 ± 1.1 (0.7)	20.9 ± 1.8 (0.7)		Small et al. (2017)
T7	T7MIN02	Mingulay	Mingulay	56.82096	-7.63059	223	Boulder	Lewisian Gneiss	18.7 ± 1.0 (0.5)	18.7 ± 1.6 (0.5)		Small et al. (2017)
T7	T7MIN03	Mingulay	Mingulay	56.82096	-7.63059	223	Bedrock	Lewisian Gneiss	21.6 ± 1.1 (0.6)	21.6 ± 1.8 (0.6)		Small et al. (2017)
T7	T7MIN04	Mingulay	Mingulay	56.81998	-7.63172	196	Boulder	Lewisian Gneiss	17.4 ± 0.9 (0.5)	17.4 ± 1.5 (0.5)		Small et al. (2017)
T7	T7MIN06	Mingulay	Mingulay	56.81521	-7.63793	52	Boulder	Lewisian Gneiss	19.2 ± 1.0 (0.5)	19.2 ± 1.6 (0.5)		Small et al. (2017)
T7	T7MIN07	Mingulay	Mingulay	56.81521	-7.63793	52	Bedrock	Lewisian Gneiss	20.9 ± 1.1 (0.6)	20.9 ± 1.8 (0.6)		Small et al. (2017)
T7	T7SGU02	North Barra	North Barra	57.05256	-7.44933	65	Boulder	Lewisian Gneiss	17.4 ± 1.0 (0.6)	17.4 ± 1.5 (0.6)		Small et al. (2017)
T7	T7SGU03	North Barra	North Barra	57.05273	-7.44955	69	Boulder	Lewisian Gneiss	19.8 ± 1.1 (0.6)	19.8 ± 1.7 (0.6)		Small et al. (2017)
T7	T7SGU04	North Barra	North Barra	57.05349	-7.45106	78	Boulder	Lewisian Gneiss	17.0 ± 0.9 (0.6)	17.0 ± 1.5 (0.6)		Small et al. (2017)
T7	T7TMC01	Torr Mor a'Chonairst	Ross of Mull	56.28791	-6.34428	42	Boulder	Schist	17.3 ± 0.9 (0.5)	17.3 ± 1.5 (0.5)		Small et al. (2017)
T7	T7TMC05	Torr Mor a'Chonairst	Ross of Mull	56.28716	-6.34287	57	Boulder	Granite	17.8 ± 0.9 (0.5)	17.8 ± 1.5 (0.5)		Small et al. (2017)
T7	T7TMC06	Torr Mor a'Chonairst	Ross of Mull	56.28617	-6.3411	46	Boulder	Granite	17.9 ± 1.0 (0.6)	18.0 ± 1.5 (0.6)		Small et al. (2017)
T7	S1	Scriob na Caillich	Jura	55.9176	−6.0509	106	Boulder	Quartzite	17.6 ± 1.2 (0.8)	17.5 ± 1.6 (0.8)		Small et al. (2017)
T7	S2	Scriob na Caillich	Jura	55.9172	−6.0512	106	Boulder	Quartzite	16.5 ± 1.1 (0.8)	16.4 ± 1.5 (0.8)		Small et al. (2017)
T7	S3	Scriob na Caillich	Jura	55.9176	−6.0522	92	Boulder	Quartzite	15.0 ± 1.1 (0.8)	14.9 ± 1.4 (0.8)		Small et al. (2017)

[1]Calculated with calculator formerly known as the CRONUS-Earth calculator (Developmental version; Wrapper script 2.3, Main calculator 2.1, constants 2.2.1, muons 1.1; Balco, et al., 2008) with LM scaling method, Loch Lomond reference production rate (LLPR) (see text), 1mm ka^{-1} erosion rate, and one sigma external uncertainty (internal in brackets).
[2]Calculated with CRONUScalc v2.0 (Marrero et al. 2016) with LM scaling method, default global reference production rate, 1mm ka^{-1} erosion rate, and one sigma external uncertainty (internal in brackets).

Table 5 All legacy and other TCN ages published after the beginning of the BRITICE-CHRONO project and included in the Bayesian age modelling.

Site	Sample	^{10}Be (ka)[1]	CRONUScalc v2.0 ^{10}Be (ka)[2]	CRONUScalc v2.0 ^{36}Cl (ka)[2]	Material and context	Reference
DONEGAL						
Malin Head				25.1 ± 1.1	Glacially smoothed quartzite bedrock	Bowen et al. (2002)
Bloody Foreland				31.0 ± 17.0	Not specified, but granite bedrock or boulder	Bowen et al. (2002)
Bloody Foreland	BF-01	21.2 ± 1.1 (1.0)	21.0 ± 2.0 (1.1)		Glacially transported granite boulder	Ballantyne et al. (2007)
	BF-02	18.5 ± 0.9 (0.8)	18.6 ± 1.7 (0.9)		Glacially transported granite boulder	
Bloody Foreland	BF-04-01	17.9 ± 1.7 (1.6)	18.0 ± 2.3 (1.8)		Glacially transported granite boulder	Clark et al. (2009b)
	BF-04-03	33.5 ± 2.7 (2.6)	34.0 ± 4.0 (2.9)		Glacially transported granite boulder	
	BF-04-04	21.8 ± 1.6 (1.5)	22.0 ± 2.4 (1.7)		Glacially transported granite boulder	
	BF-04-05	21.2 ± 1.7 (1.6)	21.4 ± 2.5 (1.8)		Glacially transported granite boulder	
	BF-04-06	21.2 ± 1.9 (1.9)	21.4 ± 2.7 (2.1)		Glacially transported granite boulder	
	BF-04-08	23.6 ± 2.0 (1.9)	23.8 ± 2.8 (2.1)		Glacially transported granite boulder	
	BF-04-09	21.7 ± 2.1 (2.0)	21.9 ± 2.8 (2.2)		Glacially transported granite boulder	
	BF-04-10	22.1 ± 2.0 (2.0)	22.3 ± 2.8 (2.2)		Glacially transported granite boulder	
Average		***21.6 ± 0.7***	***21.7 ± 1.8***			
Aran Island	ARAN01	21.8 ± 0.9 (0.7)	21.6 ± 1.9 (0.7)		Glacially transported granite boulder	Cullen (2012)
	ARAN02	21.5 ± 0.9 (0.7)	21.3 ± 1.8 (0.7)		Granite bedrock	
Average		***21.7 ± 0.8***	***21.5 ± 1.8***			
Glencolumbkille	MAL-03	17.8 ± 0.6 (0.5)	17.9 ± 1.5 (0.5)		Vein quartz in glacially transported schist boulder	Ballantyne et al. (2007)
	MAL-05	19.6 ± 0.7 (0.5)	19.8 ± 1.7 (0.6)		Vein quartz in schist roche moutonnée	
Errigal col	ERGL-COL-01	17.6 ± 0.8 (0.6)	17.4 ± 1.5 (0.6)		Glacially plucked quartzite bedrock	Ballantyne et al. (2013b)
	ERGL-COL-02	18.2 ± 0.7 (0.6)	18.0 ± 1.5 (0.6)		Glacially plucked quartzite bedrock	
	ERGL-COL-04	18.1 ± 0.8 (0.6)	17.9 ± 1.6 (0.6)		Glacially plucked quartzite bedrock	
Average		***18.0 ± 0.6***	***17.8 ± 1.4***			
Slieve League	SL-02	17.1 ± 0.8 (0.7)	16.9 ± 1.5 (0.7)		Quartzite boulder from rockslope-failure debris	Ballantyne et al. (2013b)
	SL-03	17.8 ± 1.0 (0.9)	17.6 ± 1.7 (0.9)		Quartzite boulder from rockslope-failure debris	
	SL-04	17.1 ± 1.0 (0.9)	16.9 ± 1.6 (0.9)		Quartzite boulder from rockslope-failure debris	
Average		***17.3 ± 0.6***	***17.1 ± 1.5***			
NORTH MAYO						
Ox Mountains	OX-03-01	16.9 ± 1.4 (1.4)	17.0 ± 2.0 (1.5)		Vein quartz in glacially transported gneissic boulder	Clark et al. (2009c)
	OX-03-02	15.7 ± 1.5 (1.4)	16.0 ± 2.0 (1.6)		Vein quartz in glacially transported gneissic boulder	
	OX-03-03	16.4 ± 1.3 (1.3)	16.4 ± 1.9 (1.4)		Vein quartz in glacially transported gneissic boulder	
	OX-03-05	16.9 ± 1.3 (1.2)	16.9 ± 1.9 (1.4)		Vein quartz in glacially transported gneissic boulder	
	OX-03-06	17.0 ± 1.7 (1.7)	17.0 ± 2.3 (1.8)		Vein quartz in glacially transported gneissic boulder	
Average		***16.6 ± 0.6***	***16.7 ± 1.5***			
	OX-03-07	19.1 ± 1.6 (1.5)	19.1 ± 2.3 (1.7)		Vein quartz in glacially transported gneissic boulder	Clark et al. (2009c)
	OX-03-09	20.9 ± 1.5 (1.4)	21.1 ± 2.3 (1.6)		Vein quartz in glacially transported gneissic boulder	
	OX-03-10	20.5 ± 1.9 (1.8)	20.7 ± 2.6 (2.0)		Vein quartz in glacially transported gneissic boulder	
Average		***20.2 ± 1.1***	***20.3 ± 1.9***			
HEBRIDES AND SCOTTISH MAINLAND						
Arran : Glen Dougarie	D1	16.1 ± 1			Glacially transported granite boulder	Finlayson et al. (2014)
	D2	16.9 ± 1			Glacially transported granite boulder	
South Uist : Beinn Mhor col	BM-2	16.3 ± 0.9			Strongly ice-moulded gneiss bedrock	Stone and Ballantyne (2006)
Jura: Scriob na Caillich RSF	SNC02	14 ± 1.7			Quartzite boulder	Ballantyne et al., 2014)
	SNC03	12.3 ± 1.4			Quartzite boulder	
	SNC06	16.8 ± 1.1			Quartzite boulder	
	SNC07	16.8 ± 1			Quartzite boulder	

[1]Calculated with calculator formerly known as the CRONUS-Earth calculator (Developmental version; Wrapper script 2.3, Main calculator 2.1, constants 2.2.1, muons 1.1; Balco, et al., 2008) with LM scaling method, Loch Lomond reference production rate (LLPR) (see text), 1mm ka^{-1} erosion rate, and one sigma external uncertainty (internal in brackets).
[2]Calculated with CRONUScalc v2.0 (Marrero et al. 2016) with LM scaling method, default global reference production rate, 1mm ka^{-1} erosion rate, and one sigma external uncertainty (internal in brackets).

Table 6 Previously published legacy ^{14}C ages.

Site	Code	Sample type	Stratigraphical context	Conventional Radiocarbon Age (years BP)	+/- 1σ (radiocarbon yrs BP)	Quality	Reference
TRANSECT 6							
Derryvree	BIRM-166	TOC	Moss-rich mud overlaid by proglacial sands and till	30500	1100	Red (because pre-LGM)	Colhoun et al. (1972)
Belderg Pier,Co. Mayo	SSR-2713	Mollusc	Laminated muds and sands and diamictons interpreted as glaciomarine sediments over glacially striated rock surface	16940	120	Green	McCabe et al. (1986)
	AA53589	Mollusc		16980	120	Green	McCabe et al. (2005)
	AA56703	Foraminifera		16627	83		
	AA56704	Foraminifera		16830	130		
	AA56706	Mollusc		16389	74		
	AA56707	Mollusc		16328	67		
Fiddauntawnanoneen Co. Mayo	SSR-2714	Mollusc		17370	100	Yellow	McCabe et al. (1986)
Kesh Corran Caves, Co. Sligo	OxA-3693	Bone (Red Deer)	Faunal remains in a very thin series of earth and clay strata above “sterile” deposit	13622.5	136.5	Yellow	Woodman et al. (1997)
	OxA-3706	Bone (Brown Bear)		13776.5	105.5		
	OxA-3708	Bone (Wolf)		13030	118		
	OxA-5736	Bone (Hare)		14029.5	210.5		
TRANSECT 7							
Sourlie	SRR3023	Antler of *Rangifer tarandus*	Fluviatile sediments between two glacial diamictons	29900	430	Red (because pre-LGM)	Jardine et al. (1998)
	SRR3146	Plant debris		29290	350		
Corvish	AA45968	Foraminifera	Glaciotectonised sediments	16120	160	Green	McCabe and Clark (2003)
	AA45967			15490	150		
	AA45966			16460	430		
	AA33831			15425	95		
West of Islay	SUERC13122	Shell	Glaciomarine sediments	13103	40	Green	Peacock (2008)
Loch Indaal	SUERC13123	Shell	Glaciomarine sediments	13054	39	Green	Peacock (2008)
	SUERC13124			13120	39		
Loch Sunart	UL2853	Mollusc (*Pecten Maximus)*	Mud with occasional dropstones and pecten in life position interpreted as glacial diamict capped by sediments indicating glaciomarine and fully marine conditions	14020	210	Green	Baltzer et al. (2010)
Lochgilphead	OxA-1697	Shell	Glaciomarine sediments	14481	303	Yellow	Hedges et al. (1989)
	OxA-1698			14848	302		

Table 7 The modelled boundary limit ages for the MSIS and DBIS. All boundary ages are expressed as ±1 sigma. Ages marked * are identified as outliers that did not influence the modelled outputs. Model structures show the named Phases in the Bayesian age models and groups of dating information for the models.

Malin Sea Ice Stream (T7)

Model structure	Age information		Modelled age	Boundary age
Boundary Base: ice-free Scotland				34.4 ± 1.8
Phase Ice free ages	Sourlie-SRR3023	29.9 ± 0.4	33.5 ± 0.5	
	Sourlie-SRR3146	29.2 ± 0.4	32.9 ± 0.5	
Boundary BL0-base				27.9 ± 2.2
Phase Zone 1	T7JC106-125VC117	22.9 ± 0.06	26.8 ± 0.2	
	T7JC106-125VC115	22.8 ± 0.06	26.7 ± 0.3	
Boundary BL1				26.3 ± 0.3
Phase Zone 2	UCIAMS-164440 T7-146VC-389	20.7 ± 0.1	24.4 ± 0.3	
	UCIAMS-176383 T7-146VC-369	22.0 ± 0.1	25.9 ± 0.1	
	UCIAMS-176382 T7-146VC-223	20.2 ± 0.08	23.9 ± 0.2	
Boundary BL2				23.5 ± 0.3
Phase Zone 3	UCIAMS-179841 T7_151VC_389	19.7 ± 0.1	23.1 ± 0.3	
	UCIAMS-164432 T7-153VC-277	19.2 ± 0.1	22.7 ± 0.3	
	UCIAMS-164433 T7-154VC-211	18.7 ± 0.1	22.2 ± 0.3	
Boundary BL3				22 ± 0.3
Phase Zone 4	BF-01 Bloody Foreland	21.2 ± 1.1	21.6 ± 0.4	
	BF-02 Bloody Foreland	18.5 ± 0.9	*	
	BF-04-01 Bloody Foreland	17.9 ± 1.7	*	
	BF-04-04 Bloody Foreland	21.8 ± 1.6	21.6 ± 0.4	
	BF-04-05 Bloody Foreland	21.2 ± 1.7	21.6 ± 0.4	
	BF-04-06 Bloody Foreland	21.2 ± 1.9	21.6 ± 0.4	
	BF-04-08 Bloody Foreland	23.6 ± 2.0	21.7 ± 0.4	
	BF-04-09 Bloody Foreland	21.7 ± 2.0	21.6 ± 0.4	
	BF-04-10 Bloody Foreland	22.1 ± 2.0	21.6 ± 0.4	
	T7ALTB02 Altwinny Bay	30.4 ± 4.9	*	
	T7FAWN02 Fawnmore	25.8 ± 4.2	21.7 ± 0.4	
	T7FAWN03 Fawnmore	27.1 ± 3.7	21.7 ± 0.4	
	T7MH04, Malin Head	25.5 ± 2.1	21.7 ± 0.4	
	T7MH02 Malin Head	23.2 ± 1.4	21.7 ± 0.4	
	T7MH03 Malin Head	20.7 ± 1.1	21.6 ± 0.4	
Boundary BL4				21.2 ± 0.5
Phase Zone 5	T7CAR02 Tiree	21.1 ± 1.2	20.6 ± 0.5	
	T7CAR05 Tiree	20.2 ± 1.1	20.5 ± 0.4	
	T7CAR07 Tiree	20.8 ± 1.1	20.5 ± 0.5	
	T7CARV01 Carey Valley	22.6 ± 2.4	20.6 ± 0.5	
	T7CARV02 Carey Valley	22.1 ± 2.4	20.6 ± 0.5	
	T7GLEN01 Glenshesk Valley	30.4 ± 4.2	*	
	T7GLEN02 Glenshesk Valley	23.6 ± 3.4	20.6 ± 0.5	
	SUERC-59509 T7-149VC-421	17.1 ± 0.05	20.3 ± 0.2	
Boundary BL5				20 ± 0.3
Phase Zone 6	T6ROS01 Rosguill	18.7 ± 1.0	19.7 ± 0.3	
	T6ROS02 Rosguill	21.4 ± 1.4	19.8 ± 0.3	
	T6ROS03 Rosguill	18.9 ± 1.0	19.7 ± 0.3	
Boundary BL6				19.5 ± 0.3
Phase Zone 7	T7MIN02 Mingulay	18.7 ± 1.0	19.3 ± 0.3	
	T7MIN03 Mingulay	21.6 ± 1.1	19.3 ± 0.3	
	T7MIN04 Mingulay	17.4 ± 0.9	19.2 ± 0.3	
	T7MIN06 Mingulay	19.2 ± 1.0	19.3 ± 0.3	
	T7MIN07 Mingulay	20.9 ± 1.1	19.3 ± 0.3	
Boundary BL7				19 ± 0.3
Phase Zone 8	AA45968 Corvish	16.1 ± 0.2	18.8 ± 0.3	
	AA45967 Corvish	14.5 ± 0.2	18.4 ± 0.2	
	AA45966 Corvish	16.5 ± 0.4	18.8 ± 0.3	
	AA33831 Corvish	15.4 ± 0.1	18.3 ± 0.2	
Boundary BL8				18.1 ± 0.7
Phase Zone 9	S1 Jura	17.6 ± 1.2	17.1 ± 0.9	
	S2 Jura	16.5 ± 1.1	16.5 ± 1	
	S3 Jura	15.0 ± 1.1	15 ± 1.1	
	SNC-06 Jura	16.8 ± 1.1	16.7 ± 1	
	SNC-07 Jura	16.8 ± 1.0	16.7 ± 0.9	
	SNC-02 Jura	14.0 ± 1.7	*	
	SNC-03 Jura	12.3 ± 1.4	*	
	T7SGU02 North Barra	17.4 ± 1.0	17.1 ± 0.9	
	T7SGU03 North Barra	19.8 ± 1.1	*	
	T7SGU04 North Barra	17.0 ± 0.9	16.9 ± 0.9	
	T7TMC01 Torr Mor a'Chonairst	17.3 ± 0.9	17.1 ± 0.9	
	T7TMC05 Torr Mor a'Chonairst	17.8 ± 0.9	17.3 ± 0.9	
	T7TMC06 Torr Mor a'Chonairst	17.9 ± 1.0	17.3 ± 0.9	
	Arran D1	16.1 ± 1.0	16.2 ± 0.9	
	Arran D2	16.9 ± 1.0	16.8 ± 0.9	
	SUERC13122 W Islay	13.1 ± 0.04	15.2 ± 1.6	
	SUERC13123 Loch Indaal	13.1 ± 0.04	15.1 ± 1.2	
	SUERC13124 Loch Indaal	13.1 ± 0.04	15.2 ± 1.4	
	UL2853 Baltzer	14.0 ± 0.2	17 ± 0.9	
Boundary BL9				14.9 ± 1.5
Phase Zone 10	OxA-1698	14.9 ± 0.3	14.7 ± 1.6	
	OxA-1697	14.5 ± 0.3	14.6 ± 1.5	
Boundary BL10-end				14.3 ± 1.8

Donegal Bay Ice Stream (T6)

Model structure	Age information		Modelled age	Boundary age
Boundary Base: ice-free Ireland				35.1 ± 3.2
Phase Zone 1	Derryvree: BIRM-166	30.5 ± 1.1	33.5 ± 1.2	
Boundary BL0-Build-up of ice				26.6 ± 1.3
	JC106-112VC-51	22.6 ± 0.07	26.4 ± 0.1	
Phase Zon	JC106-112VC-59.5	22.6 ± 0.07	26.4 ± 0.1	
Boundary BL1				26.3 ± 0.1
Phase Zone 2	T6CE_08-018_CC	20.2 ± 0.09	23.8 ± 0.2	
	SUERC-63558 T6-103VC-145	22.5 ± 0.07	26.2 ± 0.2	
	UCIAMS-164437 T6-102VC-247	21.0 ± 0.1	24.8 ± 0.2	
	UCIAMS-164431 T6-101VC-548-551	20.1 ± 0.1	23.8 ± 0.2	
Boundary BL2				22.9 ± 0.7
Phase Zone 3	ARAN01	21.8 ± 0.9	21.6 ± 0.6	
	ARAN02	21.5 ± 0.9	21.5 ± 0.6	
	BF-01 Bloody Foreland	21.2 ± 1.1	21.4 ± 0.6	
	BF-02 Bloody Foreland	18.5 ± 0.9	*	
	BF-04-01 Bloody Foreland	17.9 ± 1.7	*	
	BF-04-04 Bloody Foreland	21.8 ± 1.6	21.6 ± 0.7	
	BF-04-05 Bloody Foreland	21.2 ± 1.7	21.5 ± 0.7	
	BF-04-06 Bloody Foreland	21.2 ± 1.9	21.5 ± 0.7	
	BF-04-08 Bloody Foreland	23.6 ± 2.0	21.8 ± 0.7	
	BF-04-09 Bloody Foreland	21.7 ± 2.0	21.6 ± 0.7	
	BF-04-10 Bloody Foreland	22.1 ± 2.0	21.6 ± 0.7	
Boundary BL3				20.5 ± 0.3
Phase Zone 4	UCIAMS-164429 T6-099VC-474		20.2 ± 0.2	
	SSR-2713 Belderg Pier,Co. Mayo	16.9 ± 0.1	19.9 ± 0.2	
	SSR-2714 Fiddauntawnanoneen,Co. Mayo	17.4 ± 0.1	20.3 ± 0.3	
	AA56707 Belderg Pier,Co. Mayo	16.3 ± 0.07	19.3 ± 0.2	
	AA56706 Belderg Pier,Co. Mayo	16.4 ± 0.07	19.3 ± 0.1	
	AA56704 Belderg Pier,Co. Mayo	16.8 ± 0.1	19.8 ± 0.2	
	AA53589 Belderg Pier,Co. Mayo	16.6 ± 0.08	20 ± 0.2	
	AA56703 Belderg Pier,Co. Mayo	16.6 ± 0.08	19.6 ± 0.1	
	Beta432794 JC106-97VC-468cm	16.8 ± 0.06	19.8 ± 0.1	
	Beta432793 JC106-92VC-259cm	16.5 ± 0.06	19.5 ± 0.1	
	T6GULR01	24.1 ± 1.9	*	
	T6GULR02	25.2 ± 1.9	*	
Boundary BL4				19 ± 0.4
Phase Zone 5	T6ROS01 Rosguill	18.7 ± 1.0	18.2 ± 0.6	
	T6ROS02 Rosguill	21.4 ± 1.4	*	
	T6ROS03 Rosguill	18.9 ± 1.0	18.2 ± 0.6	
	T6GCS-02	16.2 ± 1.0	17.3 ± 0.6	
	T6GCS-03	17.3 ± 1.1	17.7 ± 0.6	
	T6GCS-04	16.5 ± 1.0	17.4 ± 0.6	
	MAL03	17.8 ± 0.6	17.8 ± 0.5	
	MAL05	19.6 ± 0.7	*	
	T6KC-01	37.4 ± 5.4	17.9 ± 0.7	
	T6KC-02	37.5 ± 6.3	*	
	T6KC-03	42.8 ± 6.1	*	
	T6KC-04	37.4 ± 5.4	*	
	ERGL-Col-01	17.6 ± 0.8	17.7 ± 0.6	
	ERGL-Col-02	18.2 ± 0.7	18.1 ± 0.5	
	ERGL-Col-04	18.1 ± 0.8	18 ± 0.6	
	SL-02	17.1 ± 0.8	17.5 ± 0.6	
	SL-03	17.8 ± 1.0	17.8 ± 0.6	
	SL-04	17.1 ± 1.0	17.6 ± 0.6	
	T6PG-01	17.2 ± 1.1	17.7 ± 0.6	
	T6PG-04	16.2 ± 1.0	17.3 ± 0.6	
	T6PG-05	13.0 ± 0.9	*	
Boundary BL5				16.8 ± 0.5
Phase Zone 6	OX-03-01	16.9 ± 1.4	16.2 ± 0.6	
	OX-03-02	15.7 ± 1.5	16.1 ± 0.6	
	OX-03-03	16.4 ± 1.3	16.1 ± 0.6	
	OX-03-05	16.9 ± 1.3	16.2 ± 0.6	
	OX-03-06	17.0 ± 1.7	16.2 ± 0.6	
Boundary BL6				15.3 ± 0.6
Phase Zone 7	T6BS-04	14.4 ± 0.8	14.5 ± 0.5	
	T6BS-01	13.1 ± 0.9	*	
	T6BS-02	15.4 ± 1.0	*	
	T6BS-03	14.9 ± 0.9	14.6 ± 0.5	
	T6BEN01	13.0 ± 0.7	*	
	T6BEN02	14.3 ± 0.8	14.5 ± 0.5	
	T6BEN03	14.3 ± 0.8	14.5 ± 0.5	
	T6BEN04	15.7 ± 0.9	15.7 ± 0.9	
Boundary Ice free Midlands				13.9 ± 0.4
Phase Zone 7	OxA-3706	13.8 ± 0.1	13.4 ± 0.3	
	OxA-3693	13.6 ± 0.14	*	
	OxA-3708	13.0 ± 0.1	*	
	OxA-5736	14.0 ± 0.2	13.6 ± 0.3	
Boundary End of sequence				13.1 ± 0.9

Figure captions

Figure 1: Main map presents an overview of the study area showing the west coast of Scotland and northwest of Ireland with the locations of legacy and BRITICE-CHRONO samples used in this paper, as well as other locations mentioned in the text. Background bathymetry and topography were downloaded from the EMODnet data services (https://portal.emodnet-bathymetry.eu/services/) and are presented here as shaded-relief with 20x vertical exaggeration to visualise specifically the geomorphological features on the shelf (colour scale is only indicative due to processing). Inset presents the proposed maximum ice extent, the outline of the Donegal-Barra Fan (DBF) and mapped moraines and grounding-zone wedges (GZW) in the region (from BRITICE Glacial Map v2.0; Clark et al., 2017 and references therein); the location of ice streams, main ice flow directions and ice flow divides (see Greenwood and Clark, 2009a, Greenwood and Clark, 2009b); and the location of BRITICE-CHRONO transects 6 (Donegal Bay) and 7 (Malin Sea) discussed in this paper.

Figure 2: A) Serial section of the main exposure at Altwinny Bay. OSL sample locations are indicated by the labelled red dots, whilst the boxes labelled B-F show the coverage of the facies photographs in panels B-F. Note that clast depictions are not to scale but are instead representative of relative grain size variation between units. B-F) photographs of the main facies exposed. The OSL sample locations T7ALTB01 and 02 are indicated by the red circles. The white arrows highlight some of the abundant erratic clasts within the section that are likely carried to the site by Malin Sea ice.

Figure 3: Optically-stimulated luminescence data. Abanico plots (Dietze, et al., 2016) of the De values determined for OSL dating applied at (A) Altwinny Bay, (B) Carey Valley, (C) Castleroe, (D) Fawnmore, and (E) Glenshesk Valley. The plots present the De distributions in two plots that share a common z-axis of De values: (i) a bivariate plot where each De value is presented in relation to its precision (shown on the x-axis, where those more precisely known are plotted to the right); and (ii) a univariate plot showing the age frequency distribution of De values, which does not give any presentation of the precision of individual De values. The grey shading across both plots shows the De used in age calculation for each distribution (2σ shown on they-axis). The combination of these two plots aids interpretation of the scatter in the De distributions, where samples with a greater range of De values on the z-axis have larger amounts of scatter in the De distribution.

Figure 4: Photographs of exposures at Fawnmore Quarry A) section 1 and B) section 2. The labelled boxes show the locations covered by the photographs in C-E. Close-up photographs of the units from which C) T7FAWN01, D) T7FAWN02, and E) T7FAWN03 were sampled. The circles highlight sample positions.

Figure 5 A) Generalized vertical log and environmental interpretation of the sediments exposed at Castleroe with X-axis scaling denoting C (clay), Si (silt), S (sand), G (Gravel) and Dm (diamicton). Standard lithofacies codes follow Evans and Benn (Fig. 2.15: 2004), with prefixes F (fines), S (sand), G (gravel), D (diamict), and suffixes planar (p) or trough (t) cross-stratification, delta foresets (fo), massive or structureless (S/Fm), horizontal stratification (h), rippled (r), laminations (l) with or without drop-stones (d), gravels matrix-supported massive (Gms), gravels clast-supported massive (Gm), diamict matrix-supported, massive (Dmm) and diamict matrix-supported stratified (Dms). OSL sample positions are indicated by the labelled crossed circles. The labelled bars along the depth axis indicate the coverage of photographs in B-C. B, C) Photographs of the units sampled for OSL dating. The OSL sample locations are indicated by the labelled circles.

Figure 6 A) Photomontage of the main section at Glenshesk Valley. Lithofacies codes are the same as Fig. 5 (see Evans and Benn, 2004). The labelled boxes show the locations covered by the photographs in B-C. Close-up photographs of the units from which B) T7GLEN01 and C) T7GLEN02 were sampled. The circles highlight sample positions.

Figure 7: A) Generalized vertical succession of sediments exposed within Carey Valley (after McCabe and Eyles, 1988). Lithofacies codes are the same as Fig. 5 (see Evans and Benn, 2004). OSL sample positions are indicated by the labelled crossed circles. The labelled bars along the depth axis indicate the coverage of photographs in B-C. B, C) Photographs of the units sampled for OSL dating. The OSL sample locations are indicated by the circles.

Figure 8: A) Annotated photo-montage of the main section at Lough Nacung quarry. Lithofacies codes are the same as Fig. 5 (see Evans and Benn, 2004). The labelled boxes indicate the locations of photographs shown in B-C. Close-up photographs of the units sampled for B) T6LNAC01 and C) T6LNAC02. The circles highlight the position of the OSL samples.

Figure 9: Optically-stimulated luminescence data. Abanico plots (Dietze, et al., 2016) of the De values determined for OSL dating applied at (A) Brockhill Quarry, (B) Glenulra, and (C) Lough Nacung. The plots present the De distributions in two plots that share a common z-axis of De values: (i) a bivariate plot where each De value is presented in relation to its precision (shown on the x-axis, where those more precisely known are plotted to the right); and (ii) a univariate plot showing the age frequency distribution of De values, which does not give any presentation of the precision of individual De values. The grey shading across both plots shows the De used in age calculation for each distribution (2σ shown on they-axis). The combination of these two plots aids interpretation of the scatter in the De distributions, where samples with a greater range of De values on the z-axis have larger amounts of scatter in the De distribution.

Figure 10: A) Generalized vertical succession of the sediments in Glenulra valley (after McCabe, et al., 2007a). Lithofacies codes are the same as Fig. 5 (see Evans and Benn, 2004). The location of photographs in panels B and C are indicated by the labelled bars along the depth axis. Photographs of the units sampled for B) T6GULR02 and C) T6GULR01 with sample locations are indicated by the circles.

Figure 11: A) Generalized vertical succession of the sediments at Brockhill Quarry (after McCabe, et al., 1986). Lithofacies codes are the same as Fig. 5 (see Evans and Benn, 2004). The location of photographs in panels B and C are indicated by the labelled bars along the depth axis. Photographs of the units sampled for B) T6BROC01 and C) T6BROC02 with sample locations are indicated by the circles.

Figure 12: Bayesian chronosequence age-model output of dating constraints using Oxcal 4.3. (A) the MSIS (T7) and (B) DBIS (T6). The model structure shown uses OxCal brackets (left) and keywords that define the relative order of events (Bronk Ramsey, 2009a). Each original distribution (hollow) represents the relative probability of each age estimate with posterior density estimate (solid) generated by the modelling. Shown are 14C ages (black), OSL ages (orange), cosmogenic nuclide ages (blue) and modelled boundary ages (Red). Outliers are denoted by '?' and their probably (P) of being an outlier indicated by low values <5 (95% confidence). Model agreement indices for individual ages

show their fit to the model with >60% the widely used threshold for 'good' fit (Bronk Ramsey, 2009b).

Figure 13: Maximum and retreat grounding-line positions for the Malin Shelf Ice Stream (T7 transect) and across the present-day coastal hinterland. Location of the geochronological sites constraining the Bayesian modelling, modelled ages for retreat positions, major moraines and grounding-zone wedges on the shelf and on land (from BRITICE Glacial Map v2.0; Clark et al., 2017 and references therein) and isochrones are shown. 'BL' = Boundary Layers pre-LGM ice free to 10. Background bathymetry and topography from EMODnet data services (https://portal.emodnet-bathymetry.eu/services/).

Figure 14: Maximum and retreat grounding-line positions for the Donegal Bay Ice Stream (T6 transect) and across the present-day coastal hinterland. Location of the geochronological sites constraining the Bayesian modelling, modelled ages for retreat positions, moraines on the shelf and on land (from BRITICE Glacial Map v2.0; Clark et al., 2017 and references therein) and isochrones are shown. 'BL' = Boundary Layers pre-LGM ice free to 8. Background bathymetry and topography from EMODnet data services (https://portal.emodnet-bathymetry.eu/services/).

Figure 15: For A) the Donegal Bay Ice Stream and B) the Malin Sea Ice Stream, all plotted against age (ka) showing, (bottom) the boundary ages (circle and ±1 sigma whisker plots) and retreat zones of the respective Bayesian models and the rates of net axial ice margin retreat. (Middle) Modelled palaeo water depths (relative to present day bathymetry) for the inner and outer shelf derived from a glacial isostatic adjustment (GIA) model (Bradley, et al., 2011) updated to include the latest BRITICE-CHRONO ice sheet reconstruction and accounting for global ice sheet variations. (Top) Mean and 95% ice bed elevations from the NextMap elevation and EMODnet bathymetry (www.emodnet-hydrography.eu/). C) Ice rafted debris (IRD) flux records from marine cores within the Donegal-Barra Fan MD04-2822 (Hibbert, et al., 2009) and MD05-2006 (Knutz, et al., 2001, Knutz, et al., 2002) plotted against an updated (Waelbroeck, et al., 2019). Heinrich Events H2 and H1 are highlighted grey (Bond, et al., 1992). D) Ocean-climate parameters showing (bottom) sea surface temperature records determined for the North Atlantic using SST (°C) calculated using planktonic foraminifera for core SO82-02 at 59°N, 31°W (red line) (Rasmussen, et al., 2016, Van Kreveld, et al., 2000) plotted using an updated age model (Waelbroeck, et al., 2019) and the MD01-2461 site from the Porcupine Seabight at 51.7°N, 12.9°W (blue line) (Peck, et al., 2006, Peck, et al., 2007). (Middle) $\delta^{18}O$ concentrations, Greenland Stadials (GS) and Interstadials (GI) from the GISP2 and GRIP Greenland ice cores (Rasmussen, et al., 2014), plotted with and modelled surface-air temperatures (black line) relative to present for land masses north of ~45°N (Bintanja, et al., 2005). (Top) Ice volume equivalent sea level (Lambeck, et al., 2014) and summer insolation (pecked) for 60°N (Berger and Loutre, 1991).

Figure 16: Overview of modelled isochrones and retreat rates across the two transects of the Malin Sea and Donegal Bay Ice Streams with relevant geomorphological context (from BRITICE Glacial Map v2.0; Clark et al., 2017 and references therein). Dashed lines indicate more tentative isochrone positions due to lack of geomorphological evidence at the required spatial resolution. Background bathymetry and topography from EMODnet data services (https://portal.emodnet-bathymetry.eu/services/).

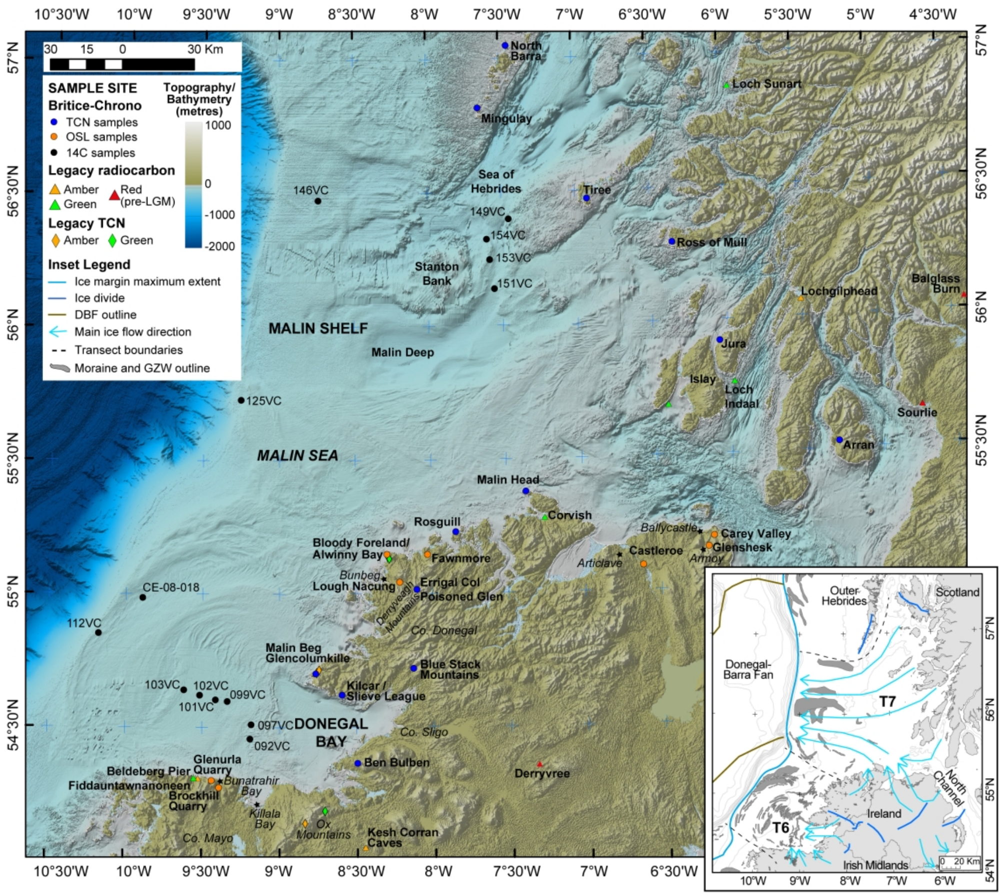

Figure 1: Main map presents an overview of the study area showing the west coast of Scotland and northwest of Ireland with the locations of legacy and BRITICE-CHRONO samples used in this paper, as well as other locations mentioned in the text. Background bathymetry and topography were downloaded from the EMODnet data services (https://portal.emodnet-bathymetry.eu/services/) and are presented here as shaded-relief with 20x vertical exaggeration to visualise specifically the geomorphological features on the shelf (colour scale is only indicative due to processing). Inset presents the proposed maximum ice extent, the outline of the Donegal-Barra Fan (DBF) and mapped moraines and grounding-zone wedges (GZW) in the region (from BRITICE Glacial Map v2.0; Clark et al., 2017 and references therein); the location of ice streams, main ice flow directions and ice flow divides (see Greenwood and Clark, 2009a, Greenwood and Clark, 2009b); and the location of BRITICE-CHRONO transects 6 (Donegal Bay) and 7 (Malin Sea) discussed in this paper.

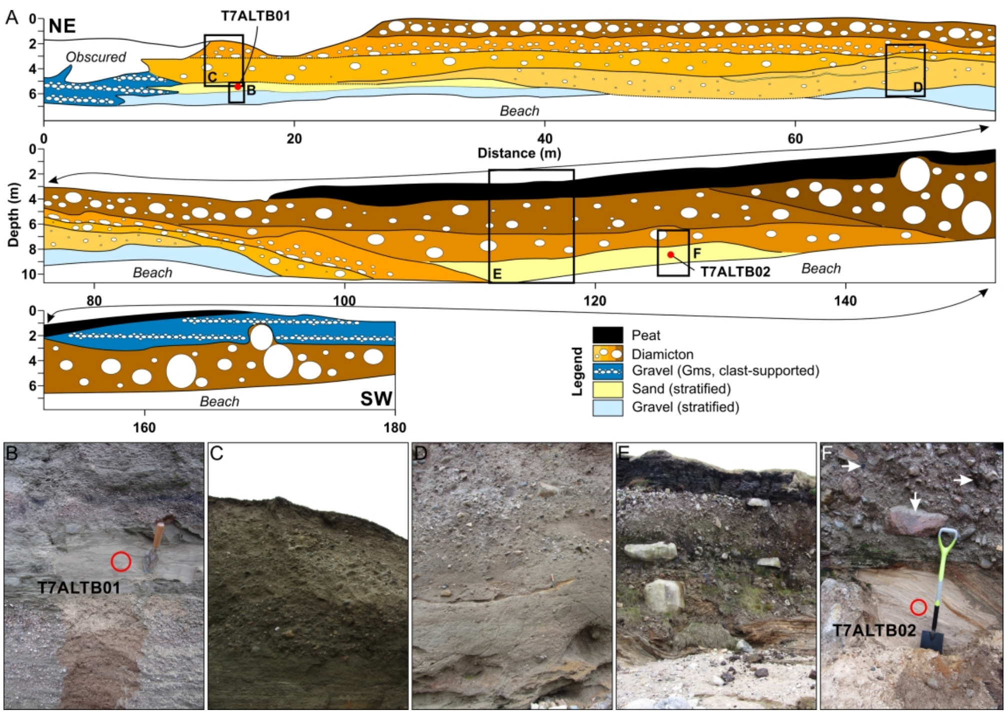

Figure 2: A) Serial section of the main exposure at Altwinny Bay. OSL sample locations are indicated by the labelled red dots, whilst the boxes labelled B-F show the coverage of the facies photographs in panels B-F. Note that clast depictions are not to scale but are instead representative of relative grain size variation between units. B-F) photographs of the main facies exposed. The OSL sample locations T7ALTB01 and 02 are indicated by the red circles. The white arrows highlight some of the abundant erratic clasts within the section that are likely carried to the site by Malin Sea ice.

252x176mm (300 x 300 DPI)

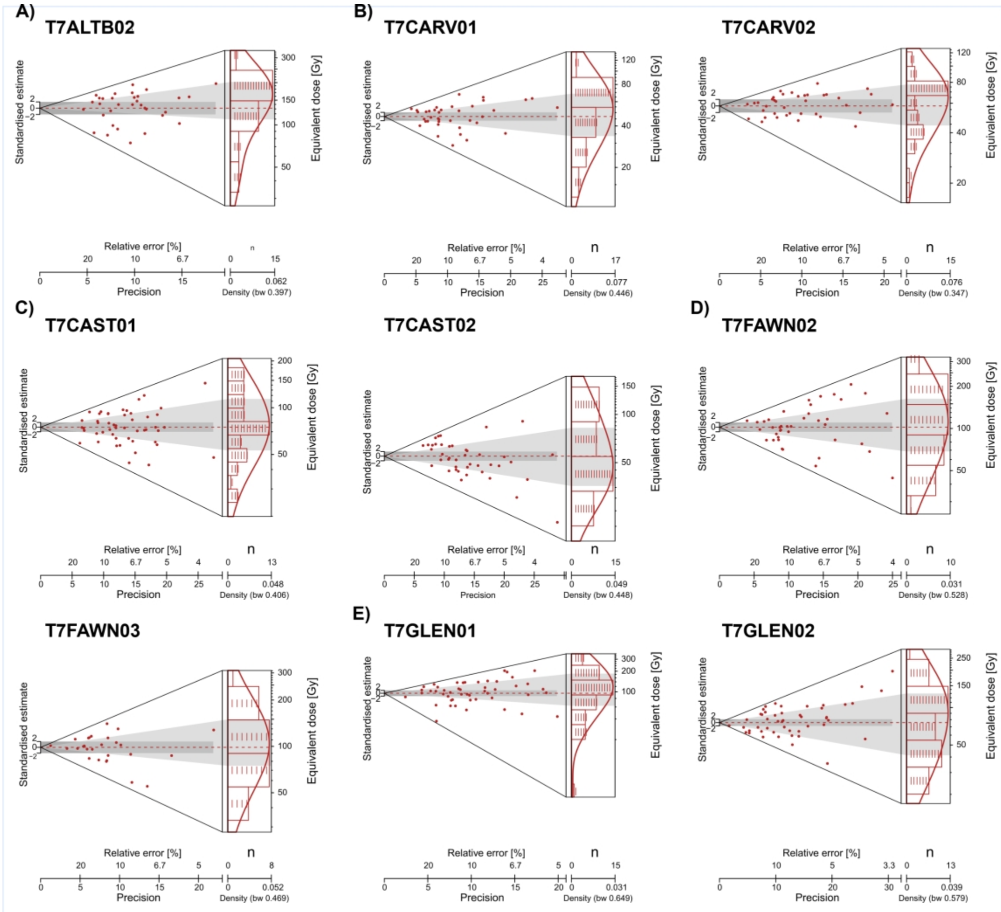

Figure 3: Optically-stimulated luminescence data. Abanico plots (Dietze et al., 2016) of the De values determined for OSL dating applied at (A) Altwinny Bay, (B) Carey Valley, (C) Castleroe, (D) Fawnmore, and (E) Glenshesk Valley. The plots present the De distributions in two plots that share a common z-axis of De values: (i) a bivariate plot where each De value is presented in relation to its precision (shown on the x-axis, where those more precisely known are plotted to the right); and (ii) a univariate plot showing the age frequency distribution of De values, which does not give any presentation of the precision of individual De values. The grey shading across both plots shows the De used in age calculation for each distribution (2σ shown on they-axis). The combination of these two plots aids interpretation of the scatter in the De distributions, where samples with a greater range of De values on the z-axis have larger amounts of scatter in the De distribution.

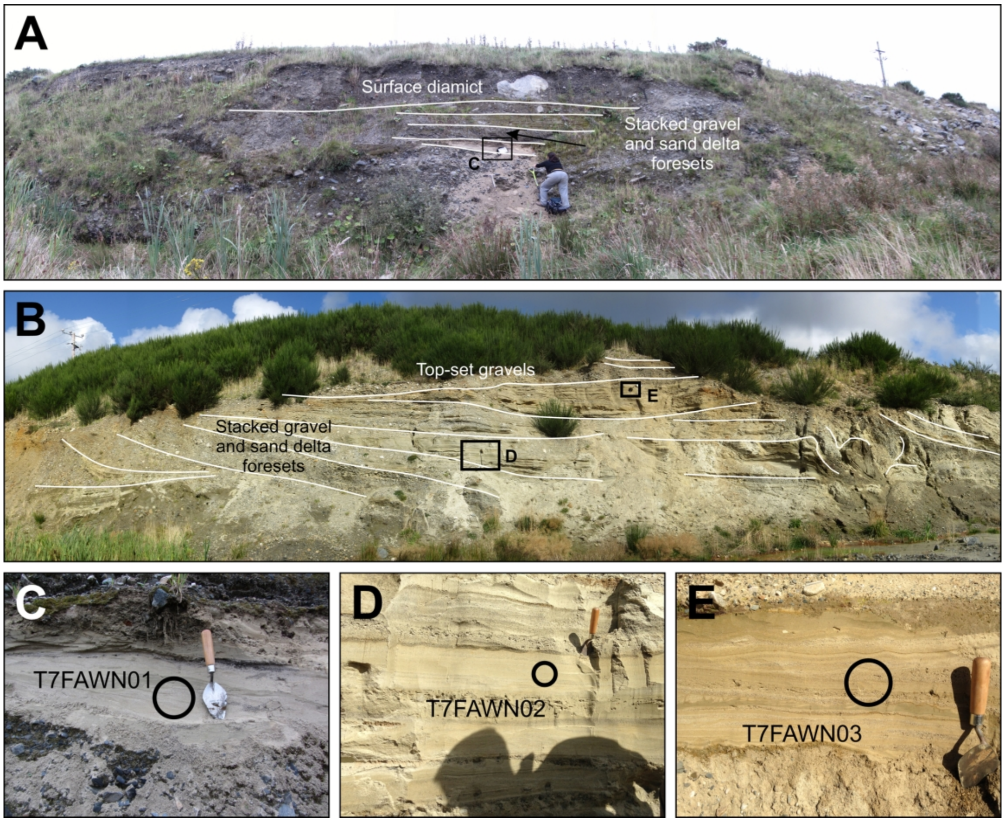

Figure 4: Photographs of exposures at Fawnmore Quarry A) section 1 and B) section 2. The labelled boxes show the locations covered by the photographs in C-E. Close-up photographs of the units from which C) T7FAWN01, D) T7FAWN02, and E) T7FAWN03 were sampled. The circles highlight sample positions.

180x146mm (300 x 300 DPI)

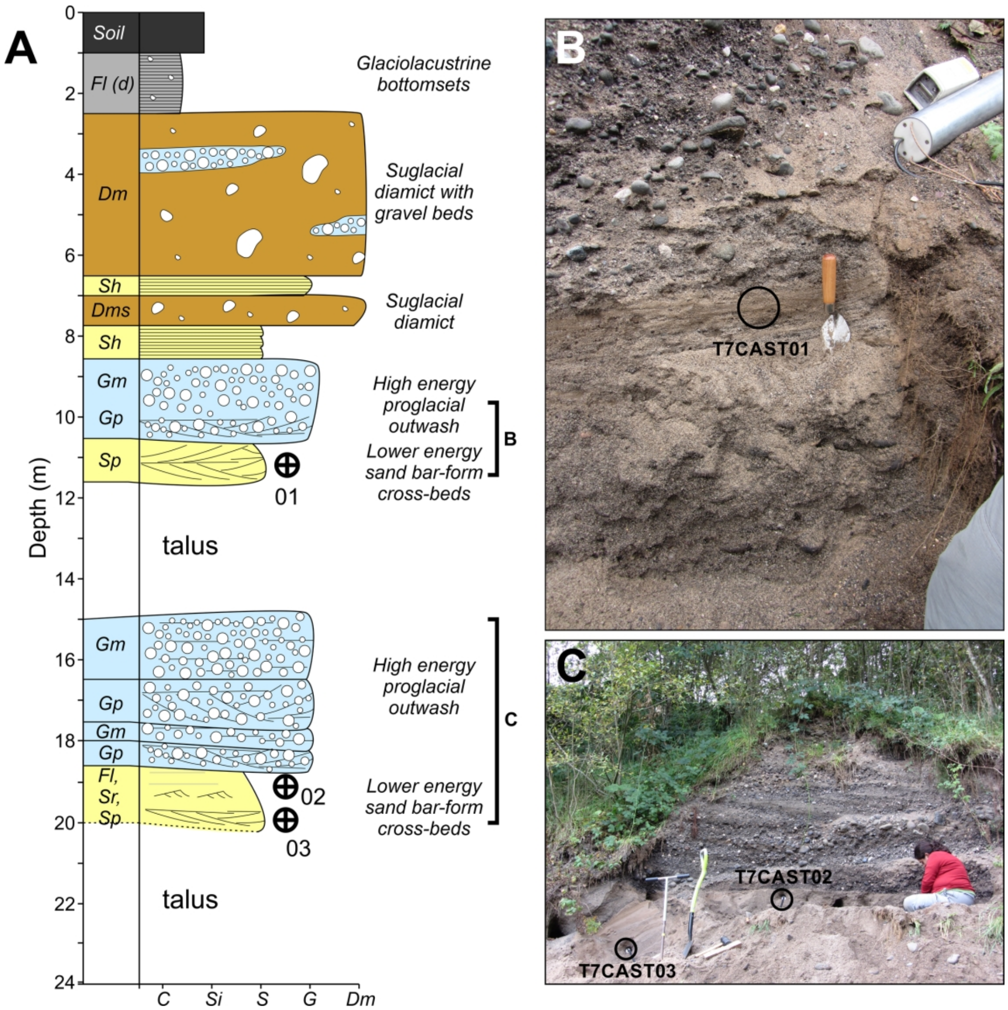

Figure 5 A) Generalized vertical log and environmental interpretation of the sediments exposed at Castleroe with X-axis scaling denoting C (clay), Si (silt), S (sand), G (Gravel) and Dm (diamicton). Standard lithofacies codes follow Evans and Benn (Fig. 2.15: 2004), with prefixes F (fines), S (sand), G (gravel), D (diamict), and suffixes planar (p) or trough (t) cross-stratification, delta foresets (fo), massive or structureless (S/Fm), horizontal stratification (h), rippled (r), laminations (l) with or without drop-stones (d), gravels matrix-supported massive (Gms), gravels clast-supported massive (Gm), diamict matrix-supported, massive (Dmm) and diamict matrix-supported stratified (Dms). OSL sample positions are indicated by the labelled crossed circles. The labelled bars along the depth axis indicate the coverage of photographs in B-C. B, C) Photographs of the units sampled for OSL dating. The OSL sample locations are indicated by the labelled circles.

185x185mm (300 x 300 DPI)

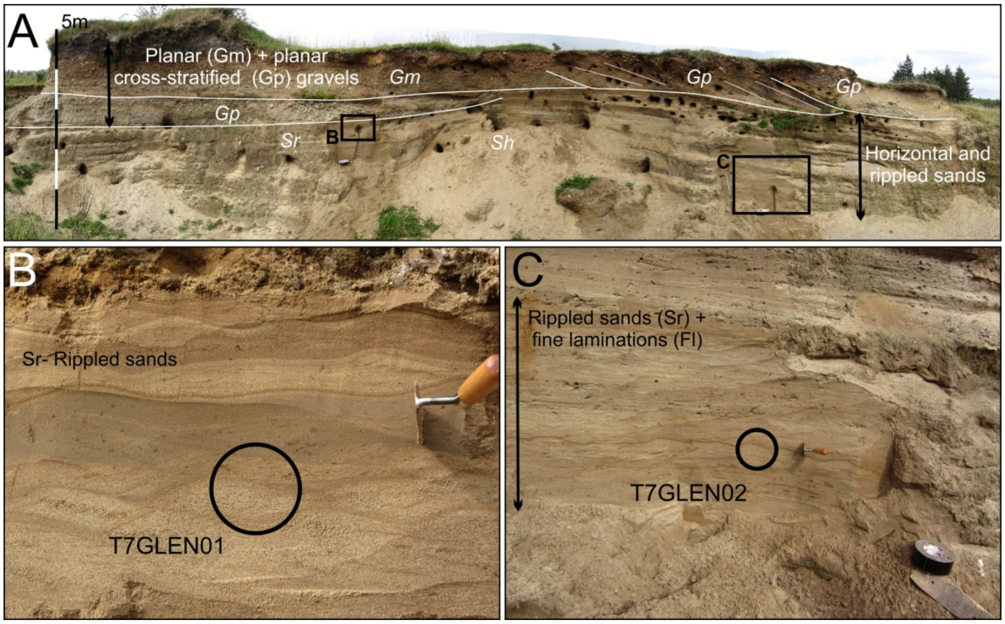

Figure 6 A) Photomontage of the main section at Glenshesk Valley. Lithofacies codes are the same as Fig. 5 (Fig. 2.15: Evans and Benn, 2004). The labelled boxes show the locations covered by the photographs in B-C. Close-up photographs of the units from which B) T7GLEN01 and C) T7GLEN02 were sampled. The circles highlight sample positions.

180x111mm (300 x 300 DPI)

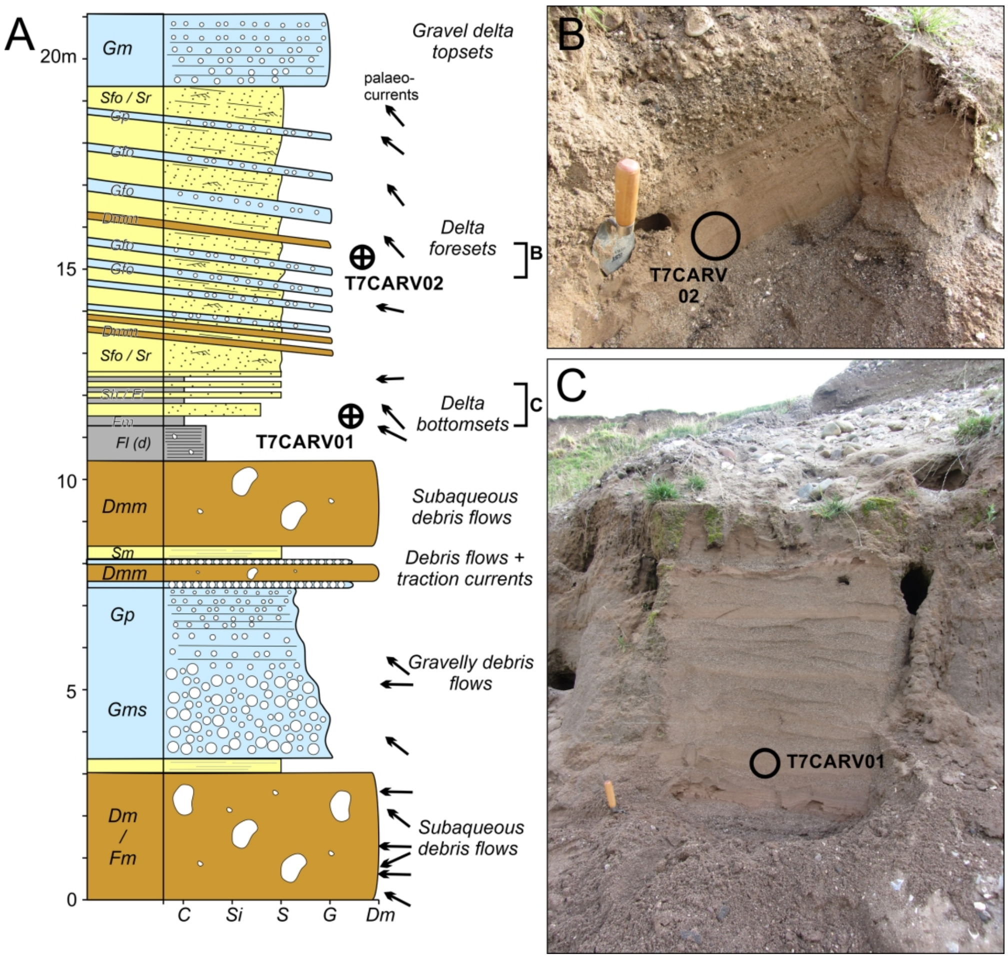

Figure 7: A) Generalized vertical succession of sediments exposed within Carey Valley (after McCabe and Eyles, 1988). Lithofacies codes are the same as Fig. 5 (Fig. 2.15: Evans and Benn, 2004). OSL sample positions are indicated by the labelled crossed circles. The labelled bars along the depth axis indicate the coverage of photographs in B-C. B, C) Photographs of the units sampled for OSL dating. The OSL sample locations are indicated by the circles.

186x176mm (300 x 300 DPI)

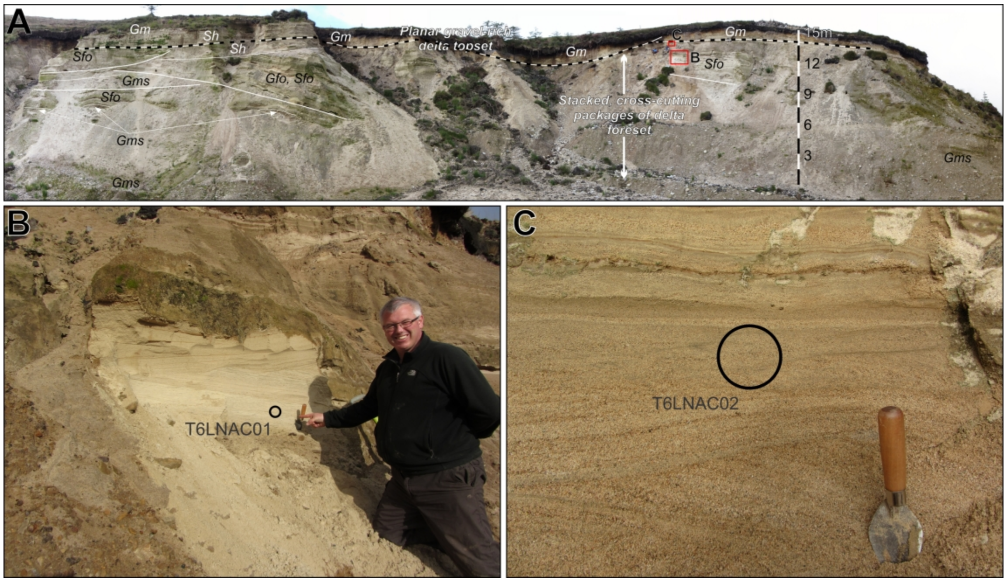

Figure 8: A) Annotated photo-montage of the main section at Lough Nacung quarry. Lithofacies codes are the same as Fig. 5 (Fig. 2.15: Evans and Benn, 2004). The labelled boxes indicate the locations of photographs shown in B-C. Close-up photographs of the units sampled for B) T6LNAC01 and C) T6LNAC02. The circles highlight the position of the OSL samples.

240x138mm (300 x 300 DPI)

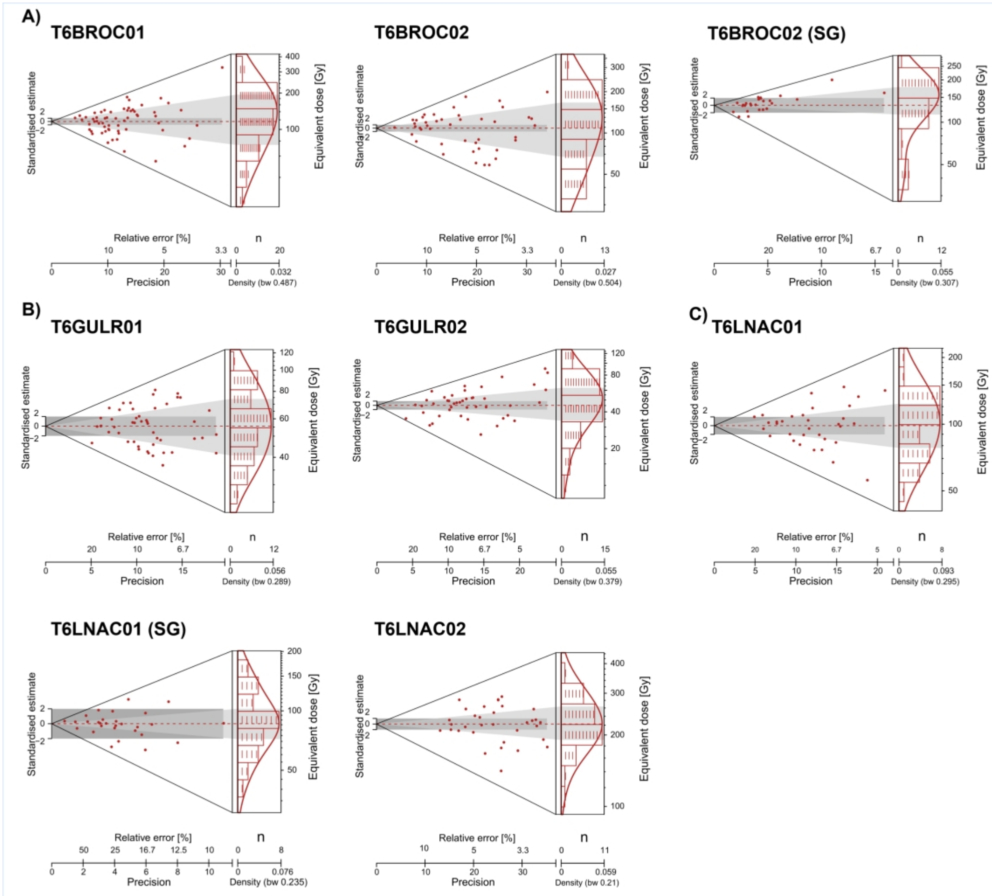

Figure 9: Optically-stimulated luminescence data. Abanico plots (Dietze et al., 2016) of the De values determined for OSL dating applied at (A) Brockhill Quarry, (B) Glenulra, and (C) Lough Nacung. The plots present the De distributions in two plots that share a common z-axis of De values: (i) a bivariate plot where each De value is presented in relation to its precision (shown on the x-axis, where those more precisely known are plotted to the right); and (ii) a univariate plot showing the age frequency distribution of De values, which does not give any presentation of the precision of individual De values. The grey shading across both plots shows the De used in age calculation for each distribution (2σ shown on they-axis). The combination of these two plots aids interpretation of the scatter in the De distributions, where samples with a greater range of De values on the z-axis have larger amounts of scatter in the De distribution.

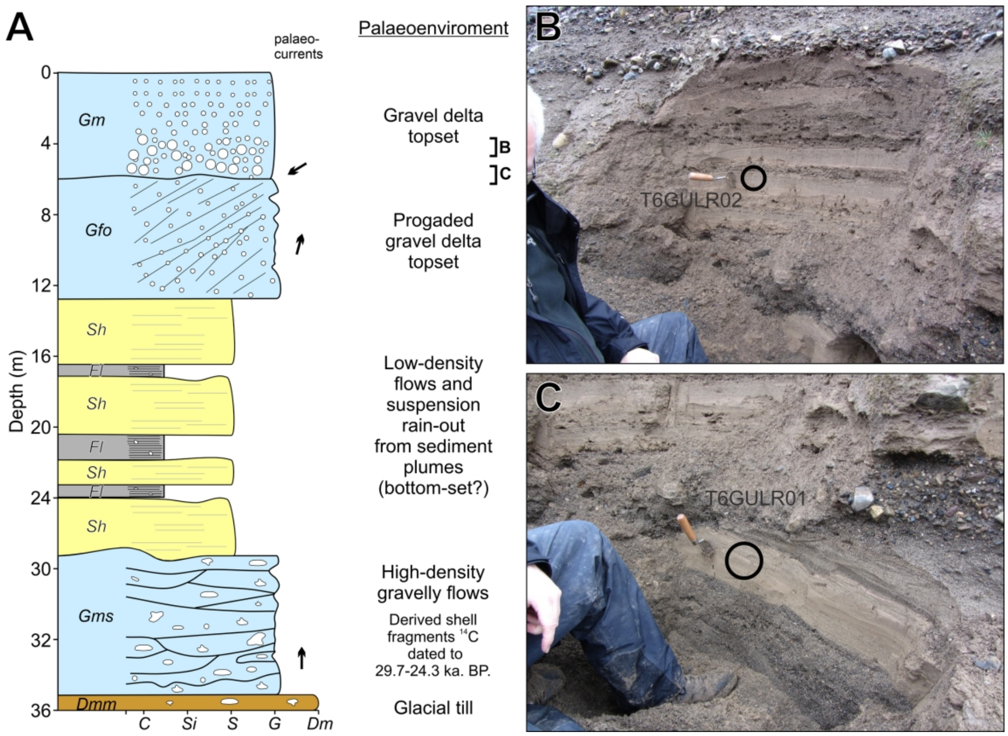

Figure 10: A) Generalized vertical succession of the sediments in Glenulra valley (after McCabe et al., 2007a). Lithofacies codes are the same as Fig. 5 (Fig. 2.15: Evans and Benn, 2004). The location of photographs in panels B and C are indicated by the labelled bars along the depth axis. Photographs of the units sampled for B) T6GULR02 and C) T6GULR01 with sample locations are indicated by the circles.

208x151mm (300 x 300 DPI)

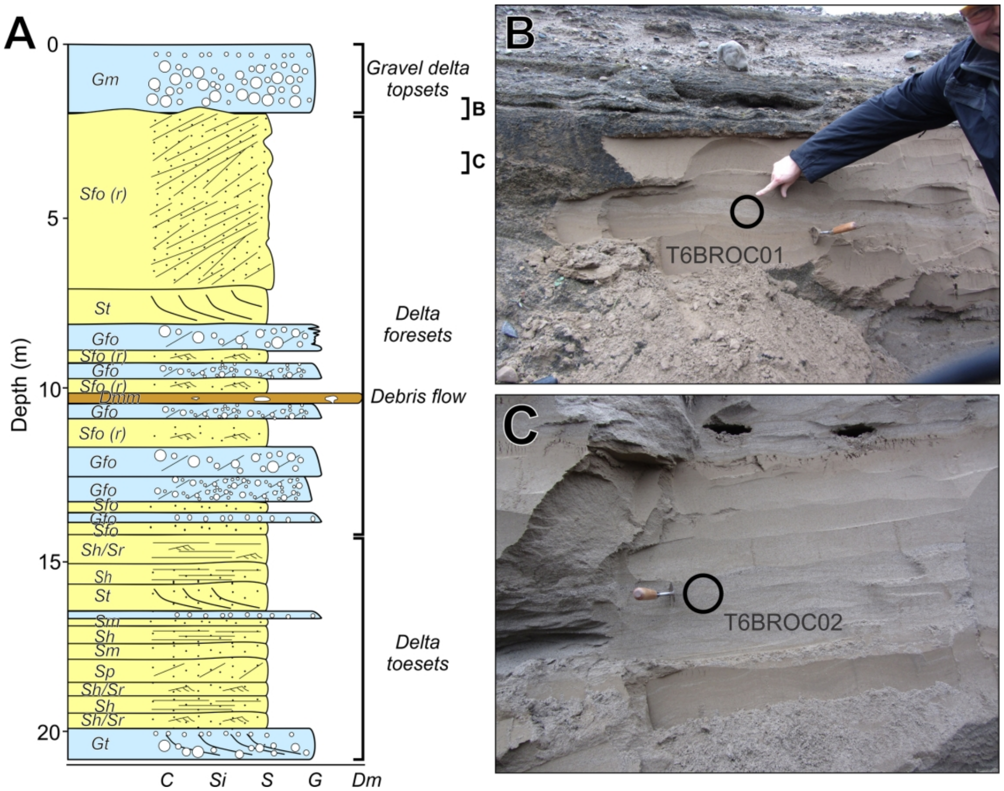

Figure 11: A) Generalized vertical succession of the sediments at Brockhill Quarry (after McCabe et al., 1986). Lithofacies codes are the same as Fig. 5 (Fig. 2.15: Evans and Benn, 2004). The location of photographs in panels B and C are indicated by the labelled bars along the depth axis. Photographs of the units sampled for B) T6BROC01 and C) T6BROC02 with sample locations are indicated by the circles.

182x142mm (300 x 300 DPI)

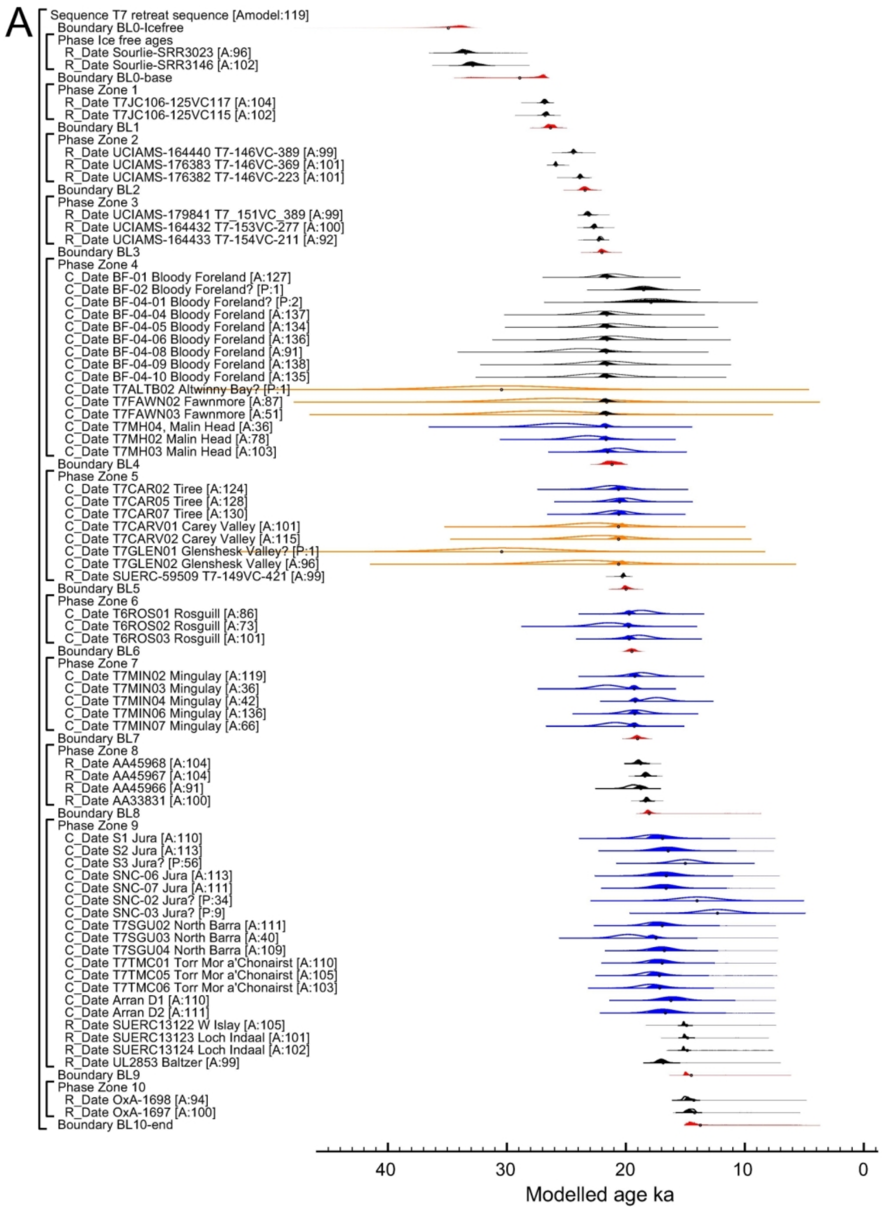

Figure 12: Bayesian chronosequence age-model output of dating constraints using Oxcal 4.3. (A) the MSIS (T7) and (B) DBIS (T6). The model structure shown uses OxCal brackets (left) and keywords that define the relative order of events (Bronk Ramsey, 2009a). Each original distribution (hollow) represents the relative probability of each age estimate with posterior density estimate (solid) generated by the modelling. Shown are 14C ages (black), OSL ages (orange), cosmogenic nuclide ages (blue) and modelled boundary ages (Red). Outliers are denoted by '?' and their probably (P) of being an outlier indicated by low values <5 (95% confidence). Model agreement indices for individual ages show their fit to the model with >60% the widely used threshold for 'good' fit (Bronk Ramsey, 2009b).

136x186mm (300 x 300 DPI)

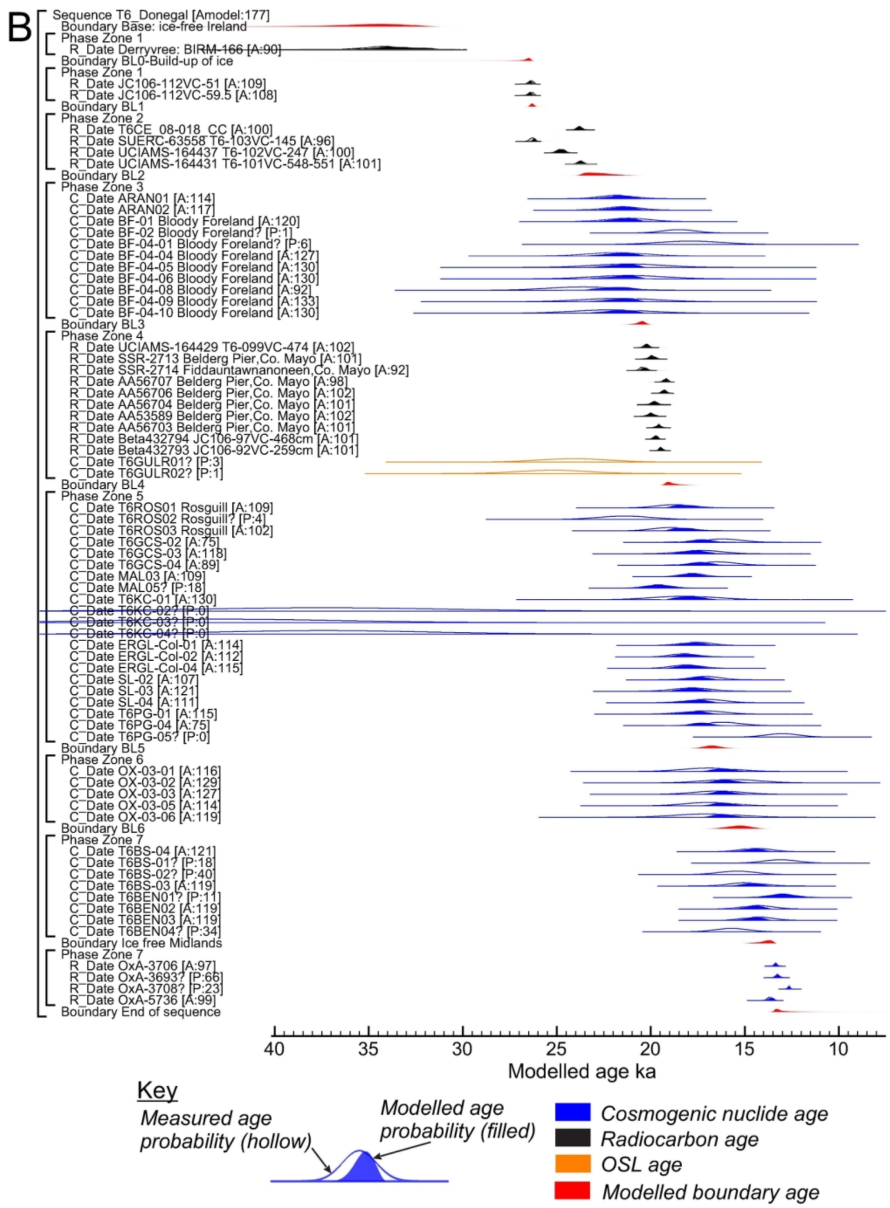

Figure 12: Bayesian chronosequence age-model output of dating constraints using Oxcal 4.3. (A) the MSIS (T7) and (B) DBIS (T6). The model structure shown uses OxCal brackets (left) and keywords that define the relative order of events (Bronk Ramsey, 2009a). Each original distribution (hollow) represents the relative probability of each age estimate with posterior density estimate (solid) generated by the modelling. Shown are 14C ages (black), OSL ages (orange), cosmogenic nuclide ages (blue) and modelled boundary ages (Red). Outliers are denoted by '?' and their probably (P) of being an outlier indicated by low values <5 (95% confidence). Model agreement indices for individual ages show their fit to the model with >60% the widely used threshold for 'good' fit (Bronk Ramsey, 2009b).

137x186mm (300 x 300 DPI)

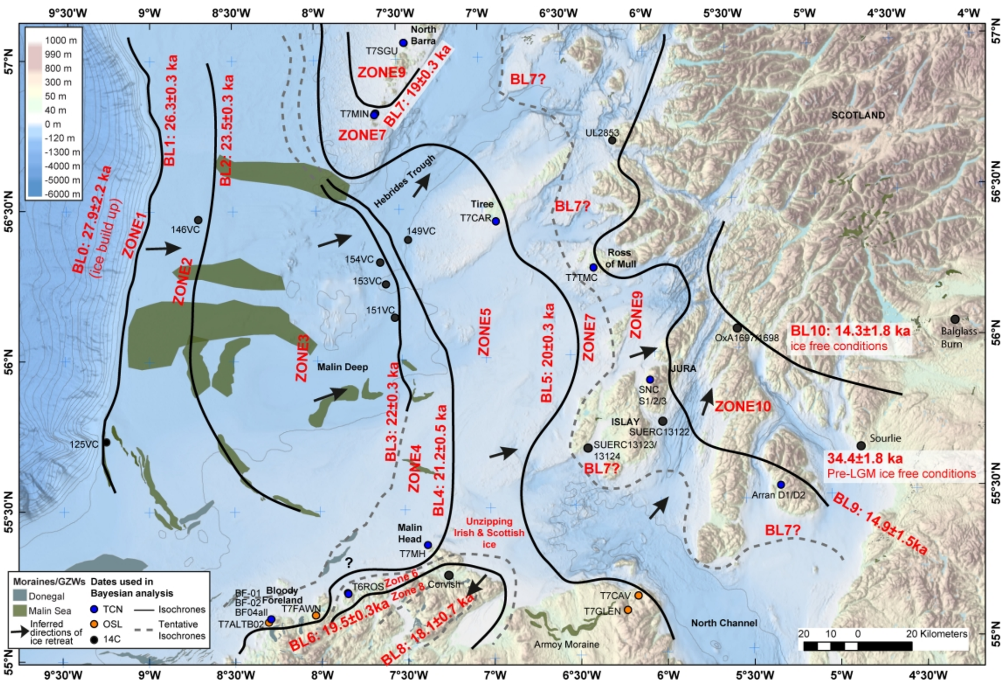

Figure 13: Maximum and retreat grounding-line positions for the Malin Shelf Ice Stream (T7 transect) and across the present-day coastal hinterland. Location of the geochronological sites constraining the Bayesian modelling, modelled ages for retreat positions, major moraines and grounding-zone wedges on the shelf and on land (from BRITICE Glacial Map v2.0; Clark et al., 2017 and references therein) and isochrones are shown. 'BL' = Boundary Layers pre-LGM ice free to 10. Background bathymetry and topography from EMODnet data services (https://portal.emodnet-bathymetry.eu/services/).

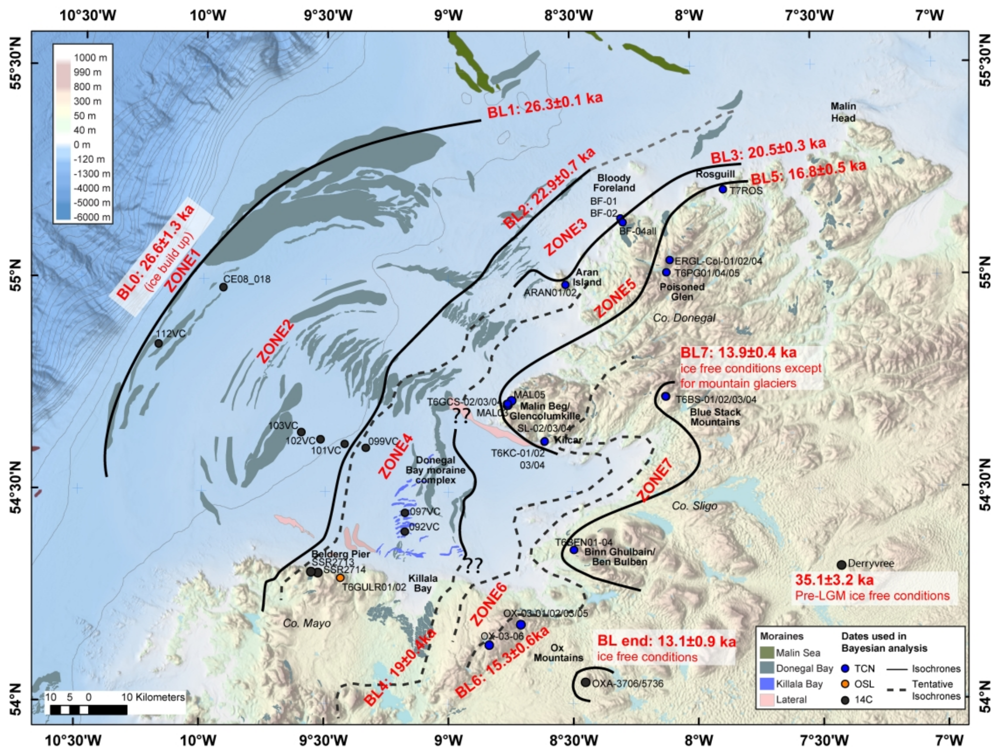

Figure 14: Maximum and retreat grounding-line positions for the Donegal Bay Ice Stream (T6 transect) and across the present-day coastal hinterland. Location of the geochronological sites constraining the Bayesian modelling, modelled ages for retreat positions, moraines on the shelf and on land (from BRITICE Glacial Map v2.0; Clark et al., 2017 and references therein) and isochrones are shown. 'BL' = Boundary Layers pre-LGM ice free to 8. Background bathymetry and topography from EMODnet data services (https://portal.emodnet-bathymetry.eu/services/).

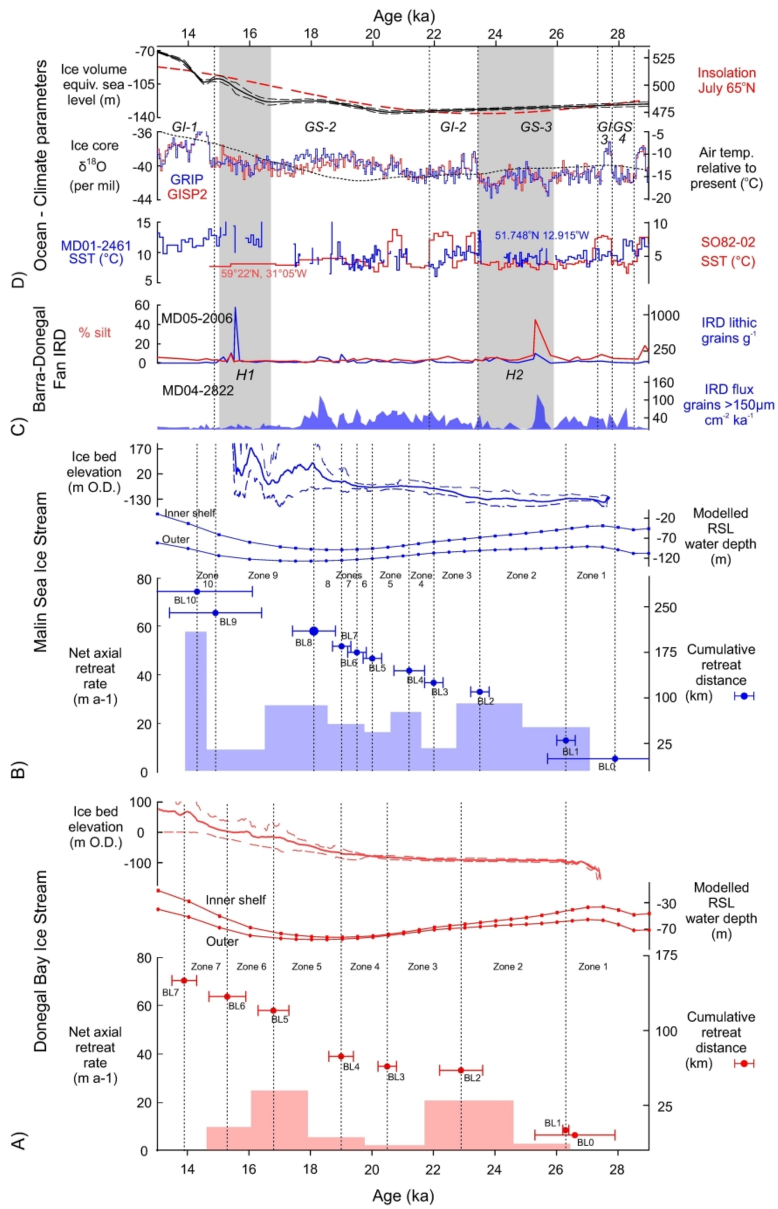

Figure 15: For A) the Donegal Bay Ice Stream and B) the Malin Sea Ice Stream, all plotted against age (ka) showing, (bottom) the boundary ages (circle and ±1 sigma whisker plots) and retreat zones of the respective Bayesian models and the rates of net axial ice margin retreat. (Middle) Modelled palaeo water depths (relative to present day bathymetry) for the inner and outer shelf derived from a glacial isostatic adjustment (GIA) model (Bradley et al., 2011) updated to include the latest BRITICE-CHRONO ice sheet reconstruction and accounting for global ice sheet variations. (Top) Mean and 95% ice bed elevations from the NextMap elevation and EMODnet bathymetry (www.emodnet-hydrography.eu/). C) Ice rafted debris (IRD) flux records from marine cores within the Donegal-Barra Fan MD04-2822 (Hibbert et al., 2009) and MD05-2006 (Knutz et al., 2001; Knutz et al., 2002) plotted against an updated (Waelbroeck et al., 2019). Heinrich Events H2 and H1 are highlighted grey (Bond et al., 1992). D) Ocean-climate parameters showing (bottom) sea surface temperature records determined for the North Atlantic using SST (°C) calculated using planktonic foraminifera for core SO82-02 at 59°N, 31°W (red line) (Rasmussen et al., 2016; Van Kreveld et al., 2000) plotted using an updated age model (Waelbroeck et al., 2019) and the MD01-2461 site from the Porcupine Seabight at 51.7°N, 12.9°W (blue line) (Peck et al., 2006; Peck et al., 2007). (Middle) δ18O

concentrations, Greenland Stadials (GS) and Interstadials (GI) from the GISP2 and GRIP Greenland ice cores (Rasmussen et al., 2014), plotted with and modelled surface-air temperatures (black line) relative to present for land masses north of ~45°N (Bintanja et al., 2005). (Top) Ice volume equivalent sea level (Lambeck et al., 2014) and summer insolation (pecked) for 60°N (Berger and Loutre, 1991).

177x276mm (300 x 300 DPI)

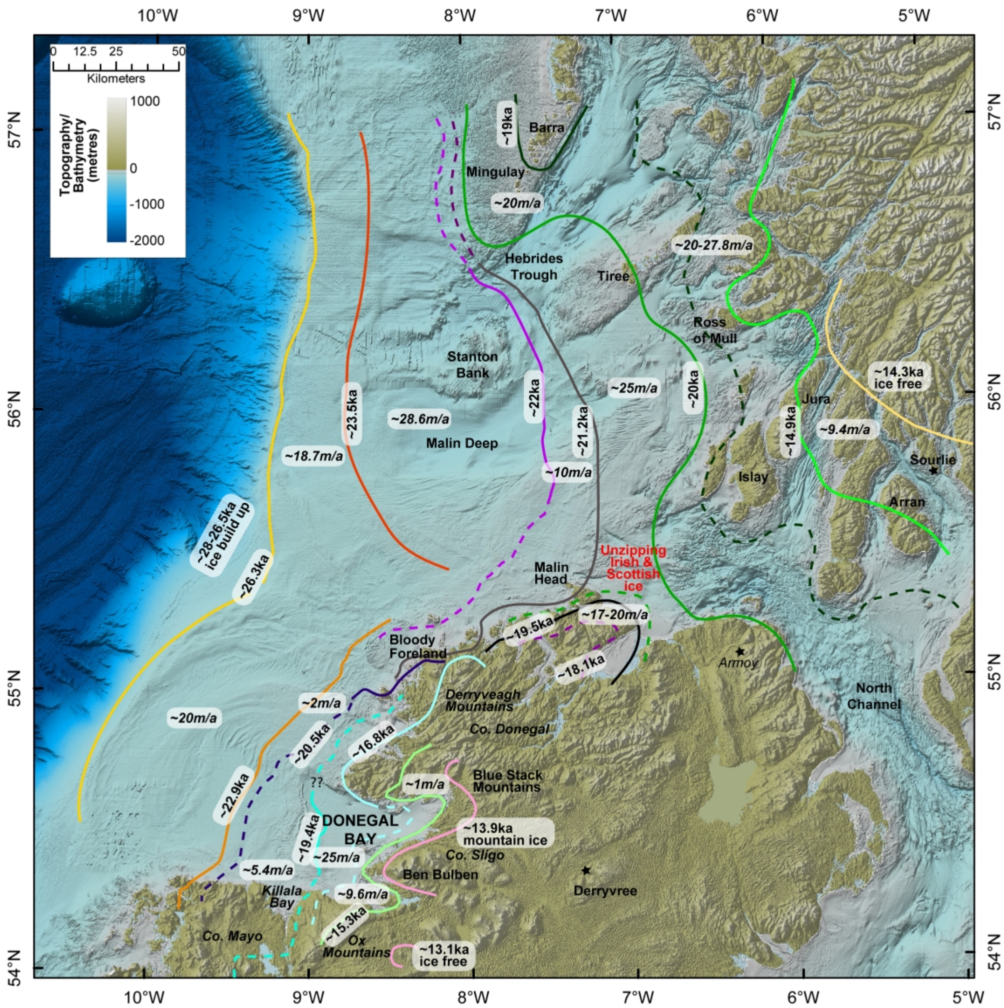

Figure 16: Overview of modelled isochrones and retreat rates across the two transects of the Malin Sea and Donegal Bay Ice Streams with relevant geomorphological context (from BRITICE Glacial Map v2.0; Clark et al., 2017 and references therein). Dashed lines indicate more tentative isochrone positions due to lack of geomorphological evidence at the required spatial resolution. Background bathymetry and topography from EMODnet data services (https://portal.emodnet-bathymetry.eu/services/).